KfK 3552
November 1983

UO_2/Zircaloy-4 Chemical Interactions and Reaction Kinetics from 1000 to 1700° C under Isothermal Conditions

(Final Report)

P. Hofmann, D. K. Kerwin-Peck
Institut für Material- und Festkörperforschung
Projekt Nukleare Sicherheit

Kernforschungszentrum Karlsruhe

KERNFORSCHUNGSZENTRUM KARLSRUHE

Institut für Material- und Festkörperforschung

Projekt Nukleare Sicherheit

KfK 3552

UO_2/Zircaloy-4 Chemical Interactions and Reaction Kinetics from 1000 to 1700°C under Isothermal Conditions

(Final Report)

P. Hofmann, D.K. Kerwin-Peck*

in Cooperation with

Ch. Adelhelm
J. Burbach
G. Gausmann
H. Metzger
E. Nold
S.O. Peck*

* EG & G Idaho, Inc., P.O. Pox 1625, Idaho Falls, Idaho 83415, presently the NRC Sponsored Delegate to the Kernforschungszentrum Karlsruhe

Kernforschungszentrum Karlsruhe GmbH., Karlsruhe

Kernforschungszentrum Karlsruhe GmbH
ISSN 0303-4003

Summary

Chemical interactions between UO_2 fuel and Zircaloy-4 cladding up to the melting point of zircaloy (Zry) are described in this report. Out-of-pile UO_2/zircaloy reaction experiments have been performed to investigate the chemical interaction behavior under possible severe fuel damage conditions (very high temperatures and external overpressure). The tests were conducted in inert gas (1 to 80 bar) with 10-cm long zircaloy cladding specimens filled with UO_2 pellets. The annealing temperature varied between 1000 and 1700°C and the annealing period between 1 and 150 minutes.

The extent of the chemical reaction depends decisively on whether or not good contact between UO_2 and zircaloy has been established. If solid contact exists, zircaloy reduces the UO_2 to form oxygen-stabilized α-Zr(O) and uranium metal. The uranium reacts with zircaloy low in oxygen to form a (U,Zr) alloy rich in uranium. The (U,Zr) alloy, which is liquid above about 1150°C, lies between two α-Zr(O) layers. The affinity of zirconium for oxygen, which results in an oxygen gradient across the cladding, is the driving force for the reaction. The UO_2/zircaloy reaction obeys a parabolic rate law. The degree of chemical interaction is determined by the extent of oxygen diffusion into the cladding, and hence by the temperature and time.

The growth of the reaction layers can be represented in an Arrhenius diagram. The UO_2/Zry-4 reaction occurs as rapidly as the steam/Zry-4 reaction above about 1100°C. The extent of the interaction is independent of the external pressure above about 10 bar at 1400°C and 5 bar at 1700°C. The maximum measured oxygen content of the cladding is about 6 wt.%, which corresponds approximately to saturated α-Zr(O). Up to about 9 vol.% of the UO_2 can be chemically dissolved by the zircaloy. In an actual fuel rod, complete release of the volatile fission products in this region of the fuel must therefore be assumed.

Chemische Wechselwirkungen und Reaktionskinetik zwischen UO_2 und Zircaloy-4 von 1000 bis 1700°C

Zusammenfassung

In diesem Bericht werden die chemischen Wechselwirkungen zwischen UO_2-Brennstoff und Zircaloy-4-Hüllmaterial bis zum Schmelzpunkt von Zircaloy (Zry) beschrieben. Es wurden out-of-pile UO_2/Zry-Reaktionsexperimente unter möglichen SFD (Severe Fuel Damage)-Bedingungen, d.h. bei hohen Temperaturen und großen äußeren Überdrucken, durchgeführt, um das Reaktionsverhalten zu studieren. Die Experimente erfolgten mit ca. 10 cm langen Hüllrohrproben, die mit UO_2-Pellets gefüllt waren, unter inerten Bedingungen (1 bis 80 bar). Die Temperaturen variierten zwischen 1000 und 1700°C und die Glühzeiten zwischen 1 und 150 min.

Das Ausmaß der chemischen Wechselwirkungen hängt entscheidend davon ab, ob ein guter Festkörperkontakt zwischen UO_2 und Zry besteht oder nicht. Falls direkter Kontakt besteht, wird das UO_2 durch das Zry unter Bildung von sauerstoffstabilisiertem α-Zr(O) und Uranmetall reduziert. Das Uran reagiert mit sauerstoffarmem Zr unter Bildung einer (U,Zr)-Legierung. Die (U,Zr)-Legierung ist oberhalb etwa 1150°C flüssig und liegt zwischen zwei α-Zr(O)-Reaktionsschichten. Die Affinität des Zirkoniums zum Sauerstoff ist die Triebkraft für die chemischen Wechselwirkungen und führt zu einem Sauerstoffgradienten im Hüllrohrquerschnitt. Die Reaktionen zwischen dem UO_2 und Zry verlaufen nach einem parabolischen Zeitgesetz. Der Reaktionsumfang wird durch das Ausmaß der Sauerstoffdiffusion in das Hüllmaterial bestimmt und hängt von der Temperatur und Zeit ab.

Das Wachstum der Reaktionsschichten kann in einem Arrheniusdiagramm dargestellt werden. Die UO_2/Zry-Reaktionen verlaufen oberhalb etwa 1100°C genau so schnell wie die Zry/Wasserdampf-Reaktion. Das Ausmaß der Wechselwirkungen ist bei 1400°C oberhalb etwa 10 bar und bei 1700°C oberhalb etwa 5 bar unabhängig vom äußeren Druck. Der maximal gemessene Sauerstoffgehalt in der Hülle beträgt ungefähr 6 Gew.%, was einem nahezu gesättigten α-Zr(O) entspricht. Bis etwa 9 Vol.% des UO_2 werden durch das Zry chemisch aufgelöst. In einem Brennstab muß daher mit einer vollständigen Freisetzung der flüchtigen Spaltprodukte aus diesem Brennstoffbereich gerechnet werden.

Contents

FIGURES

TABLES

1. Introduction

In hypothetical light water reactor (LWR) accidents, nuclear fuel rods may be subjected to very high temperatures for periods sufficient to cause severe fuel damage. A wide variety of scenarios can be postulated in which severe fuel damage may occur. Power-cooling imbalance conditions, for example, in which the heat generated in the fuel rod exceeds the heat removal capability of the coolant, can result in an increase in cladding temperatures at an essentially unchanged high coolant pressure. Since zircaloy (Zry) is thermodynamically unstable with respect to UO_2, chemical interactions take place between the cladding and fuel. A quantitative description of the UO_2/Zry chemical interaction as a function of temperature and time is needed to predict fuel rod behavior in severe fuel damage accidents.

Extensive out-of-pile and in-pile experiments have been performed under a variety of postulated conditions as part of a cooperative arrangement for LWR fuel rod behavior research between the Federal Ministry of Research and Technology (Federal Republic of Germany) and the Nuclear Regulatory Commission (USA) /1-8/. Out-of-pile single effects UO_2/Zry reaction experiments /1,2/ and integral rod and bundle tests /3,4/ have been performed at the Karlsruhe Nuclear Research Center as part of the German Nuclear Safety Project. The primary objectives of the out-of-pile integral rod and bundle tests are to reach cladding temperatures up to 2200°C to investigate UO_2 dissolution by liquid zircaloy, the temperature escalation due to the steam/zircaloy interaction, the influence of spacer, absorber, and control rod guide tube materials on fuel rod behavior and failure, and the fragmentation of severely embrittled fuel rods on quench /3,4/. In-pile tests performed by EG & G Idaho, Inc., in the Power Burst Facility (PBF) at the Idaho National Engineering Laboratory include an extensive series of power-cooling-mismatch tests completed in 1980 /5-8/, and a series of in-pile bundle tests currently in progress to investigate fuel rod behavior under a variety of severe fuel damage (SFD) conditions /9,10/. The primary objectives of the PBF SFD program include characterization of fuel rod damage resulting from severe cladding oxidation and melting, UO_2 dissolution and melting, and fuel rod fragmentation. The Severe Core Damage Analysis Package (SCDAP)

is being developed by EG & G Idaho for the detailed analysis of LWR fuel rod bundle behavior under severe fuel damage conditions /11/. The results of the UO_2/Zry-4 chemical interaction experiments up to the melting point of Zry-4 (~1760°C), which are presented in this paper, and the results of UO_2/Zry-4 dissolution experiments above the melting point of Zry-4 /12/ are used for the interpretation of out-of-pile and in-pile SFD test results and for the modeling of fuel rod behavior.

The reaction of UO_2 with zirconium and zirconium alloys was studied systematically and reported by Mallett et al. in 1957 /13/ and by Grossman and Rooney in 1965 /14/ at temperatures up to 1200°C. Their studies, however, were performed primarily at temperatures below 1200°C for long reaction times. Extrapolation of these results to higher temperatures and shorter reaction times has limited validity, particularly since pure zirconium and Zircaloy-2 were used in these reaction experiments rather than Zircaloy-4. In addition, solid contact between the fuel and cladding materials did not exist in all cases, and the geometry of the specimens did not correspond to that of a fuel rod in a LWR. More recently, the kinetics of the reaction at high temperatures were reported in 1979 by Hofmann and Politis /1/, who performed extensive UO_2/Zry-4 out-of-pile experiments between 900 and 1500°C in an inert atmosphere with an external overpressure for annealing times of 3 and 60 minutes, and in 1980 by Paul et al. /15/, who performed UO_2/Zry-2 experiments between 1000 and 1500°C in vacuum for times of 3 to 600 minutes. In 1983, Rosinger /16/ published results of UO_2/Zry-4 experiments performed at 1100 and 1200°C in argon at 1 bar for periods of 5 to 120 minutes, and Parsons et al. /17/ of experiments performed between 1500 and 1850°C in vacuum for times of 1 to 125 minutes. The present work describes the results of out-of-pile UO_2/Zry-4 experiments conducted from 1300 to 1700°C in an inert atmosphere with an external overpressure for annealing times of 1 to 150 minutes, and includes the results of the earlier experiments performed at 1000, 1100, and 1200°C /1/.

2. Experiment Design and Conduct

The out-of-pile UO_2/Zry-4 reaction experiments were performed in argon with short Zry-4 cladding specimens filled with stoichiometric high-density UO_2 pellets. The specimen dimensions and other important parameters are summarized in table 1. The chemical composition of the Zry-4 cladding is given in table 2. The specimens were sealed in helium at atmospheric pressure and room temperature.

A schematic of the high temperature/high pressure autoclave equipment MONA is shown in figure 1. Experiments can be performed up to a maximum temperature of about 2200°C, and a maximum pressure of 200 bar in argon or 40 bar in an argon/oxygen mixture. The specimen is contained in a high pressure vessel and inductively heated, with the cladding as susceptor. Cladding temperature is monitored continuously by pyrometer and can be measured at three different axial elevations and orientations of the specimen. In the present experiments, an infrared pyrometer calibrated against thermocouple measurements was used.

The UO_2/Zry-4 experiments were performed at temperatures from 1300 to 1700°C and reaction times from 1 to 150 minutes. Each specimen was heated at 10 K/s at atmospheric pressure up to the desired temperature, and held at this temperature for 60 seconds to allow the cladding and fuel to reach thermal equilibrium (figure 2). External pressure was applied within 2 to 3 seconds to collapse the cladding onto the fuel. The external pressure ranged from 1 to 80 bar, with the majority of the tests conducted at 40 bar. At the end of the test, the specimen was cooled under pressure at 5 K/s (figure 2). The cooldown rate was regulated to minimize the formation of cracks in the embrittled cladding, which simplified metallographic evaluation of the reaction zones.

The UO_2/Zry-4 reaction was also investigated as a function of external pressure at 1400 and 1700°C. Specimens were tested at 2, 5, 10, 20, 40, 60 and 80 bar external pressure for 10 minutes. Additional experiments were performed with tungsten foil (20 µm x 2 mm) between the cladding and fuel to determine the location of the original UO_2/Zry-4 interface. The reaction temperature ranged from 1400 to 1700°C with an annealing time of 10 minutes and an external pressure of 40 bar.

All of the specimens were examined metallographically to determine the extent of the UO_2/Zry-4 reaction. Some specimens were examined by scanning electron microscope (energy dispersive analyses) and electron microprobe (wavelength dispersive analyses) to identify the reaction products, and by Auger electron spectroscopy to determine the oxygen content of the cladding as afunction of distance from the UO_2/Zry-4 interface.

3. Experiment Results

3.1 UO_2/Zircaloy-4 Reaction Layer Description

The extent of the chemical interaction between UO_2 and Zry depends decisively on whether or not solid fuel-cladding contact exists. In the absence of direct UO_2/Zry contact, oxygen can be transported from the UO_2 to the Zry via the gas phase only. With no external pressure, no UO_2/Zry reaction layers have been observed up to 1500°C since no contact existed /1/. Above 1500°C, localized fuel cladding contact always occurs due to the greater thermal expansion of the fuel than of the cladding, which causes the fuel-cladding gap to close. With sufficient external pressure, the cladding collapses completely onto the fuel pellets and solid UO_2/Zry contact exists. Under these conditions, the chemical interaction between UO_2 and Zry is circumferentially and axially very uniform. Zircaloy reduces UO_2 (to UO_{2-x}) to form metallic oxygen-stabilized α-Zr(O) and uranium metal. The uranium reacts only with zirconium low in oxygen and therefore penetrates and/or diffuses into the cladding to form a (U,Zr) alloy rich in uranium. The (U,Zr) alloy lies between two oxygen-stabilized α-Zr(O) layers and is liquid above about 1150°C, depending on the Zr content. The α-Zr(O) layer adjacent to the fuel contains small amounts of the (U,Zr) alloy, primarily along grain boundaries. The α-Zr(O) layer adjacent to the β-Zry region contains no (U,Zr) alloy. During cooldown of the specimen, the hypostoichiometric UO_{2-x} decomposes into stoichiometric $UO_{2.00}$ and additional metallic uranium. The sequence of the individual reaction layers from the fuel to the cladding outside surface at room temperature is:

$$[UO_2 + U] \rightarrow [\alpha\text{-Zr(O)}_a + (U,Zr)] \rightarrow (U,Zr) \rightarrow \alpha\text{-Zr(O)}_b \rightarrow \text{prior}^{*}\ \beta\text{-Zry}$$

which are shown schematically in figure 3. In general, the number of reaction layers and their sequence is the same for all temperatures and reaction times.

Optical photomicrographs of a typical specimen (1600°C for 3 minutes) are shown in figure 4 in the as-polished condition (bright field), and

* During the experiment, this portion of the cladding was β-phase, and on cooldown transformed into α-phase. At room temperature, it is therefore referred to as prior β-Zry.

after oxidation in air (both bright field and polarized light). In the as-polished photomicrograph, metallic U and Zr inclusions are visible in the UO_2 matrix as shiny particles. In air, the metallic U and the U in the (U,Zr) alloy oxidize readily to UO_2, and the Zr remains metallic. Comparison of the as-polished and oxidized-in-air photomicrographs thus shows the amount of Zr which has diffused into the UO_2 ahead of the $UO_2/\alpha\text{-Zr(O)}_a$ reaction interface. The $\{\alpha\text{-Zr(O)}_a + (U,Zr)\}$ and (U,Zr) reaction layers and interfaces are easily recognized after the U has oxidized in air. The $\alpha\text{-Zr(O)}_b$ interface with the relatively unreacted portion of the cladding is not visible in bright field and is therefore examined in polarized light. The extent of the reaction differs greatly, increasing with increasing temperature and time. The dependence of the reaction on temperature at 1400, 1500, 1600, and 1700°C after 10 minutes is shown in polarized light in figure 5. The dependence of the reaction on time at 1600°C for 3, 6, 10, and 20 minutes is shown in bright field (oxidized in air) in figure 6.

The overall distributions of U and Zr at the $UO_2/\alpha\text{-Zr(O)}_a$ interface are shown in electron microprobe (EMP) photographs in figure 7 (1600°C for 10 minutes). In the fuel region, metallic uranium and zirconium particles are clearly apparent, and are shown in more detail in scanning electron microscope (SEM) photographs in figure 8 (1700°C for 10 minutes). The U particles (which contain some Zr) are designated U(Zr), and the Zr particles (which contain some O) are designated Zr(O). Uranium particles are evident across the entire pellet cross section, with a much higher concentration of U near the $UO_2/\alpha\text{-Zr(O)}_a$ interface. At the interface (figure 9), some UO_2 grains are completely surrounded by metallic U and have been chemically dissolved to varying extents by Zr. At longer times this process is more pronounced. The U does not remain at the interface. It penetrates (as a liquid) along the $\alpha\text{-Zr(O)}_a$ grain boundaries (and, to a small extent, probably diffuses through the $\alpha\text{-Zr(O)}_a$ matrix) into the cladding to form the (U,Zr) layer or globules. Figure 8 clearly shows that Zr diffuses or penetrates into the UO_2. The extent of Zr diffusion depends on temperature and time, and Zr has been observed up to ∿500 μm from the $UO_2/\alpha\text{-Zr(O)}_a$ interface. The amount of Zr in the fuel decreases rapidly with increasing distance from the interface.

The {α-Zr(O)$_a$ + (U,Zr)} layer (figures 4, 5, and 6) is made up of relatively small, radially elongated α-Zr(O) grains (compared to the α-Zr(O)$_b$ grains). The (U,Zr) alloy is present along the grain boundaries as "stringers" and as small globules within the grains, with some U dissolved in the α-Zr(O) matrix. The results of the tungsten marker experiments show that the original UO_2/Zry-4 interface lies between the {α-Zr(O)$_a$ + (U,Zr)} and (U,Zr) layers* (figure 10). In the figure, one edge of the tungsten foil is clearly shown in the upper right hand photograph. As is evident in the upper left hand photograph, the position of the foil corresponds to the {α-Zr(O)$_a$ + (U,Zr)}/(U,Zr) interface. The {α-Zr(O)$_a$+ (U,Zr)} layer therefore forms in the fuel region. Metallic U then penetrates and/or diffuses into the α-Zr(O), primarily along grain boundaries, to interact with oxygen-poor Zr. The interfaces with UO_2 and with the (U,Zr) layer are quite distinct.

The (U,Zr) alloy layer, which consists primarily of uranium and contains almost no oxygen, is liquid above about 1150°C, depending on the Zr content. Up to about 1400°C, the (U,Zr) alloy forms as a uniform, closed layer between two α-Zr(O) layers (figure 11). After very long annealing times, the (U,Zr) layer is transformed into many small spherical particles (figure 11). At 1500°C and above, large globules of (U,Zr) alloy form within the α-Zr(O)$_b$ layer (figure 12). After short annealing times, small α-Zr(O) platelets are present at the edges of the (U,Zr) globules. With increasing time, the α-Zr(O) platelets (which contain some U) grow in size, consuming large portions of the (U,Zr) globules (figure 12). The formation of small spherical particles at lower temperatures and large globules at higher temperatures may be due to the change in interfacial energy between the liquid (U,Zr) alloy and the α-Zr(O)$_b$ matrix, which is determined by the O and Zr contents of the (U,Zr) alloy and by the O content of, and gradient across, the surrounding α-Zr(O)$_b$ phase /18/.

---

* Tungsten marker experiments were performed by Hofmann and Politis in the earlier experiment series /1/, and the original UO_2/Zry-4 interface was determined to lie between the (U,Zr) alloy and the α-Zr(O)$_b$ layers. At that time, relatively few marker experiments were conducted, with varying results. In the present work, several experiments were performed and the results clearly show that the original interface lies between the {α-Zr(O)$_a$ + (U,Zr)} and (U,Zr) alloy layers (figure 10).

The α-Zr(O)$_b$ layer is made up of large α-Zr(O) grains (figures 4, 5 and 6). In contrast to the α-Zr(O)$_a$ layer, it contains no (U,Zr) alloy along the grain boundaries and, in general, no U in the matrix. The boundary between the α-Zr(O)$_b$ layer and the remainder of the cladding (prior β-zircaloy) is generally distinct, but can be very irregular in places where large α-Zr(O) incursions extend into the prior β-zircaloy. The cladding is severely embrittled when the thickness of the total reaction zone is large compared to the thickness of the remaining Zry-4. After 10 minutes at 1700°C (figure 5), and 20 minutes at 1600°C (figure 6), the cladding is completely embrittled. That is, the α-Zr(O)$_b$ region extends to the outside surface of the cladding. On cooldown, the severely embrittled cladding fractures in many places throughout the α-Zr(O)$_b$ layer (figures 4, 5, and 6).

3.2 UO_2/Zry-4 Measured Reaction Zone Thickness

The essential objective of the UO_2/Zry-4 reaction experiments is a quantitative analytical description of the chemical interaction. It is therefore necessary to determine the thickness of the various reaction zones as functions of temperature and time. As shown in figure 3, Zone I is defined as the thickness of the {α-Zr(O$_a$ + (U,Zr)} layer, Zone II as the thickness of Zone I plus that of the (U,Zr) alloy layer, and Zone III as the thickness of Zone II plus that of the α-Zr(O)$_b$ layer.

The individual reaction zone thicknesses were measured directly with an optical microscope or from photomicrographs at a minimum of sixteen orientations on each sample. The average and standard deviation were calculated for each reaction zone of each specimen and are given in table 3. The standard deviation of the zone II values tended to be the largest, particularly at 1500°C and above, because of large variations in the size of the globules. Two test series were performed at 1600°C and 2 additional samples were tested at 1700°C (table 3) due to the relatively large uncertainty in temperature measurements at very high temperatures. The results show good agreement. The tungsten marker specimens were evaluated at azimuthal locations away from the tungsten foil and the results are included in table 3.

As a result of the external overpressure, some of the liquid (U,Zr) alloy may flow into the dishing volumes in the fuel stack. In figure 13, a longitudinal section of a specimen tested at 1700°C for 60 minutes is shown. All three pellet interfaces are filled with (U,Zr) alloy, shown at higher magnification on the right. It should be emphasized, therefore, that the thickness of the (U,Zr) "layer" corresponds only approximately to the actual amount of (U,Zr) alloy formed during the UO_2/Zry-4 interaction. In addition, due to the globule formation of the (U,Zr) alloy at and above 1500°C, the (U,Zr) layer thickness was arbitrarily defined and actually contains some α-Zr(O)$_b$.

3.3 UO_2/Zry-4 Reaction Kinetics

The chemical interaction between UO_2 and Zry-4 is a diffusion-controlled process. The reaction obeys a parabolic rate law. The reaction zone thicknesses are therefore plotted versus the square root of time at 1300, 1400, 1500, 1600, and 1700°C in figures 14 through 18, respectively. A linear regression using the method of least squares was performed for each reaction zone at each temperature. All of the data corresponding to parabolic reaction kinetics (up to but not including the plateau) for each zone at each temperature was used for each regression. For simplicity, only the average values with uncertainty bands of $\pm 1\sigma$ for each zone at each reaction time are shown in the figures. Since the reaction zones have zero thickness at time zero, the y-intercept in all cases is zero. The calculated regression constants (slopes of the lines) and standard errors of estimate are given in table 4. The total reaction zone thickness is plotted versus the square root of time for all test temperatures in figure 19.

The affinity of zirconium for oxygen, which results in an oxygen gradient across the cladding, is the driving force for the UO_2/Zry-4 reaction. Therefore, as the cladding becomes saturated with oxygen, the parabolic dependence of the reaction zone thickness on time ceases. Once the α-Zr(O)$_b$ layer has reached the outside surface of the cladding, the thicknesses of the individual reaction zones remain essentially constant with increasing time, although the total oxygen content of the cladding

continues to increase. The $Zr-ZrO_2$ phase diagram is shown in figure 20. The O content of α-Zr(O) varies between 2.1 and 6.7 wt.% at 1300°C, and 3.5 and 7.6 wt.% at 1700°C. Thus, a small increase in the thickness of the cladding may occur after the $\alpha\text{-Zr(O)}_b$ layer has reached the cladding outside surface due to the additional uptake of O up to saturation of the $\alpha\text{-Zr(O)}_b$ phase. The $\alpha\text{-Zr(O)}_b$ layer reached the cladding outside surface after approximately 70 minutes at 1400°C, 30 minutes at 1500°C, 12 minutes at 1600°C, and 6 minutes at 1700°C (figures 15 through 18). The maximum measured O content (from AES analyses) was 6.5 wt.% O after 100 minutes at 1600°C (see Section 3.4).

The total reaction zone reached a maximum thickness of about 870 μm for all temperatures, which compares to an original cladding wall thickness of 725 μm. This increase in thickness is due primarily to the penetration of liquid U into the cladding to form the (U,Zr) layer or globules. In figures 15 through 18, after the plateau has been reached, the thickness of the (U,Zr) layer ranges from 90 to 150 μm. The cladding thickness also increases due to the collapse of the cladding onto the fuel pellet (up to 45 μm) and, to a lesser extent, due to the small volume increase which accompanies the uptake of oxygen by zircaloy to form α-Zr(O).

The depth of oxygen diffusion into the cladding from the original UO_2/Zry-4 interface, in addition to the growth of the individual reaction zones, is also important for predicting fuel rod behavior. As mentioned in the previous section, the tungsten marker experiments showed that the original interface lies between the $\{\alpha\text{-Zr(O)}_a + \text{(U,Zr)}\}$ and the (U,Zr) layers (figure 10). Diameter measurements across the specimens from the different reaction layer interfaces showed that the diameter of the $\{\alpha\text{-Zr(O)}_a + \text{(U,Zr)}\}$ / (U,Zr) interface is approximately constant with both increasing time and temperature (figures 21 and 22, respectively) which also indicates that this is the position of the original interface. Therefore, the thickness of Zone I was subtracted from the total reaction zone thickness (Zone III) to obtain an adjusted reaction zone thickness. The calculated regression constants and standard errors of estimate are given in table 4.

Reaction zone growth rate is plotted versus reciprocal temperature in an Arrhenius diagram in figure 23 for each reaction zone. All of the data corresponding to parabolic reaction kinetics for each zone at each temperature was used to perform each regression. The following analytical expressions were calculated:

$x^2/t = 5.50 \exp(-57{,}700/RT)$ (1) Zone I

$x^2/t = 0.707 \exp(-50{,}100/RT)$ (2) Zone II ($\leq 1400^{\circ}C$)

$x^2/t = 1.62 \exp(-45{,}200/RT)$ (3) Zone III

$x^2/t = 0.259 \exp(-41{,}300/RT)$ (4) Zone III - Zone I (adjusted with respect to position of original UO_2/Zry-4 interface)

where the growth rate coefficient x^2/t is in cm^2/s, R is 1.987 cal/mol-K, and T is in K. Ninety-five percent confidence limits for the predicted values and standard errors of estimate for each equation and for the individual coefficients (intercept and activation energy) were determined. Details of the calculations are presented in the appendix.

The equation for Zone II is only valid up to $1400^{\circ}C$. From 1000 to $1400^{\circ}C$, the (U,Zr) layer is a uniform,closed layer between the two α-Zr(O) layers (figure 3,11). At $1500^{\circ}C$ and above, because of the large globules of (U,Zr) which form within the $\alpha\text{-Zr(O)}_b$ layer (figure 12), an arbitrary (U,Zr) layer thickness was defined which contains some $\alpha\text{-Zr(O)}_b$. This data was therefore not included in the Zone II regression. Also, since the (U,Zr) alloy is liquid above $1150^{\circ}C$, the formation of this layer is not strictly a diffusion-controlled process. In theory, therefore, it is not correct to represent the growth of this layer in an Arrhenius diagram.

The total and adjusted growth rate equations are compared to UO_2/Zr, UO_2/Zry-2, and steam/Zry-4 results from the literature in figure 24 and in table 5. Mallett et al. /13/ examined the UO_2/Zr interaction up to $1100^{\circ}C$, and the activation energy of 37,000 kcal/mol is somewhat lower than our result of 45,200 kcal/mol for the growth of the total reaction zone (Zone III). Grossman and Rooney /14/ studied the UO_2/Zry-2 interaction up to $1300^{\circ}C$, and Paul et al. /15/ up to $1500^{\circ}C$. The activation energies from the two studies are very similar (50,000 and 47,540 kcal/mol, respectively) and somewhat higher than our result. The steam/Zry-4 results of six investi-

gations (growth of the α-Zr(O) + ZrO_2 double layer) are shown as a region in figure 24 /19-24/. Note that the adjusted growth rate curve (Zone III - Zone I) lies below this region, but the total growth rate curve overlaps the steam/Zry-4 region above about 1100°C. That is, the UO_2/Zry-4 reaction occurs as rapidly as the steam/Zry-4 reaction above about 1100°C.

3.4 O, Zr, and U Contents of the Reaction Layers

The O, Zr, and U contents of the individual reaction layers were determined by Auger electron spectroscopy (AES) and electron microprobe (EMP) analyses of specimens tested at 1500, 1600, and 1700°C. Concentrations of lighter elements, e.g., oxygen, can be determined very accurately by AES analysis using suitable standards, and of heavier elements, e.g., Zr and U, more accurately by EMP analysis using suitable standards and correction factors.

Of particular importance with respect to cladding embrittlement are the maximum O content and the O distribution across the cladding as functions of temperature and time. The AES and EMP results for the $\alpha\text{-Zr(O)}_a$ and $\alpha\text{-Zr(O)}_b$ matrices (the (U,Zr) alloy contains very little or no O) are presented and compared in table 6. The uncertainty* in O content from AES analysis of all reaction zones is less than ±0.5 wt.%. The uncertainties in Zr and U content from AES analysis of the α-Zr(O) matrices are somewhat larger. The uncertainties in the AES results are described in detail in Reference 25. The Sn content was not determined. The uncertainties in Zr, U, and Sn contents from EMP analysis of the α-Zr(O) matrices are ±3.0, ±0.2, and ±0.1 wt.%, respectively. The O content was determined by difference {100 wt.% - (Zr + U + Sn contents)} and has an uncertainty of ±3.0 wt.%. The agreement between the AES and EMP results is excellent.

EMP results of a specimen tested for 6 minutes at 1500°C are shown graphically in figure 25, with Zr and U contents in each of the reaction layers plotted as functions of distance from the $UO_2/\alpha\text{-Zr(O)}_a$ interface. In the $\{\alpha\text{-Zr(O)}_a + \text{(U,Zr)}\}$ region, the results for the $\alpha\text{-Zr(O)}_a$ matrix and the (U,Zr) stringers are plotted separately.

---

* All uncertainties are ±3σ.

The AES results of four specimens tested for 6, 30, 100, and 150 minutes at 1500°C are shown in figure 26, of three specimens tested for 3, 20, and 100 minutes at 1600°C in figure 27, and of three specimens tested for 3, 10, and 60 minutes at 1700°C in figure 28. (The complete AES results for all specimens examined are published in Reference 25.) The O and U content in the α-Zr(O)$_a$, α-Zr(O)$_b$, and prior β-Zry matrices are plotted as functions of distance from the UO_2/α-Zr(O)$_a$ interface at the top of each figure, with Zr, O, and U elemental distribution maps below. The compositions of the α-Zr(O)$_a$, α-Zr(O)$_b$, and prior β-Zry matrices as determined from both AES and EMP analyses can be described as follows:

- Initially, an O gradient exists across the zircaloy from the UO_2 to the cladding outside surface (with an O minimum in the (U,Zr) region). With increasing time, the O gradient across the cladding levels off and the total O content of the cladding increases up to a maximum of about 6 wt.%.
- The O concentration profile across the α-Zr(O)$_a$ layer is relatively flat for annealing times of 3 minutes or more. The matrix contains up to 10 wt.% U (with an average value of about 6 wt.%) and up to 1.6 wt.% Sn. The overall composition of α-Zr(O)$_a$ remains relatively constant with increasing time. With the exception of very long annealing times, the Sn content is always less than in the α-Zr(O)$_b$ matrix.
- The O concentration profile across the α-Zr(O)$_b$ layer is also relatively flat, and drops rather abruptly at the α-Zr(O)$_b$/prior β-Zry interface. The matrix contains up to about 6 wt.% O (although in general slightly less than the α-Zr(O)$_a$ matrix), no U (in general), and up to 1.6 wt.% Sn. After very long annealing times, the O contents of the two α-Zr(O) matrices are about equal and, near the (U,Zr) globules, the α-Zr(O)$_b$ matrix also contains up to about 6 wt.% U.
- The prior β-Zry matrix contains up to 3 wt.% O and up to 1.6 wt.% Sn (which corresponds to the initial Sn content of Zry-4). In no case does the matrix contain U, even after very long annealing times.

The O, Zr, and U contents of the uranium-rich (U,Zr) alloy regions were also determined by AES and EMP analyses. Unfortunately, discrepancies exist between the two sets of measurements for many different specimens. The AES results show much higher O and Zr contents in the alloy (up to 5 wt.% O and up to 55 wt.% Zr) than the EMP results (no O and up to 35 wt.% Zr), especially in the stringers. The width of the electron beam used in the

AES measurements was relatively large (4 μm), and in the EMP measurements much smaller (0.1 to 1.0 μm). The stringers are on the average about 0.5 μm wide, with globules up to about 10 μm in diameter. Therefore, one possible explanation for the discrepancy between the AES and EMP results in the stringers is that the AES beam analysed a portion of the surrounding α-Zr(O)$_a$ matrix, resulting in erroneously large O and Zr contents. Since EMP analysis gives in general more accurate results for heavier elements, the EMP results are presented alone in table 7. (The AES results are shown graphically in the lower portions of figures 26, 27 and 28). The uncertainties in Zr, U and Sn contents from EMP analyses of the (U,Zr) alloy are ±1.1, ±3.0 and ±0.1 wt.%, respectively. The O content was determined by difference {100 wt.% - (Zr + U + Sn contents)} and has an uncertainty of ±3.2 wt.%. The compositions of the U-rich metallic phase in the UO_2 near the UO_2/α-Zr(O)$_a$ interface, the (U,Zr) stringers in the α-Zr(O)$_a$ layer, and the (U,Zr) layer and/or globules as determined by EMP analysis can be described as follows:

- In general, the uranium-rich (U,Zr) metallic phases contain no O and no Sn.
- In the fuel near the UO_2/α-Zr(O)$_a$ interface, metallic U particles containing small amounts of Zr (up to about 2 wt.%) are present.
- The (U,Zr) alloy stringers and particles in the α-Zr(O)$_a$ matrix contain slightly more Zr (up to about 5 wt.%). With increasing time, the Zr content decreases and the U content increases correspondingly. No Zr or U concentration gradients are evident in this region.
- The (U,Zr) alloy layer or globules contain up to 35 wt.% Zr and up to 1 wt.% Sn after very short annealing times. With increasing time (and increasing O content of the surrounding α-Zr(O) matrix), the Zr content decreases to a minimum of about 3 wt.% as the Zr reacts with O to form additional α-Zr(O) along the edges of the globules (figure 12), and the U content increases correspondingly. The Sn content in the (U,Zr) alloy decreases to zero as the Sn reacts with Zr to form a Zr-rich (Zr,Sn) alloy at the edges of and in some cases within the globules. The (Zr,Sn) alloy contains up to 15 wt.% Sn.

- After very long annealing times, the compositions of all of the (U,Zr) alloy phases across the entire oxidized cladding cross section are very similar (no oxygen, 2 to 3 wt.% Zr, 97 to 98 wt.% U, and no Sn).

With increasing temperature, the phenomena and tendencies described above for all of the α-Zr(O) and (U,Zr) alloy phases are accelerated. For example, at 1500°C the cladding is saturated with O after about 60 minutes, and at 1600°C after about 30 minutes.

After very long annealing times at high temperatures, the compositions of the (U,Zr) globules and of the surrounding α-Zr(O)$_b$ matrix become more complex. EMP results of a specimen tested at 1600°C for 100 minutes are shown in figure 29. The globule is made up of (U,Zr) alloy regions within a lattice rich in O, Fe, and Cr, and is surrounded by a Sn-rich layer. (The O-, Fe-, and Cr-rich lattice and Sn-rich border were also observed in globules of specimens tested at 1500°C for 100 and 150 minutes). Above the globule is an isolated (U,Zr)O_2 ceramic particle. The α-Zr(O)$_b$ near the globule contains about 5 wt.% U (see also figures 26,27, 28). Uranium was found in the α-Zr(O)$_b$ matrix near the (U,Zr) globules in several specimens tested for very long annealing times. When the cladding is completely saturated with O, i.e., an O gradient is no longer present, the Zr in the (U,Zr) alloy preferentially reacts with O from the surrounding α-Zr(O) matrix to form additional α-Zr(O) (figure 12), and the U content of the remaining (U,Zr) alloy increases. The movement of Zr and U within the globules is probably very rapid since the (U,Zr) alloy is a liquid at test temperatures. The composition of the additional α-Zr(O) (or prior (U,Zr) alloy) which forms is very similar to that of the α-Zr(O)$_a$ matrix (up to 6 wt.% each of O and U).

The (U,Zr) alloy is liquid above about 1150°C and may flow into the dishing volumes between pellets (and into cracks and open porosity) due to the external overpressure (figure 13). AES analyses were performed on this material from the specimen tested at 1700°C for 60 minutes (figure 30). In close contact with UO_2, Zr from the (U,Zr) alloy reacts with O from the UO_2 to form a thin homogeneous layer of α-Zr(O). In some cases, α-Zr(O) incursions

extend into the (U,Zr) region. The compositions of the α-Zr(O) and (U,Zr) phases are included in tables 6 and 7. The α-Zr(O) phase contains 3 to 5 wt.% O and 6 to 10 wt.% U. The (U,Zr) phase contains no O, about 4 wt.% Zr, and is predominately a single phase. Some second-phase particles with a higher Zr content are also present in the (U,Zr) region. Some of the Zr(O) which was observed within the UO_2 near the fuel/cladding interface may have formed by a similar process, i.e., the liquid (U,Zr) penetrated along connected pores into the UO_2 pellet and the Zr interacted with the UO_2 to form α-Zr(O) within the fuel region.

3.5 UO_2/Zry-4 Chemical Interaction as a Function of External Pressure

The influence of external pressure (1 to 80 bar) on the UO_2/Zry-4 interaction under non-oxidizing conditions was investigated at 1400 and 1700°C. In figure 31, reaction zone thickness is plotted versus pressure for the three reaction zones at 1400 and 1700°C. At 1400°C, the interaction is independent of external pressure above about 10 bar, and at 1700°C above about 5 bar. Internal pressure at room temperature was 1 bar, which corresponds to 5.6 bar at 1400°C and 6.6 bar at 1700°C, assuming constant internal volume. The actual internal pressure at test temperatures is difficult to calculate because the internal volume at temperature is not easily determined. However, the internal pressures were probably somewhat higher than 5.6 and 6.6 bar since the internal volume decreases with increasing temperature due to the greater thermal expansion of the fuel than of the cladding. The significance of these results is that at 1400°C a minimum differential pressure of approximately 5 bar is required for good UO_2/Zry contact and uniform reaction layer formation. At 1700°C, the interaction is independent of differential pressure in the examined range of 1 to 80 bar. That is, differential thermal expansion of the fuel and cladding alone is sufficient for good fuel/cladding contact. At very low external pressures where the fuel/cladding contact was not good, many pores were observed in the $\alpha\text{-Zr(O)}_a$ phase near the UO_2 interface.

3.6 Uncertainties

Random variations in the reaction zone thicknesses were principally caused by uncertainties in the measurements of: (a) reaction zone thickness, (b)

reaction time, and (c) reaction temperature (calibration error and reproducibility). The equations describing the data are presented with 95% confidence limits in the appendix, which indicate the portion of the data variation not explained by the diffusion-based model. Probable and possible sources of error in the data-taking process and the adequacy of the assumed model are discussed below.

Variations in reaction zone thickness were quantified by performing a number of measurements (at least 16) for each reaction zone of each specimen. For each specimen, the variability was characterized by calculating the standard deviation (1σ) for each reaction zone thickness, as shown in figures 14 through 18 and given in table 3. The Zone I interfaces were uniform and well-defined, and in most cases $\pm 1\sigma$ for Zone I was less than ± 10 μm. The Zone II interfaces at 1300 and 1400°C were also uniform and well-defined, except after very long annealing times, and in most cases $\pm 1\sigma$ was less than ± 10 μm. However, at 1500, 1600, and 1700°C, the variation in Zone II values was larger due to the globule formation of the (U,Zr) layer and the irregularity of the (U,Zr)/α-Zr(O)$_b$ interface (figure 6). One standard deviation for Zone II at the higher temperatures was, in general, 60 μm or less. The Zone III interfaces were relatively uniform but in several cases large incursions of α-Zr(O) extended into the prior β-Zry region, making it difficult to define this interface. One standard deviation for Zone III was, in general, 30 μm or less.

The uncertainty associated with performing the thickness measurements was estimated to be ± 10 μm ($\pm 3\sigma$). This uncertainty includes the resolution limit of the optical microscope and the ability of the operator to align the specimen. This error is small compared to the sources discussed below.

The uncertainty in reaction time arises from the heatup and cooldown periods, during which additional UO_2/Zry-4 reaction may occur. As shown in figure 2, heatup and thermal equilibration were performed without external pressure, preventing (in most cases) any fuel/cladding interaction. Localized contact did occur at 1500°C and above, even without external pressure, due to the greater thermal expansion of the fuel than of the cladding. At 1600°C,

therefore, the maximum additional reaction time due to heatup was (100°C ÷ 10 K/s + 60 s) = 70 s and at 1700°C, 80 s. However, the extent of the reaction during this time was probably limited since uniform fuel/cladding contact did not exist. Cooldown was performed at 5 K/s under pressure (figure 2). Substantial additional fuel/cladding interaction probably occurred within the first 200°C of cooldown. Therefore, the maximum additional reaction time due to cooldown was (200°C ÷ 5 K/s) = 40 s. Up to and including 1500°C, the maximum total error in reaction time was thus +40 s. This error is small for reaction times of 3 minutes or more. Above 1500°C, the maximum total error was +120 s, which becomes significant at the shorter reaction times. However, this estimate seems to be somewhat large since shifting all of the data points at 1600 and 1700°C (figures 17 and 18) 120 s to the right results in substantial negative reaction zone thicknesses at time zero. From the data in figures 17 and 18, it appears that only the specimens tested for 1 minute have a noticeable error, indicating that the total error in reaction time at high temperatures is probably closer to +60 s than +120 s.

The uncertainty in reaction temperature is by far the largest and most difficult to quantify. The uncertainty arises in calibrating the emissivity (which is actually measured) against temperature (the desired result). The calibration was performed by direct comparison of thermocouple-measured temperatures and infrared pyrometer-measured emissivities. The thermocouples were Pt-10% Rh/Pt with an uncertainty of ±(0.5% T) from 700 to 1700°C, as given by the manufacturer. The calibration was performed at 1300 and 1400°C, at which the thermocouple has an uncertainty of ±7°C. All of the temperatures determined by pyrometer measurements above 1400°C were therefore extrapolations of the calibration curve. Emissivity is a function of the temperature of the material, the wavelength of the radiation, and the chemical composition of the material. Emissivity also varies depending on the radiation direction and the material surface condition. All of these factors contribute to the uncertainty in the emissivity measurement. However, several factors indicate that the temperature measurement was relatively good. First, related experiments performed recently in a different apparatus showed that the melting point of Zry-4 is 1760 ± 30°C /26/. Cladding melting was observed in several specimens tested at 1750°C in MONA but in none of the specimens tested at 1700°C. Second, the results at 1500 and 1600°C are reasonably spaced with respect to the results at 1400 (the upper limit of the thermocouple calibration) and 1700°C (figure 19).

Third, the two test series performed at 1600°C showed good repeatability. Therefore, the temperature uncertainty is estimated to be ± 30°C.

The equations developed to describe the data (Eqs. 1,2,3,4) assume that the UO_2/Zry-4 interaction can be modelled by considering only the diffusion of oxygen into the cladding. However, although oxygen diffusion is the predominant force for the reaction, other phenomena may be important as well. For example, the liquid (U,Zr) alloy may flow into the dishing volumes between pellets and into pellet cracks and open porosity due to the external overpressure. The observed amount of (U,Zr) alloy was probably less than the amount actually formed during the reaction. In addition, the irregularity of the (U,Zr)/α-Zr(O)$_b$ interface at high temperatures and definition of a (U,Zr) "layer" resulted in errors in the Zone II values. Since the maximum extents of the globules were measured and no attempt was made to convert the actual globule area into a layer thickness, the (U,Zr) "layer" actually contains some α-Zr(O)$_b$. That is, the reported Zone II thicknesses at high temperatures are too large. The 95% confidence limits given in the appendix for the growth rate equations therefore contain contributions from stochastic processes affecting the experimental data and physical phenomena not considered by the assumed model.

4. Discussion

4.1 UO_2/Zry-4 Chemical Interaction Phenomena

The chemical interaction between UO_2 and Zry-4 results in the following individual reaction layers at room temperature:

$$[UO_2 + U] \rightarrow [\alpha\text{-Zr(O)}_a + (U,Zr)] \rightarrow (U,Zr) \rightarrow \alpha\text{-Zr(O)}_b \rightarrow \text{prior } \beta\text{-Zry}$$

which are shown in schematically in figure 3. In general, the number of reaction layers and their sequence is the same for all temperatures and reaction times.

Metallic U has been observed in the fuel across the entire pellet cross section, with a much higher concentration of U near the $UO_2/\alpha\text{-}Zr(O)_a$ interface (figure 8). At the pellet center, most of the U forms during cooldown as hypostoichiometric UO_{2-x} decomposes into stoichiometric $UO_{2.00}$ and elemental U (figure 32). Near the interface, a large part of the U forms at temperature due to the reduction of UO_2 below the $UO_{2-x}/(UO_{2-x} + U)$ phase boundary. As Zry takes up O and reduces the UO_2 to UO_{2-x} at high temperatures, the fuel region remains a single phase (figure 32) until the $UO_{2-x}/(UO_{2-x} + U)$ phase boundary is reached (O/U = 1.92 at 1700°C). Reduction of the fuel below the phase boundary results in the formation of U in the fuel region at test temperatures, particularly near the fuel/cladding interface due to the diffusion of Zr into the UO_2.

Metallic Zr particles containing some O have also been observed in the fuel up to about 500 µm from the $UO_2/\alpha\text{-}Zr(O)_a$ interface (figure 8). Elemental Zr clearly diffuses or penetrates into the UO_2 ahead of the reaction interface. Therefore, the interface region has to be treated as a ternary system. Only ternary diffusion couples can result in the formation of two-phase zones /27/.

The $\alpha\text{-}Zr(O)_a$ layer forms by diffusion of O into the cladding. The fuel is chemically dissolved by Zry to form metallic α-Zr(O) and elemental U. The U does not remain at the $UO_2/\alpha\text{-}Zr(O)_a$ interface. It penetrates as a liquid along the $\alpha\text{-}Zr(O)_a$ grain boundaries into the cladding to interact with O-poor Zr and form a (U,Zr) alloy. The (U,Zr) alloy is present in small amounts (up to about 10% of the area) along the $\alpha\text{-}Zr(O)_a$ grain boundaries and as small globules wihtin the $\alpha\text{-}Zr(O)_a$ grains. No pronounced composition gradients in the alloy as a function of distance from the reaction interface were found. The $\alpha\text{-}Zr(O)_a$ matrix itself contains elemental U (up to about 6 wt.%). In specimens tested at higher temperatures (1500°C and above), some of the U is present at room temperature as very small, homogeneously distributed inclusions (figure 33). The number of inclusions increases with increasing temperature. The α-Zr(O) can dissolve a small amount of U at high temperatures to form a homogeneous solid solution of

Zr, O, and U, and on cooling, metallic U may precipitate in the matrix /1/. At lower temperatures (1300 and 1400°C), U precipitates have not been observed in the α-Zr(O) matrix (although U is present in the matrix), even after very long annealing times (figure 34), which indicates that the solubility limit of U in α-Zr(O) was not exceeded. No gradients in U content of the $\alpha\text{-Zr(O)}_a$ matrix as a function of distance from the reaction interface were found. At the lowest temperatures (1200°C and below), no U is present in the matrix.

The appearance and composition of the (U,Zr) layer and globules change substantially with increasing temperature and reaction time. Up to about 1400°C, the (U,Zr) alloy forms initially as a uniform, closed layer between the two α-Zr(O) layers. At 1500°C and above, large globules of (U,Zr) alloy form within the $\alpha\text{-Zr(O)}_b$ layer. As the cladding becomes saturated with O (with increasing time), the Zr in the (U,Zr) alloy, which has a greater affinity for O than for U, begins to react with O from the surrounding α-Zr(O) matrix to form additional α-Zr(O). The U content of the (U,Zr) alloy therefore increases with increasing time, and the Zr content decreases. At lower temperatures (1300 and 1400°C) after very long annealing times, the (U,Zr) layer is transformed into many small spherical particles (figure 11), which is probably the result of two processes: (a) the growth of additional α-Zr(O) into the (U,Zr) region, isolating portions of the liquid alloy, and (b) the tendency of the U-rich alloy to form spheres to reduce its interfacial energy with respect to the surrounding α-Zr(O) matrix /18/. At higher temperatures (1500°C and above) after long annealing times, the additional α-Zr(O) consumes large portions of the (U,Zr) globules (figure 12), leaving a complex structure of (U,Zr) alloy and Zry-4 alloying elements (Sn, Fe, and Cr) (figure 29). At the lowest temperatures (1200°C and below), the growth of additional α-Zr(O) into the (U,Zr) region after long annealing times was not observed. At these temperatures, the reaction kinetics are relatively slow and the examined reaction times (up to 60 minutes) were not long enough for the cladding to become saturated with oxygen /1/.

Wetting behavior studies of the U/Zry-4 and U/α-Zr(O) systems have shown that the wettability of Zry by liquid U worsens with increasing O content of the Zry. That is, a U-rich (U,Zr) alloy or metallic U wets O-poor Zry much better than α-Zr(O). Therefore, as the O content of the cladding increases, the (U,Zr) alloy will preferentially take on a spherical or globular shape to reduce its surface area, and thereby minimize the integral interfacial energy of the system /18/.

The compositions of the (U,Zr) globules at 1500°C and above range from about 65 wt.% U and 35 wt.% Zr after short annealing times to about 97 wt.% U and 3 wt.% Zr after long annealing times. The U-Zr phase diagram is shown in figure 35. The compositions of the globules all lie in the two-phase (α-U + δ) region at room temperature. The α-U phase contains 99 wt.% U and 1 wt.% Zr and the δ phase contains 49 to 57 wt.% U and 43 to 51 wt.% Zr (at room temperature). It is reasonable, therefore, that the range in composition of the (U,Zr) alloy under non-equilibrium conditions lies between the α-U and δ phase compositions. At higher temperatures, up to the solidus line in figure 35, U and Zr are completely miscible (isomorphous system). At the higher Zr contents (30 to 35 wt.%) for the test temperatures examined (1300 to 1700°C), the alloy can range from solid to partially liquid to completely liquid. At the lower Zr contents, the alloy is completely liquid at all examined temperatures and times. (It should be emphasized that the phase diagram has not been precisely determined - the dashed curves in figure 35 indicate that the phase boundaries have not been reliably established - and only represents equilibirum conditions which, in general, were not the case for these specimens. There is a great deal of discussion in the literature about whether the δ phase is a metastable or stable intermediate phase /28/.)

The $\alpha\text{-Zr(O)}_b$ layer forms in the original cladding region by diffusion of O from the $UO_2/\alpha\text{-Zr(O)}_a$ reaction interface through the $\alpha\text{-Zr(O)}_a$ and (U,Zr) regions to the O-poor β-Zry region. In contrast to the $\alpha\text{-Zr(O)}_a$ layer, the $\alpha\text{-Zr(O)}_b$ layer contains no (U,Zr) alloy along grain boundaries or within grains and no metallic U in the matrix (except after very long annealing times). The transitions in composition from the $\alpha\text{-Zr(O)}_a$ region and (U,Zr) layer or globules to the $\alpha\text{-Zr(O)}_b$ region are, in general, distinct and abrupt (figures 25, 26, 27, 28). Although the O contents in the $\alpha\text{-Zr(O)}_a$ and

α-Zr(O)$_b$ layers are very similar or nearly identical, the U content changes abruptly. After very long annealing times, the α-Zr(O)$_b$ region near the (U,Zr) globules may also contain up to 5 wt.% U. The additional α-Zr(O) {or prior (U,Zr) alloy)} which forms along the edges of the (U,Zr) globules contains U. The original α-Zr(O)$_b$ matrix contains no U. The compositions of the α-Zr(O)$_a$ and additional α-Zr(O) matrices are very similar (up to about 6 wt.% each O and U) and both formed in U-rich regions (the UO_2 pellet and the (U,Zr) alloy, respectively). The α-Zr(O)$_b$ matrix, however, formed in a U-free region (the Zry-4 cladding). Apparently, if α-Zr(O) forms in a U-rich region at high temperatures, the matrix will contain U, and vice versa. The absence of U in α-Zr(O)$_b$ away from the (U,Zr) globules (and the absence of any gradients in U content in the α-Zr(O)$_a$ matrix indicates that U diffuses very slowly in α-Zr(O) {the diffusion rate probably depends on the O content of the α-Zr(O)}, especially compared to O. The movement of large amounts of U from the reaction interface to the (U,Zr) layer therefore probably occurs in the liquid phase along the (U,Zr) stringers.

The prior β-Zry region contains from 1 to 3 wt.% O (figures 26,27,28 and Reference 25), as determined by AES analysis. From the Zr-ZrO_2 phase diagram (figure 20), β-Zr can contain up to 0.8 wt.% O at 1300°C and up to 1.7 wt.% O at 1700°C. The additional O which can be dissolved in β-Zry, as compared to β-Zr, can probably be attributed to the presence of the alloying elements in β-Zry (Sn, Fe, and Cr).

The isothermal section of the U-Zr-O ternary phase diagram at 1000°C is shown in figure 36 /29/. The initial tie-line for the fuel/cladding interaction lies between UO_2 at point A and Zr at point B. As the reaction proceeds, point B moves continuously from Zr toward oxygen-saturated α-Zr(O), the final stable reaction product between Zr and O in the UO_2/Zr interaction under solid state conditions (point C). Oxygen-stabilized α-Zr(O) contains a maximum of about 30 at.% oxygen, as shown in figure 20. Point A moves relatively little (toward UO_{2-x}) since the amount of UO_2 in the experiments was always much larger than the amount of zircaloy (6.8 g/cm UO_2 and 1.5 g/cm Zry). The final tie-line for the interaction is therefore AC. When this equilibrium position has been reached, the quasi-binary α-Zr(O) (with 30 at.% oxygen)- UO_2 phase diagram is applicable (figure 37 /26/).

The wetting behavior of various liquid/solid combinations of U, Zry, α-Zr(O), and UO_2 has been investigated in argon from 1800 to 2000°C /18/. The surface and interfacial energies of the various systems were determined from the measured wetting angles. Estimation of the total interfacial energy for two different reaction layer sequences of the UO_2/Zry-4 interaction shows that the observed sequence (figure 3):

$$UO_2 \rightarrow \alpha\text{-Zr(O)}_a \rightarrow (U,Zr) \rightarrow \alpha\text{-Zr(O)}_b \rightarrow \text{prior } \beta\text{-Zry}$$

is energetically more stable than another possible sequence:

$$UO_2 \rightarrow \alpha\text{-Zr(O)} \rightarrow (U,Zr) \rightarrow \text{prior } \beta\text{-Zry}.$$

That is, the total interfacial energy tends toward a minimum for the temperature range 1130 to 1700°C.

The observed sequence of reaction layers can also be explained from the U-Zr-O ternary phase diagram /1,30/. The diffusion path between final compositions of a diffusion couple need not necessarily be a straight line. Hofmann and Politis suggested a straight line between UO_2 and α-Zr(O) /1/. Olander suggested a rather complicated diffusion path which matches the observed reaction layer arrangement /30/.

4.2 UO_2/Zry-4 Reaction Kinetics

The rate-determining step in the UO_2/Zry-4 reaction is the diffusion of O into the zircaloy cladding. This is confirmed by the good agreement between the activation energies for the oxidation of zircaloy by UO_2 and by steam. In the UO_2/Zry-4 reaction, the activation energy for the growth of the total reaction zone is 45,200 cal/mol, and for the growth of the $\{(U,Zr) + \alpha\text{-Zr(O)}_b\}$ reaction zone, which corresponds approximately to the growth of the $\alpha\text{-Zr(O)}_b$ layer alone, is 41,300 (figure 23). The (U,Zr) layer should have little or no effect on the reaction kinetics since it can

dissolve very little O and it is liquid, thereby providing an easy path for O diffusion. In the steam/Zry-4 reaction (as investigated by Leistikow and Schanz), the activation energy for the growth of the $\{\alpha\text{-Zr(O)} + ZrO_2\}$ double layer is 43,900 cal/mol, and for the growth of the α-Zr(O) layer alone is 43,600 cal/mol /19/.

The kinetics of the UO_2/Zry-4 reaction have been successfully modeled by Denis and Garcia /31/. Oxygen diffusion is assumed to be the rate-determining step in the reaction and Zr diffusion is not considered. The model accurately predicts the interface movements and growth rates for the individual reaction layers, based upon the experimental results of Reference 1 and the present work. The model is more sophisticated than that developed by Cronenberg and El-Genk /32/, which considered only the transformation of β-Zry into α-Zr(O) due to O diffusion to describe the resulting O gradients in both the fuel and cladding. They did not treat the formation of a (U,Zr) alloy layer between two α-Zr(O) layers, as has been observed experimentally.

The UO_2/Zry-4 reaction occurs as rapidly as the steam/Zry-4 reaction above about 1100°C (figure 24), since both reactions are governed by the diffusion of O into the cladding. If the external reaction alone is considered in predicting cladding embrittlement, the reaction time corresponding to a specific extent of cladding embrittlement may be severely overestimated. It is shown below that the time required for the growth of a specified thickness of either the external $\{\alpha\text{-Zr(O)} + ZrO_2\}$ double layer or the internal $\{\alpha\text{-Zr(O)}_a + (U,Zr) + \alpha\text{-Zr(O)}_b\}$ total reaction zone alone is 4 times greater than the time required for the growth of the same total reaction zone thickness due to both the external and internal reactions.

To directly compare the external and internal reactions, it is necessary to express the reaction zone thicknesses in the same form, e.g., as the thickness of original cladding wall consumed. Considering the external reaction, the volume expansion accompanying the uptake of O by zircaloy to form α-Zr(O) is very small and can be neglected. That is, the α-Zr(O) thickness is assumed to correspond directly to an original cladding

thickness. However, it is known that the growth of ZrO_2 is accompanied by a volume expansion of 1.56 (which occurs predominately in the radial direction). The thicknesses of the α-Zr(O) and ZrO_2 layers can be calculated for a specific reaction temperature and time using the following correlations /19/:

$$x_{\alpha\text{-}Zr(O)} = [t \cdot 0.508 \exp(-43{,}561/RT)]^{1/2} \quad (5)$$

$$x_{ZrO_2} = [t \cdot 0.0782 \exp(-40{,}164/RT)]^{1/2} \quad (6)$$

where x is in cm, t in seconds, R is 1.987 cal/mol-K, and T is in K. The total reaction zone thickness on the outside surface can therefore be converted to a thickness of original cladding wall consumed from:

$$x_{\text{cladding consumed (external)}} = x_{\alpha\text{-}Zr(O)} + x_{ZrO_2}/1.56. \quad (7)$$

The total reaction zone thickness on the inside surface is not as easily converted to a thickness of original cladding consumed. The reaction interface moves during the test as zircaloy chemically dissolves the UO_2, oxygen diffuses into the cladding to form α-Zr(O), liquid U penetrates along the α-Zr(O) grain boundaries to form the (U,Zr) layer, and Zr diffuses into the UO_2. The thickness of original cladding wall consumed is approximately equal to the total reaction zone thickness minus the thickness of the (U,Zr) layer, or the sum of the $\alpha\text{-}Zr(O)_a$ and $\alpha\text{-}Zr(O)_b$ thickness. Due to the globule formation of the (U,Zr) alloy, it is not a simple matter to subtract this amount of material from the total reaction zone thickness. Therefore, as a first approximation, the total reaction zone thickness is assumed to represent the thickness of the original cladding wall consumed. The cladding consumed can then be calculated from Eq. 3 for a specific reaction temperature and time:

$$x_{\text{cladding consumed (internal)}} = [t \cdot 1.62 \exp(-45{,}200/RT)]^{1/2}. \quad (8)$$

A comparison of the reaction times required for the growth of equivalent thicknesses of: (a) the steam/Zry-4 total reaction zone alone, (b) the UO_2/Zry-4 total reaction zone alone, and (c) the combined external and internal reaction zones, is presented in table 8 for several different temperatures and times. Note in table 8 that the thickness of the original cladding wall consumed by the external reaction and the thickness of the internal reaction zones are very nearly equal for all temperatures and times. Using the same temperatures, the reaction times required for the growth of equivalent thicknesses of the combined external and internal reaction zones were calculated by trial and error. For example (table 8), at 1100°C after 60 minutes, 213 μm of cladding wall are consumed by the external reaction alone and 201 μm by the internal reaction alone. However, after only 15 minutes at 1100°C, 207 μm are consumed by both the external and internal reactions (106.5 + 100.5 μm, respectively). That is, if only the external reaction is considered in determining cladding embrittlement, the reaction time is overestimated by a factor of 4. Since the external and internal reactions are known to obey parabolic rate laws and occur at approximately the same rate, it is logical that halving the external and internal reaction zone thicknesses divides the reaction time by 4.

4.3 Cladding Embrittlement

Oxygen uptake embrittles zircaloy cladding by the formation of brittle α-Zr(O). The cladding is severely embrittled if the thickness of the total reaction zone is large compared to the thickness of the remaining β-Zry, which is relatively ductile. Many of the UO_2/Zry-4 specimens were severely embrittled and broke very easily during the tests, on cooldown, and/or during posttest handling. Of the specimens which broke, the majority fractured at one location, several at two, and one at six locations (the specimen tested at 1400°C for 150 minutes). All of the breaks occurred at pellet-to-pellet interfaces. A failure map for all of the specimens tested from 1300 to 1700°C (both cooldown and handling failures) up to 100 minutes is shown in figure 38. A very clear, distinct pattern of failure behavior is apparent. The specimens tested at lower temperatures withstood much longer times at reaction temperatures before breaking than those tested at the highest temperatures.

Of particular importance with respect to the mechanical stability of the cladding is the thickness of the cladding wall that has not been chemically influenced by oxygen uptake and therefore retains the original strength and ductility of the cladding, i.e., the chemically uninfluenced β-Zry. The extent of the chemical changes in the cladding can be represented by the total thickness of the two oxygen-stabilized α-Zr(O) phases. The (U,Zr) alloy can be neglected since it contains only small amounts of Zr. With respect to the strength of the total reaction zone, the (U,Zr) alloy can also be neglected since it is liquid above about 1150°C and at lower temperatures has a low yield strength. Very probably, the $\alpha\text{-Zr(O)}_a$ phase also contributes little to the overall strength of the cladding since it contains the (U,Zr) alloy along grain boundaries. This may be the reason that cracks have never been observed in the $\alpha\text{-Zr(O)}_a$ zone, since the grains are free to move with respect to each other at high temperatures, and at low temperatures thermal and mechanical stresses are relieved by plastic deformation of the (U,Zr) alloy. The mechanical properties of the oxidized cladding are therefore predominately determined by the strength and ductility of the $\alpha\text{-Zr(O)}_b$ and β-Zry phases.

Many different embrittlement criteria have been developed to predict both failures due to thermal shock on quenching and failures due to subsequent handling. Haggag of EG&G Idaho, Inc., recently published a study of the applicability of several different embrittlement criteria with respect to PBF fuel rods tested in-pile and ANL fuel rods tested out-of-pile /33/. The study concluded that the Chung and Kassner criteria for the two types of failure, which are based on the O content of the remaining β-phase and state that /34/:

- To withstand thermal shock during a reflood, the thickness of the remaining β-phase containing $\leq$0.9 wt.% O should be >0.1 mm, and
- To withstand posttest handling, the thickness of the remaining β-phase containing $\leq$0.7 wt.% O should be >0.3 mm,

are most appropriate since these criteria make it possible to differentiate between thermal shock and handling failures. A second embrittlement criterion discussed by Haggag which also shows good rod failure prediction (but does not

distinguish between the types of rod failure) is that of Pawel /35/. He suggested the values of 0.7 wt.% for the mean O concentration in the β-phase, together with a 95% saturation condition, as critical criteria for the onset of room temperature embrittlement.

In the present case, however, these embrittlement criteria cannot be directly applied to the UO_2/Zry-4 specimens since: (a) the reaction is one-sided and the criteria are based on two-sided oxidation, and (b) the specimens are much shorter (0.1 m as compared to the 1 m PBF rods), which has an influence on the forces induced during handling.

4.4. Fission Product Release

During the UO_2/Zry-4 interaction, the Zry chemically dissolves the outer portion of the UO_2 pellet. The posttest pellet diameters of eight specimens tested at 1400, 1500, 1600 and 1700°C in which the cladding had completely reacted to α-Zr(O) were measured. The average posttest diameter was 8.68 ± 0.05 mm (±1σ). Since the original pellet diameter was 9.11 mm, the maximum area of fuel dissolved was 6.01 mm^2. The cross-sectional area of the original pellet was 65.2 mm^2. Therefore, a maximum of 9.2% of the pellet can be dissolved by the Zry cladding. In an actual fuel rod, since the UO_2 crystalline structure is totally destroyed by chemical interaction with the Zry, complete release of gaseous and volatile fission products in this region must be assumed.

5. Conclusions

Out-of-pile UO_2/Zry-4 chemical interaction experiments in argon from 1000 to 1700°C and the reaction kinetics have been described. The conclusions can be summarized as follows:

- The extent of the reaction depends decisively on the fuel/cladding contact conditions.

- If solid contact exists, zircaloy reduces the UO_2 to form oxygen-stabilized α-Zr(O) and metallic U. The U reacts with Zr low in oxygen to form a (U,Zr) alloy rich in U which is liquid above about 1150°C.

- The reaction layers form in a particular sequence at all reaction temperatures and times:

$$[UO_2 + U] \rightarrow [\alpha\text{-Zr(O)}_a + (U,Zr)] \rightarrow (U,Zr) \rightarrow \alpha\text{-Zr(O)}_b \rightarrow \text{prior } \beta\text{-Zry.}$$

- The original UO_2/Zry-4 interface lies between the $\{\alpha\text{-Zr(O)}_a + (U,Zr)\}$ and (U,Zr) layers. The $\alpha\text{-Zr(O)}_a$ therefore forms in the fuel region and the (U,Zr) and $\alpha\text{-Zr(O)}_b$ layers in the cladding region.

- In the examined temperature range, the reaction obeys a parabolic rate law. The diffusion of O into the cladding is the rate-determining step in the reaction.

- O uptake by the Zry causes the cladding to become embrittled. The maximum measured O content of the α-Zr(O) is about 6 wt.%. On cooldown and/or during posttest handling, the embrittled specimens break very easily.

- The UO_2/Zry-4 reaction occurs as rapidly as the steam/Zry-4 reaction above about 1100°C. Therefore, oxidation from both the outside and inside cladding surfaces occurs 4 times faster than oxidation from either surface alone.

- Up to about 9 volume % of the UO_2 can be chemically dissolved by the Zry. In an actual fuel rod, complete release of fission products in this region of the fuel must therefore be assumed.

ACKNOWLEDGMENTS

We would like to thank Prof. Dr. W. Dienst, Dr. R.R. Hobbins, and Dr. M.L. Picklesimer for thorough technical and editorial reviews of the manuscript.

6. References

/1/ P. Hofmann, C. Politis, "The Kinetics of the Uranium Dioxide - Zircaloy Reactions at High Temperatures", Journal of Nuclear Materials, 87, 1979, pp. 375-397.

/2/ P. Hofmann, D.K. Kerwin,"Preliminary Results of UO_2/Zircaloy-4 Experiments under Severe Fuel Damage Conditions",Res Mechanica 5, 1982, pp. 293-308.

/3/ A. Fiege, Severe Fuel Damage Investigations of KfK/PNS, KfK 3431 B, January 1983.

/4/ S. Peck, S. Hagen, K. Hain, KfK/PNS Investigations on Severe Fuel Damage: The CORA Program, to be published as a KfK report.

/5/ T.E. Murley, L.S. Tong, G.L. Bennett,"Summary of LWR Safety Research in the USA", IAEA International Conference on Nuclear Power and Its Fuel Cycle, Salzburg, Austria (IAEA-CN-36), May 1977.

/6/ U.S. Nuclear Regulatory Commission, Division of Reactor Safety Research, Water Reactor Safety Research Program - A Description of Current and Planned Research, NUREG-0006, February 1979.

/7/ P.E. MacDonald, W.J. Quapp, A.S. Menner, Z.R. Martinson, R.K. McCardell. "Response of Unirradiated and Irradiated PWR Fuel Rods Tests Under Power-Cooling-Mismatch Conditions",Nuclear Safety, 19, 1978, pp. 440-464.

/8/ A.S. Mehner, W.J. Quapp, R.R. Hobbins, S.L. Seiffert, R.K. McCardell, "Performance of Unirradiated and Irradiated PWR Fuel Rods Tested Under Power-Cooling-Mismatch Conditions", ANS Thermal Reactor Safety Meeting, Sun Valley, Idaho, July 31 - August 5, 1977.

/9/ NRC Action Plan Developed as a Result of the TMI-2 Accident, NUREG-0660, Volume 1, May 1980.

/10/ P.E. MacDonald, G.P. Marino,"Power Burst Facility Severe Fuel Damage Test Program",10th Water Reactor Safety Meeting, Gaithersburg, Maryland, October 12-15, 1982.

/11/ C.M. Allison, D.L.Hagmman, S.Hsieh, E.T. Laats, J.W. Spore, Severe Core Damage Analysis Package (SCDAP), Code Conceptual Design Report, EGG-CDAP-5397, April 1981.

/12/ P. Hofmann, D. Kerwin-Peck, P. Nikolopoulos, "Physical and Chemical Phenomena Associated with the Dissolution of Solid UO_2 by Molten Zircaloy", Sixth International Conference on Zirconium in the Nuclear Industry, Vancouver, Canada, June 1982.

/13/ M.W. Mallett, J.W. Droege, A.F. Gerds, A.W. Lemmon,Jr., The Zirconium -Uranium Dioxide Reaction, BMI 1210, July 1957.

/14/ L.N. Grossman, D.M. Rooney, Interfacial Reaction Between UO_2 and Zircaloy-2, GEAP 4679, April 1965.

/15/ A.R. Paul, M.C. Naik, K.S. Venkateswarlu, Kinetics of Interfacial Reaction Between UO_2 and Zry-2, BARC-1087, 1980.

/16/ H.E. Rosinger, A Study of the Pellet/Clad (Uranium Dioxide/Zircaloy-4) Interaction at 1373 and 1473 K, AECL-7785, February 1983.

/17/ P.D. Parsons, J.A.S. Mowat, D.W.F. Dewhurst, T.E. Hughes, "The Physical and Chemical Degradation of PWR Fuel Rods in Severe Accident Conditions", OECD-NEA-CSNI/IAEA Specialists' Meeting on Water Reactor Fuel Safety and Fission Product Release in Off-Normal and Accident Conditions,RISØ National Laboratory, Roskilde, Denmark, May 1983.

/18/ P. Hofmann, D. Kerwin-Peck, P. Nikolopoulos, "Determination of Interfacial Energies in the UO_2/Zry Diffusion Couple", to be published in the Journal of Nuclear Materials.

/19/ S. Leistikow, G. Schanz, H.V. Berg, Kinetik und Morphologie der isothermen Dampf-Oxidation von Zircaloy 4 bei 700-1300°C, KfK 2587, March 1978.

/20/ V.F. Urbanic,"Method for Estimating the Exposure Time and Temperature for Zircaloy Oxidation in Steam",Journal of Nuclear Materials, 59, 1976, pp. 90-94.

/21/ J.V. Cathcart, R.E. Pawel, R.A. McKee, R.E. Druschel, G.J. Yurek, J.J. Campbell, S.H. Jury, Zirconium Metal-Water Oxidation Kinetics IV. Reaction Rate Studies, ORNL/NUREG-17, Aug. 1977.

/22/ R.R. Biedermann, R.G. Ballinger, W.G. Dobson, A Study of Zircaloy-Steam Oxidation Reaction Kinetics, EPRI NP-225, Sept. 1976.

/23/ M. Suzuki, S. Kawasaki, T. Furuta, Zircaloy-Steam Reaction and Embrittlement of the Oxidized Zircaloy Tube Under Postulated Loss-of-Coolant Accident Conditions, JAERI-M 6879, Dec. 1976.

/24/ D.O. Hobson, P.L. Rittenhouse, Embrittlement of Zircaloy-Clad Fuel Rods by Steam During LOCA Transients, ORNL 4758, Jan. 1972.

/25/ Ch. Braun, E. Nold, Augerelektronenspektroskopische Untersuchungen zur Wechselwirkung von UO_2/Zry-4 bei hohen Temperaturen, to be published in the Journal of Nuclear Materials.

/26/ P. Hofmann et al.,"Untersuchungen zu schweren Kernschäden", Projekt Nukleare Sicherheit Jahresbericht 1982, KfK 3350, August 1983. pp. 4200/196-4200/209

/27/ F.N. Rhines, Phase Diagrams in Metallurgy, McGraw-Hill, New York, 1956.

/28/ M. Hansen, Constitution of Binary Alloys, McGraw-Hill, New York, 1958.

/29/ C. Politis, Untersuchungen im Dreistoffsystem Uran-Zirkon-Sauerstoff, KfK 2167, October 1975.

/30/ D.R. Olander, "The UO_2/Zircaloy Chemical Interaction", Journal of Nuclear Materials,115, 1983, pp. 271-285.

/31/ A. Denis, E.A. Garcia, "Model to Describe the Interaction Between UO_2 and Zircaloy in the Temperature Range 1000 to 1700°C, Journal of Nuclear Materials 116, 1983, pp.44-54.

/32/ A.W. Cronenberg, M.S. El-Genk, "An Assessment of Oxygen Diffusion During UO_2/Zry Interaction", Journal of Nuclear Materials,78, 1978, pp. 390-407.

/33/ F.M. Haggag, Zircaloy Cladding Embrittlement Criteria: Comparison of In-Pile and Out-of-Pile Results, NUREG/CR-2757 EGG-2123, July 1982.

/34/ H.M Chung, T.F. Kassner, Embrittlement Criteria For Zircaloy Fuel Cladding Applicable to Accident Situations in Light-Water Reactors, NUREG/CR-1344, ANL-79-48, January 1980.

/35/ R.E. Pawel, "Oxidation Diffusion in Beta Zircaloy During Steam Oxidation", Journal of Nuclear Materials,50, 1974, pp. 247-258.

/36/ A. Skokan, K. Biemüller, G. Reiser, G. Schlickeiser, Ermittlung von Daten zu Beschreibung des Reaktions- und Freisetzungsverhaltens bei Temperaturerhöhung im RDB und beim Kernschmelzen, PNS Annual Report 1982, KfK 3350, 1983, pp. 4300/10-4300/15.

Table 1: Fuel Rod Specimen Nominal Parameters

Cladding	
material	Zry-4
outside diameter (mm)	10.75
inside diameter (mm)	9.30
wall thickness (mm)	0.725
length (mm)	102
Fuel pellet	
material	UO_2 (depleted U)
density (g/cm^3)	10.41 (95 % TD)
oxygen/uranium ratio	2.000
diameter (mm)	9.11
length (mm)	11
weight (g)	7.22
shape	Dished (both ends)
Fuel rod	
Internal pressure (bar)	1 (at 20^oC)
Fill gas	He

Table 2: Zircaloy-4 Chemical Composition (wt.%)

Sn	1.57
Fe	0.22
Cr	0.10
Ni	0.0035
H	0.0006
C	0.014
N	0.0028
O	0.13
Zr	balance

Table 3: Measured UO_2/Zry-4 Reaction Zone Thickness as a Function of Temperature and Time

Specimen	Temperature (°C)	Time (min)	Measured Reaction Zone Thickness (μm)[a]					
			I		II		III	
			$\bar{x}$	σ	$\bar{x}$	σ	$\bar{x}$	σ
59M	1300	10	55	0	63	4.5	210	4.6
60M		20	77	2.5	91	5.1	294	5.8
74M		60	115	3.2	140	3.4	502	11
62M		100	185	6.7	204	8.0	801	26
63M		150	237	14	268	15	918	26
2M	1400	3	46	3.9	67	3.6	161	8.3
3M		10	79	4.5	104	4.4	286	12
55M		10 (W)[b]	100	5.4	131	8.9	328	8.8
26M		20	139	4.2	175	7.8	465	24
27M		30	152	5.6	197	7.3	532	19
28M		60	245	10	301	15	836	14
53M		100	386	8.8	528	19	860	15
54M		150	369	11	529	21	854	14
64M	1500	3	82	3.2	146	28	275	7.8
65M		10	155	5.8	226	34	491	9.4
56M		10 (W)[b]	200	8.4	299	41	640	37
50M		30	327	9.6	425	31	835	26
67M		60	394	8.7	460	38	878	28
51M		100	390	12	488	39	871	14
52M		150	404	11	509	52	854	13
68M	1600(Series A)	1	88	2.6	175	53	277	19
69M		3	144	4.4	223	43	431	14
70M		6	192	4.0	327	62	582	22
71M		10	267	12	435	59	-	-
57M		10(W)[b]	289	11	434	73	790	10
72M		20	404	9.7	561	52	887	32
73M		30	428	12	583	47	889	21
33M		60	386	6.3	517	13	857	11
49M		100	406	13	530	42	837	19
106M	1600(Series B)	1	75	1.8	177	28	234	6.4

Table 3 (continued)

Specimen	Temperature (°C)	Time (min)	Measured Reaction Zone Thickness (μm)[a]					
			I		II		III	
			$\bar{x}$	σ	$\bar{x}$	σ	$\bar{x}$	σ
107M		3	113	4.4	252	38	351	24
108M		6	168	5.4	275	39	486	16
109M		10	221	2.7	317	27	666	12
75M	1700	1	129	2.5	296	44	433	18
104M		1	117	4.8	265	59	360	14
76M		3	222	5.8	362	72	677	49
105M		3	188	5.5	376	49	618	23
77M		6	302	15	533	75	866	40
78M		10	407	8.7	556	75	869	16
79M		10(W)[b]	385	7.5	584	66	842	17
80M		20	427	8.1	574	59	883	17
40M		30	426	15	542	42	852	19
41M		60	422	19	557	59	871	39

a. Average and standard deviation calculated from a minimum of 16 measurements.

b. Tungsten marker specimens.

Table 4: Regression Constants Calculated Using the Method of Least Squares for the Data from Table 3 ($x = a_o + a_1 \sqrt{t}$ with $a_o = 0$)

Temperature	Zone I		Zone II		Zone III		adjusted reaction zone	
	$a_1(\mu m/s^{1/2})^a$	SEE $(\mu m)^b$	$a_1(\mu m/s^{1/2})^a$	SEE $(\mu m)^b$	$a_1(\mu m/s^{1/2})^a$	SEE $(\mu m)^b$	$a_1(\mu m/s^{1/2})^a$	SEE $(\mu m)^b$
1000[c]	0.326	2.44	0.461	0.817	1.87	5.42	1.54	7.42
1100[c]	0.694	4.27	0.903	6.86	3.31	19.6	2.61	14.0
1200[c]	1.09	3.91	1.47	1.98	6.01	6.03	4.92	6.99
1300	2.34	15.3	2.66	12.2	9.71	50.8	7.37	43.3
1400	3.86	12.9	4.87	12.8	13.3	34.0	9.41	24.8
1500	7.27	20.7	9.88	33.7	19.8	19.7	12.3	31.3
1600 (Series A)	11.2	14.6	17.1	59.1	32.1	26.5	21.4	22.8
(Series B)	8.92	6.04	14.8	57.7	26.7	24.5	17.8	21.9
1700	16.0	15.7	29.1	72.3	46.8	48.5	31.0	46.3

a. The a_1 values represent the slopes of the lines in Figures 14 through 18.

b. The standard error of estimate (SEE) of x on $\sqrt{t}$ is analogous to standard deviation and is a measure of the scatter about the regression equation.

c. From Reference 1.

Table 5: Comparison of the Growth Rate Equations for the UO_2/Zry and Steam/Zry Reactions

Interaction	Investigators	Temperature Range (°C)	Growth Rate Equation[a]
UO_2/Zry-4	present work	1000 to 1700	1.62exp (-45,200/RT)[b] 0.30exp (-41,600/RT)[b]
UO_2/Zr	Mallett et al /13/	704 to 1093	0.0765exp (-37,000/RT)[b] 0.060exp (-37,400/RT)[b]
UO_2/Zry-2	Grossmann, Rooney /14/	677 to 1300	4 exp (-50,000/RT)
UO_2/Zry-2	Paul et al /16/	1000 to 1500	2.66exp (-47,540/RT)[b] 2.53exp (-50,100/RT)[b]
steam/Zry-4	Leistikow,Schanz, Berg /17/	800 to 1500	1.66exp (-43,885/RT)
steam/Zry-2 and -4	Urbanic, Heidrick /18/	1050 to 1580 1580 to 1850	0.132exp (-35,629/RT) 0.063exp (-30,846/RT)
steam/Zry-4	Cathcart et al /19/	1000 to 1500	0.682exp (-41,700/RT)
steam/Zry-4	Biederman et al /20/	982 to 1482	0.051exp (-34,230/RT)
steam/Zry-4	Suzuki et al /21/	1000 to 1330	0.396exp (-39,420/RT)
steam/Zry-4	Hobson,Rittenhouse /22/	927 to 1370	0.708exp (-41,054/RT)

a. Total reaction zone except where noted. R is 1.987 cal/mol-K.

b. Adjusted with respect to original UO_2/Zry or Zr interface.

Table 6: O, Zr, and U Contents of the α-Zr(O) Matrices from AES and EMP Analyses (in wt.%)

Temperature (°C)	Time (min)	Specimen	Element	α-Zr(O)$_a$ matrix[a] AES[b]	α-Zr(O)$_a$ matrix[a] EMP[c]	α-Zr(O)$_b$ matrix[a] AES[b]	α-Zr(O)$_b$ matrix[a] EMP[c]
1500	6	31M	O		4.9 to 6.1		5.3
			Zr		88.4 to 90.1		94.6
			U		5.0 to 5.6		0.1
	60	25M	O		11.5		10.3
			Zr		82.2		88.5
			U		5.3		0.0
			Sn		1.0		1.3
	100	51M	O	4.3 to 6.0	5.0	5.0 to 6.0	5.3
			Zr	87 to 91	87.9	94	93.1
			U	3.5 to 7.5	5.5	0.0 to 1.1	0.0
			Sn		1.6		1.6
	150	52M	O	4.7 to 6.0		4.9 to 6.3	
			Zr	87 to 90		90 to 94	
			U	4.9 to 7.0		0.0 to 4.2	
1600	3	15M	O	4.8	4.1 to 5.5	4.0 to 4.7	5.2
			Zr	87 to 89	85.7 to 89.1	95 to 96	94.7
			U	6.0 to 8.0	6.3 to 9.7	0.0	0.1
	20	18M	O	3.9 to 4.3		3.2 to 4.8	
			Zr	87 to 92		95 to 97	
			U	4.3 to 9.1		0.0	
	30	19M	O		4.8		3.7
			Zr		88.9		94.9
			U		5.3		0.0
			Sn		1.0		1.4
	100	49M	O	5.5 to 6.5	6.4	5.7 to 6.2	5.9
			Zr	86 to 90	84.5	92 to 94	87.9
			U	4.0 to 7.5	8.2	0.0 to 2.5	5.2
			Sn		0.9		1.0
1700	3	36M	O	5.2 to 5.5		4.2 to 4.6	
			Zr	92		95 to 96	
			U	2.2 to 3.2		0.0 to 0.8	

Table 6(continued)

Temperature (°C)	Time (min)	Specimen	Element	α-Zr(O)$_a$ matrix[a] AES[b]	α-Zr(O)$_a$ matrix[a] EMP[c]	α-Zr(O)$_b$ matrix[a] AES[b]	α-Zr(O)$_b$ matrix[a] EMP[c]
1700	6	37M	O		3.9		3.8
			Zr		87.2		94.7
			U		8.2		0.0
			Sn		0.7		1.5
	10	38M	O	5.0 to 6.0		4.5 to 5.0	
			Zr	84 to 91		94	
			U	3.5 to 9.5		0.0	
	20	39M	O		6.1		6.9
			Zr		87.2		91.4
			U		5.9		0.0
			Sn		0.8		1.7
	60	41M	O	5.4 to 6.0		5.2 to 5.5	
			Zr	89 to 91		95 to 96	
			U	3.1 to 4.6		0.0	
	60	41M (dishing volume)	O	4.7 to 5.1		2.5 to 3.4	
			Zr	83 to 85		90.7 to 91.5	
			U	10 to 12		5.8 to 6.1	

a. Composition corresponds to the α-Zr(O) matrix only and does not include the (U,Zr) alloy in these two regions.

b. Auger electron spectroscopy analysis. Uncertainty in O content is less than ± 0.5 wt.%. The uncertainties are described in detail in Reference 25.

c. Electron microprobe analysis. Uncertainties in Zr, U, and Sn contents are ± 3.0, ± 0.2, and ± 0.1 wt.%, respectively. O content was determined by difference (100 wt.%-(Zr+U+Sn contents) and has an uncertainty of ± 3.0 wt.%.

Table 7: O, Zr, and U Contents of the (U,Zr) Alloy from EMP Analysis (in wt.%)[a]

Temperature (°C)	Time (min)	Specimen	Element	UO_2	U-rich metallic phase in UO_2	(U,Zr) stringer	(U,Zr) layer
1500	6	31M	O	10.8	0.0	1.0	0.6 to 1.2
			Zr	0.0	1.1	4.8	13.7 to 35.1
			U	89.2	98.9	94.1	64.2 to 85.1
			Sn	0.0	0.0	0.0	0.5
	60	25M	O	11.9	0.0	0.0	0.0
			Zr	0.0	2.3	2.9	3.7
			U	88.1	97.7	97.1	96.3
			Sn	0.0	0.0	0.0	0.0
	100	51M	O		0.0	0.0	0.0
			Zr		0.9	1.8	2.4
			U		99.1	98.2	97.6
			Sn		0.0	0.0	0.0
1600	3	15M	O	10.3	0.0	0.9	0.5 to 0.8
			Zr	0.1	0.8	4.8	21.2 to 30.5
			U	89.6	99.2	94.3	69.0 to 78.0
			Sn	0.0	0.0	0.0	0.0
	30	19M	O	11.9	0.0	0.0	0.0
			Zr	0.0	2.5	3.1	10.2
			U	88.1	97.5	96.9	89.7
			Sn	0.0	0.0	0.0	0.1
	100	49M	O			0.0	0.0
			Zr			1.9	2.9
			U			98.1	97.1
			Sn			0.0	0.0
1700	6	37M	O	11.9		0.0	0.0
			Zr	0.0		2.0	30.6
			U	88.1		98.0	68.3
			Sn	0.0		0.0	1.1
	20	39M	O			0.0	0.0
			Zr			1.7	3.8
			U			98.3	96.2
			Sn			0.0	0.0

Table 7(continued)

Temperature (°C)	Time (min)	Specimen	Element	UO_2	U-rich metallic phase in UO_2	(U,Zr) stringer	(U,Zr) layer
1700	60	41M (dishing volume)	O				0.0
			Zr				3.8
			U				96.2
			Sn				0.0

a. Electron microprobe analysis. Uncertainties in Zr, U, and Sn contents are ± 1.1, ± 3.0, and ± 0.1 wt.%, respectively. O content was determined by difference (100 wt.% - (Zr + U + Sn contents) and has an uncertainty of 3.2 wt.%.

Table 8: Comparison of the Reaction Times for Equivalent Reaction Zone Thicknesses for the External Steam/Zry-4 Reaction, Internal UO_2/Zry-4 Reaction, and Combined (External + Internal) Reactions

Temperature (^oC)	Single Zone Reaction Time (min)	External Reaction Zone[a] (μm)			Internal Reaction Zone[b] (μm)	(External+Internal) Reaction Zones[c]	
		α-Zr(O)	ZrO_2	cladding wall consumed		cladding wall consumed (μm)	reaction time (min)
1100	60	145	106	213	201	106.5 + 100.5 = 207	15
1200	30	177	124	256	250	128 + 125 = 253	7.5
1300	10	164	111	235	236	117.5 + 118 = 235.5	2.5
	60	401	271	575	578	287.5 + 289 = 576.5	15
1400	30	430	281	610	630	305 + 315 = 620	7.5
1500	10	359	228	505	534	252.5 + 267 = 519.5	2.5

a. The α-Zr(O) and ZrO_2 reaction layer thicknesses were calculated from Equations 5 and 6, respectively. The thickness of cladding wall consumed was then calculated from Equation 7.

b. The total thickness of the internal reaction zone, which is assumed to represent the thickness of cladding wall consumed, was calculated from Equation 8.

c. The reaction time required for the growth of an equivalent thickness of the combined (external + internal) reaction zones was determined by trial and error. The corresponding reaction time is one-fourth of the single zone reaction time.

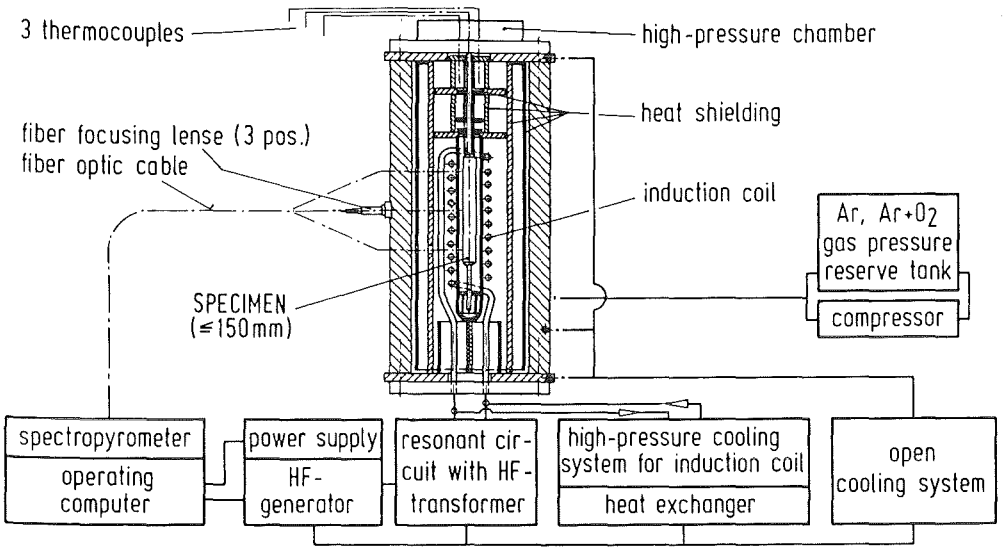

a. Schematic of MONA

b. MONA high-frequency generator and cooling system for induction coil

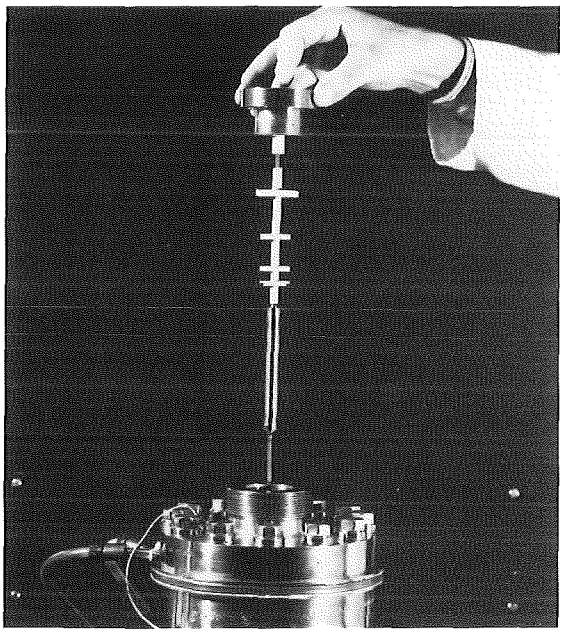

c. Test specimen with ceramic shielding before loading into MONA

Figure 1: High-temperature/high pressure experiment equipment MONA.
T_{max} = 2200°C, P_{max} = 200 bar (argon), P_{max} = 40 bar (argon/oxygen)

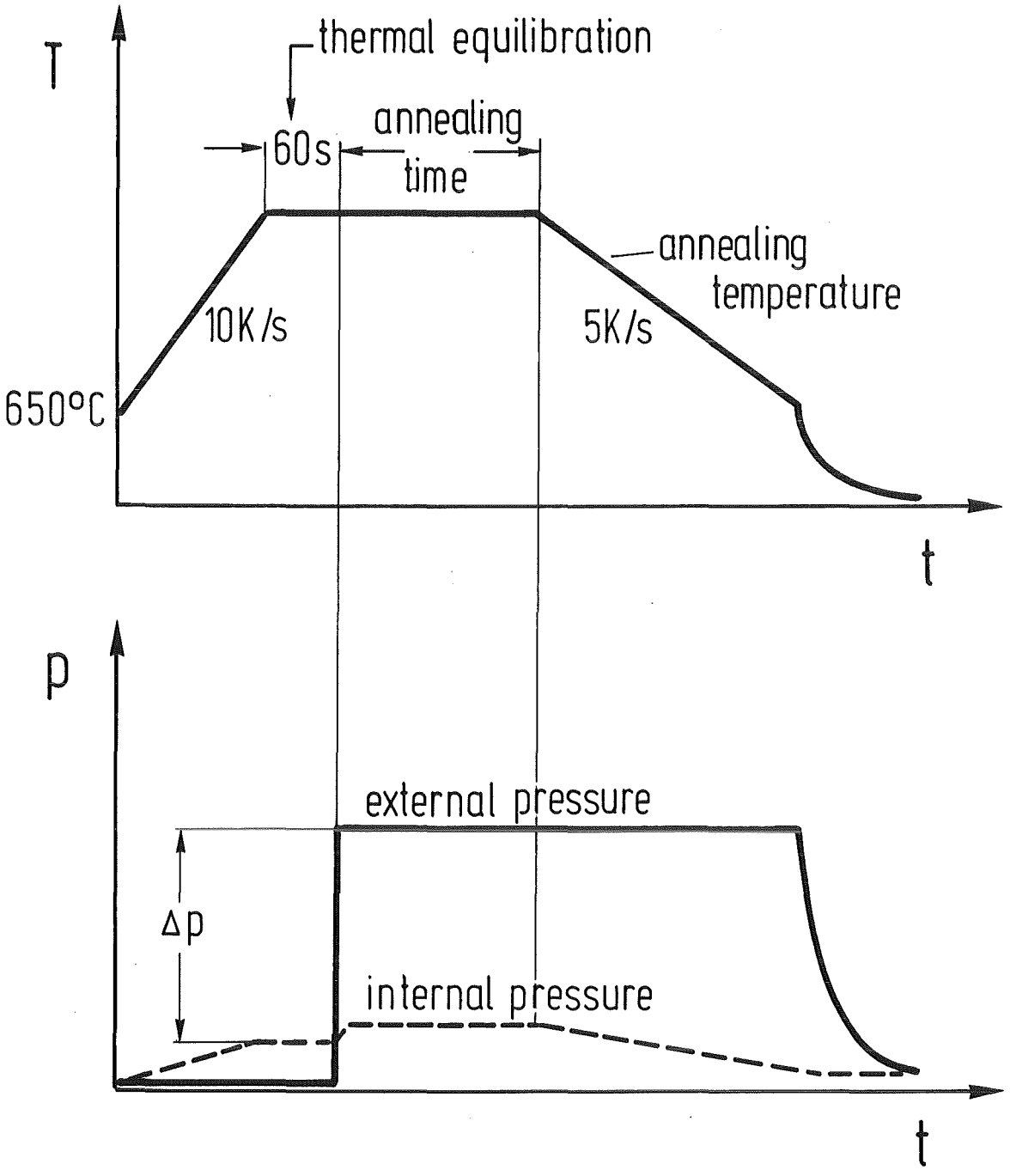

T_{max} : 2200 °C

p_{max} : 200 bar (inert atmosphere)
40 bar (oxidizing atmosph.)

Figure 2: Schematic of the test conduct

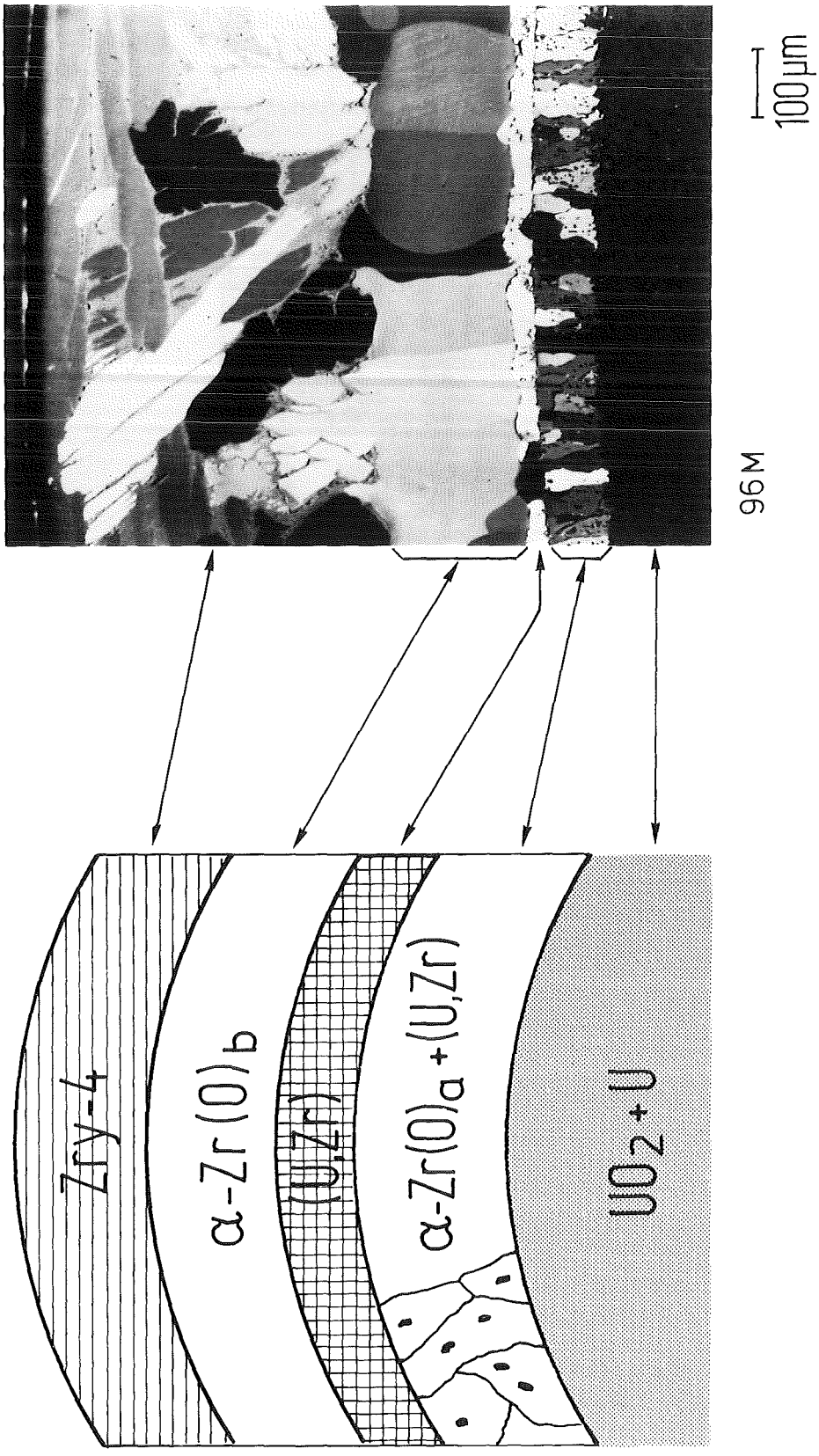

Figure 3: Sequence of the UO_2/Zry-4 reaction layers

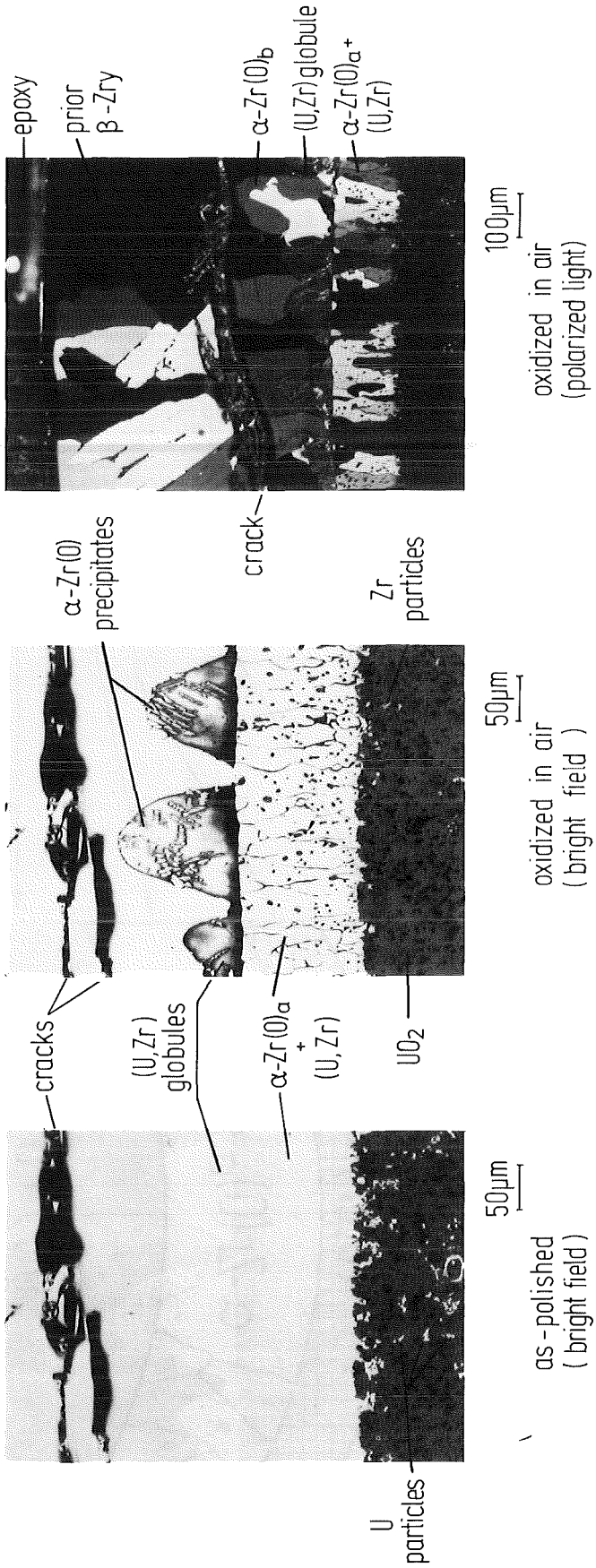

Figure 4: UO_2/Zry-4 reaction layer appearance after 3 minutes at 1600°C

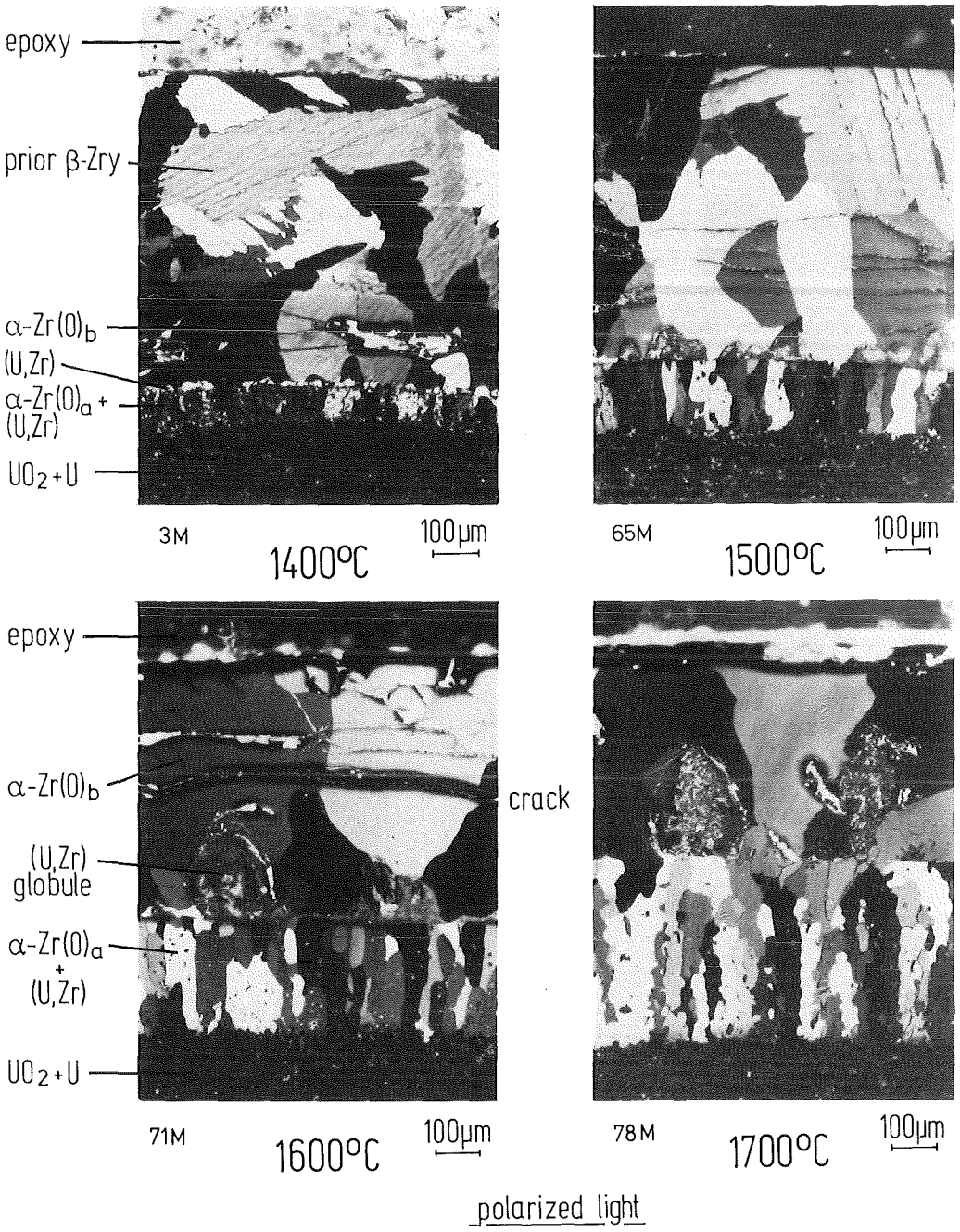

Figure 5: UO_2/Zry-4 reaction layer appearance as a function of temperature (annealing time 10 min)

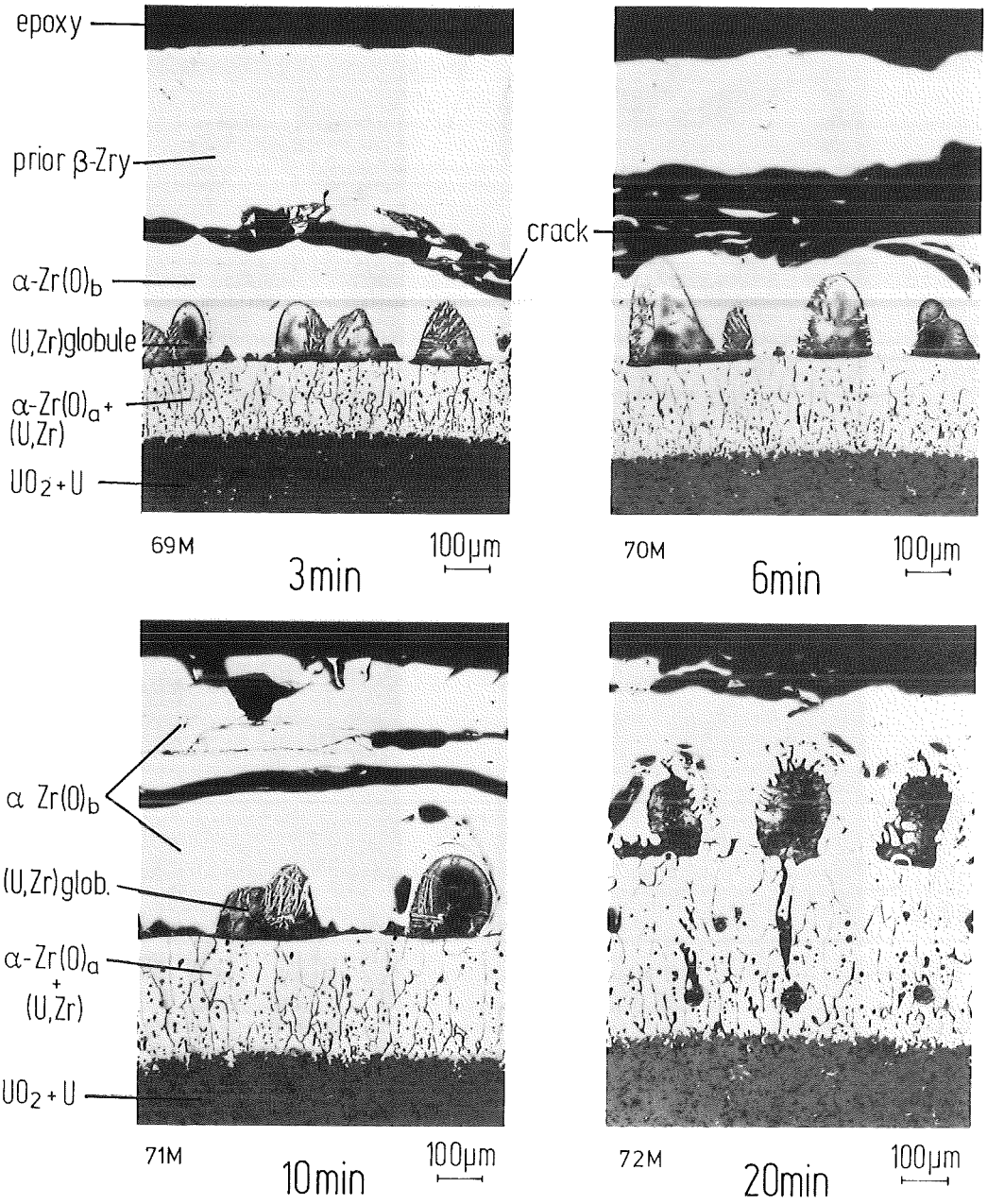

Figure 6: UO_2/Zry-4 reaction layer appearance as a function of time (annealing temperature 1600°C)

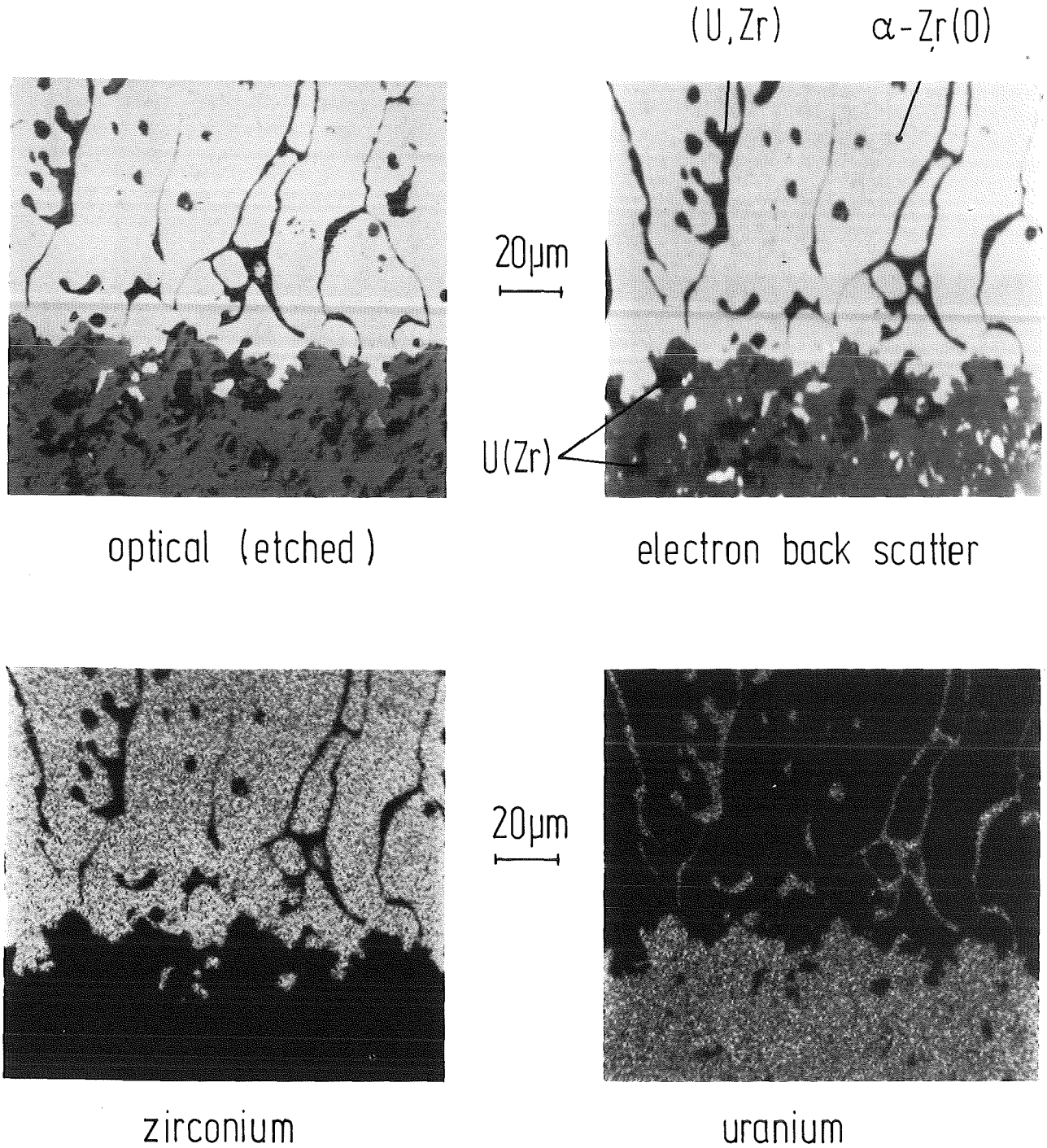

Figure 7: UO_2/α-Zr(O) reaction interface (T = 1600°C, t = 600 s) (electron microprobe analysis)

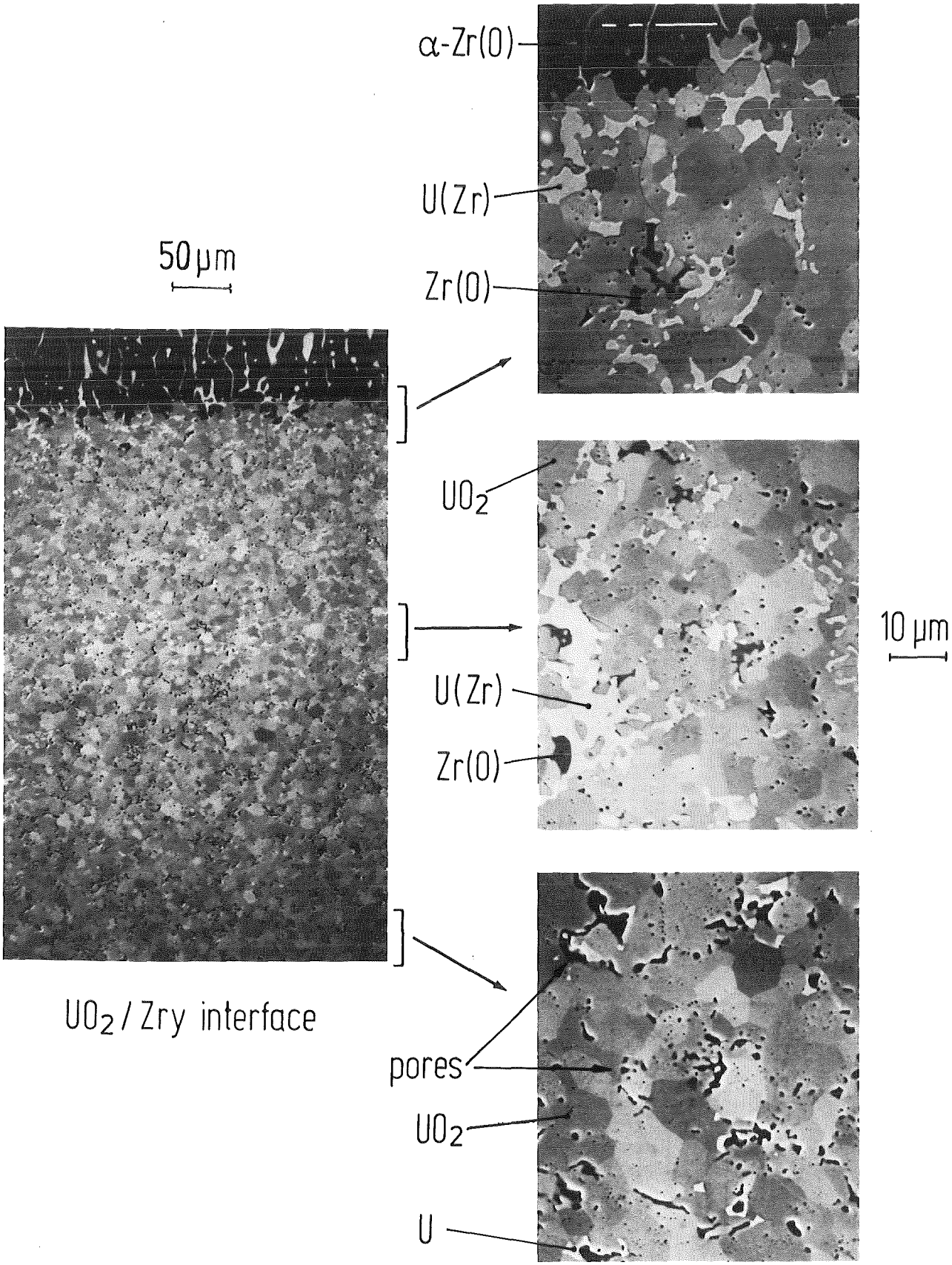

Figure 8: U and Zr distribution in UO_2 as a function of distance from the UO_2/α-Zr(O) interface (T = 1700°C, t = 600 s) (SEM photographs)

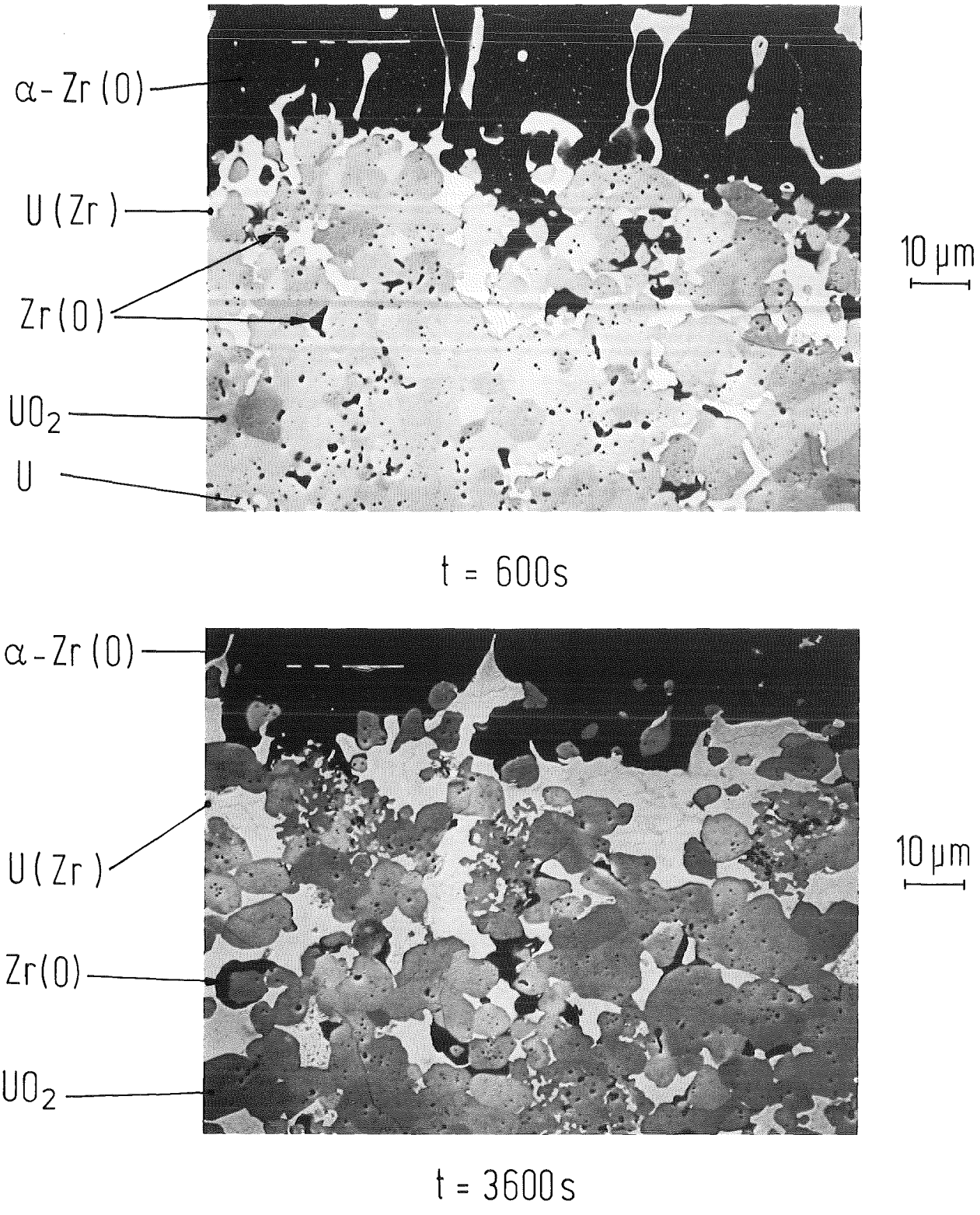

Figure 9: Formation of liquid U at the UO_2/α-Zr(O) interface and dissolution of UO_2 (T = 1700°C) (SEM photographs)

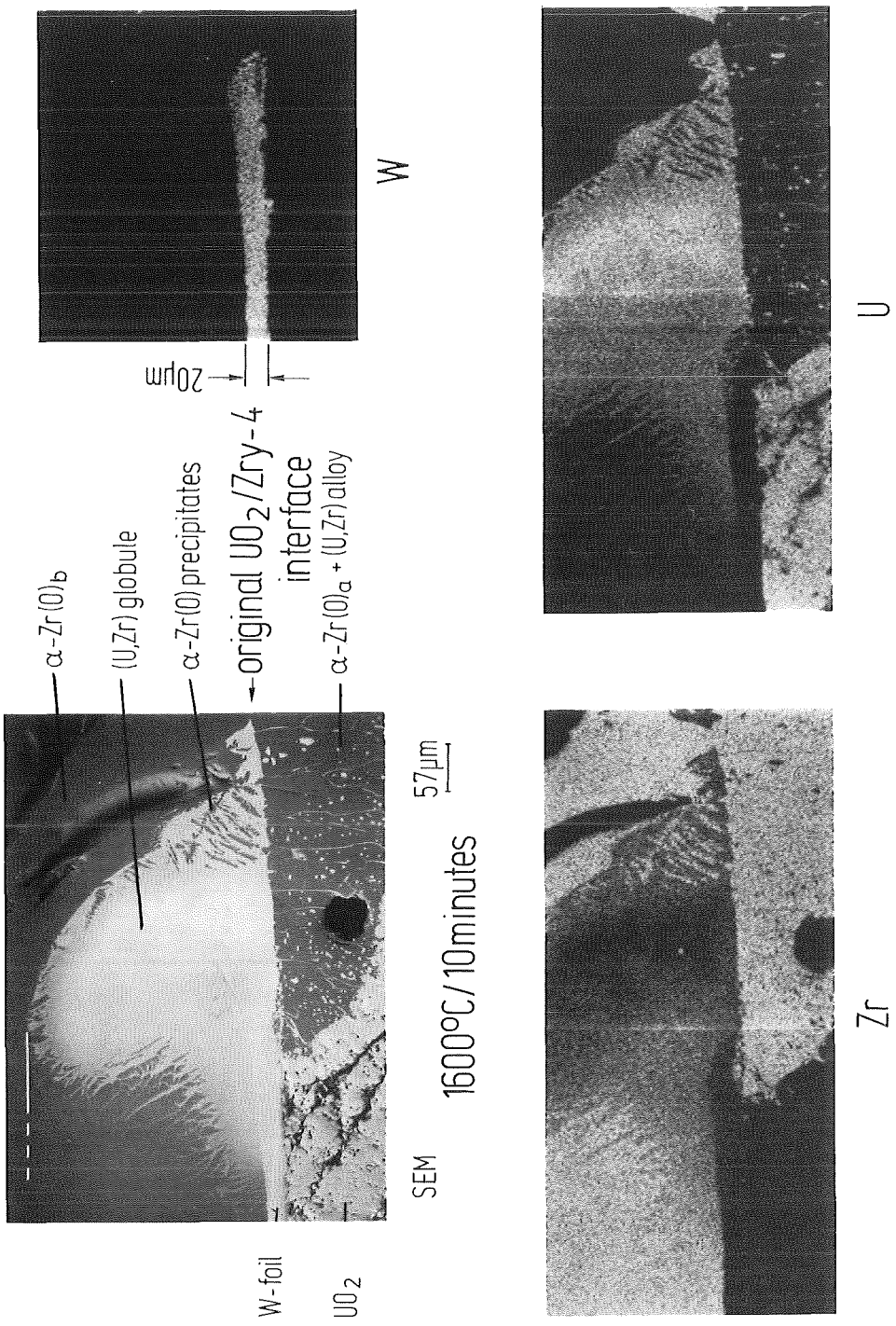

Figure 10: Location of the original UO_2/Zry-4 interface (electron microprobe analysis)

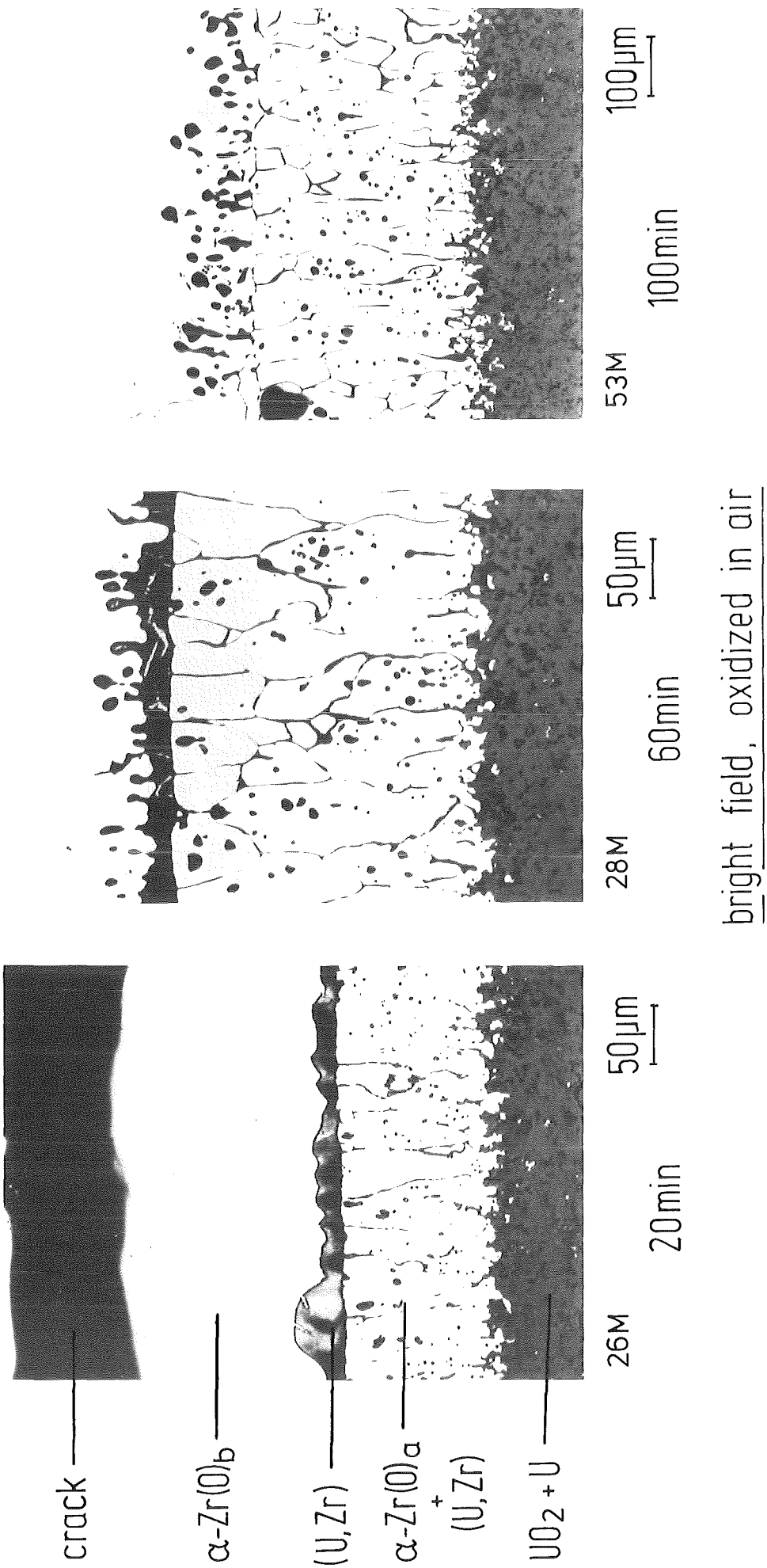

Figure 11: Transformation of (U,Zr) layer as a function of time at 1400°C

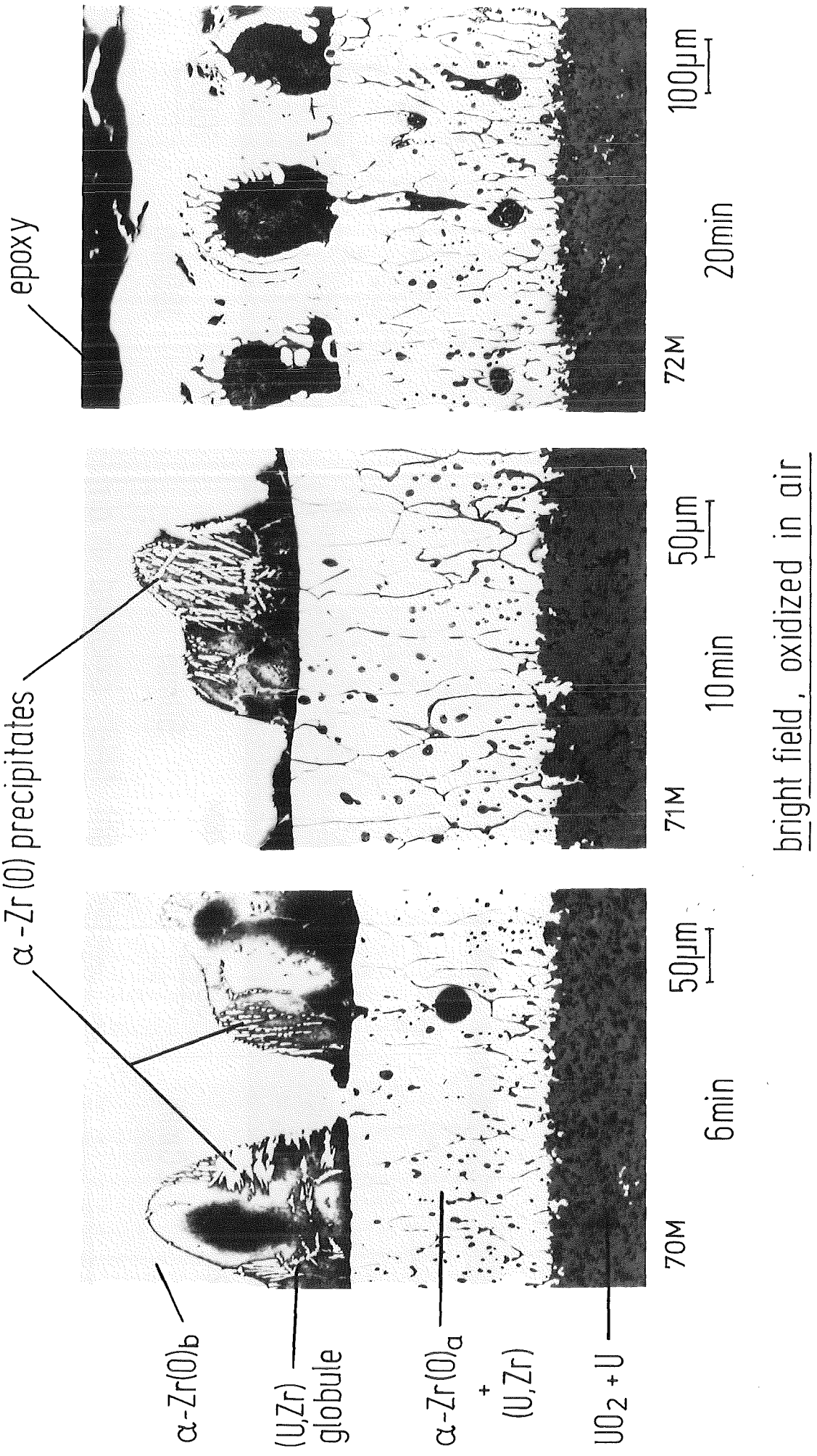

Figure 12: Growth of oxygen-stabilized α-Zr(O) into (U,Zr) globules as a function of time at 1600°C

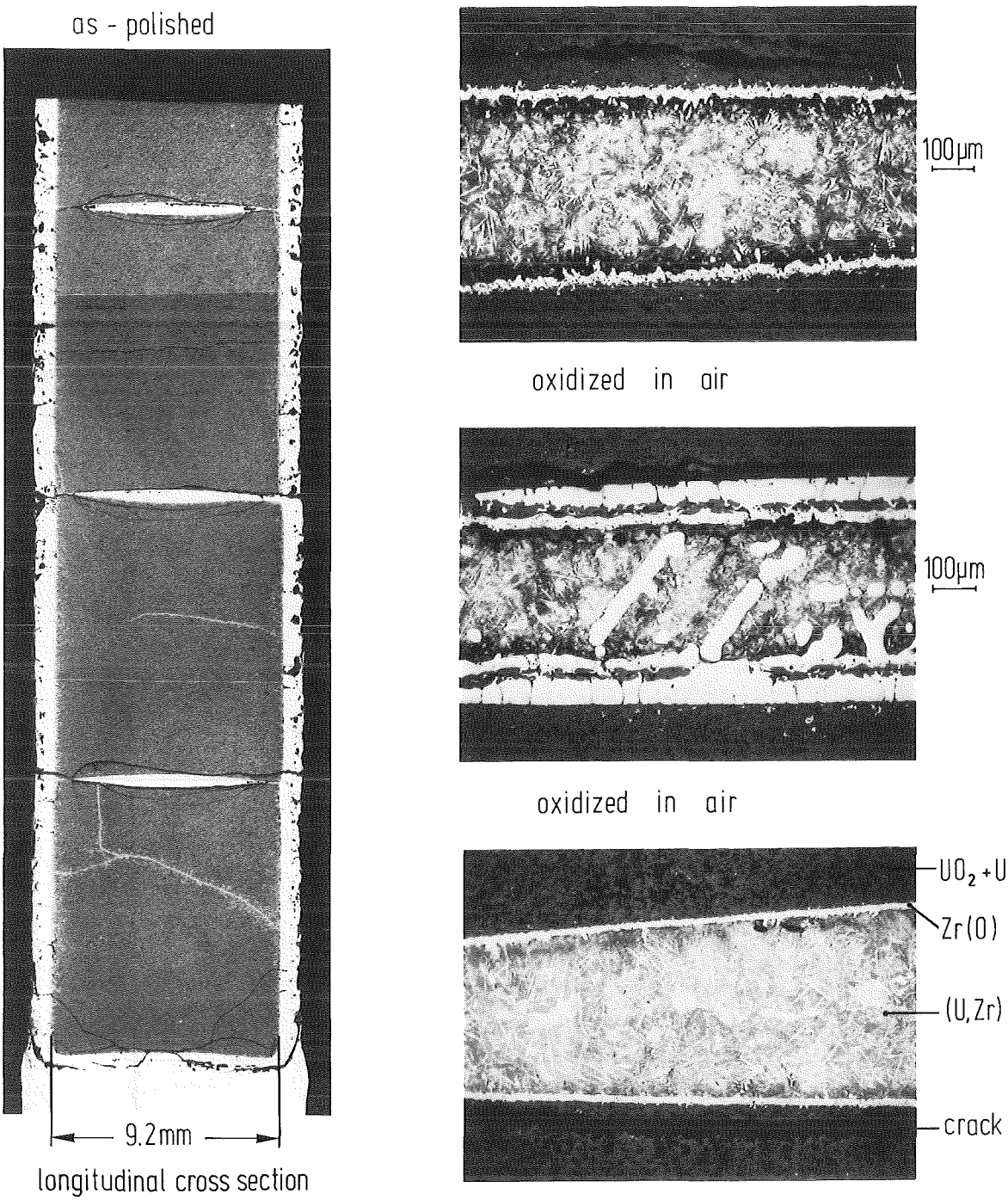

1700 °C / 3600 s ; Δp ≈ 40 bar

Figure 13: Penetration of liquid (U,Zr) alloy into pellet dishing volumes (T = 1700°C, t = 3600 s)

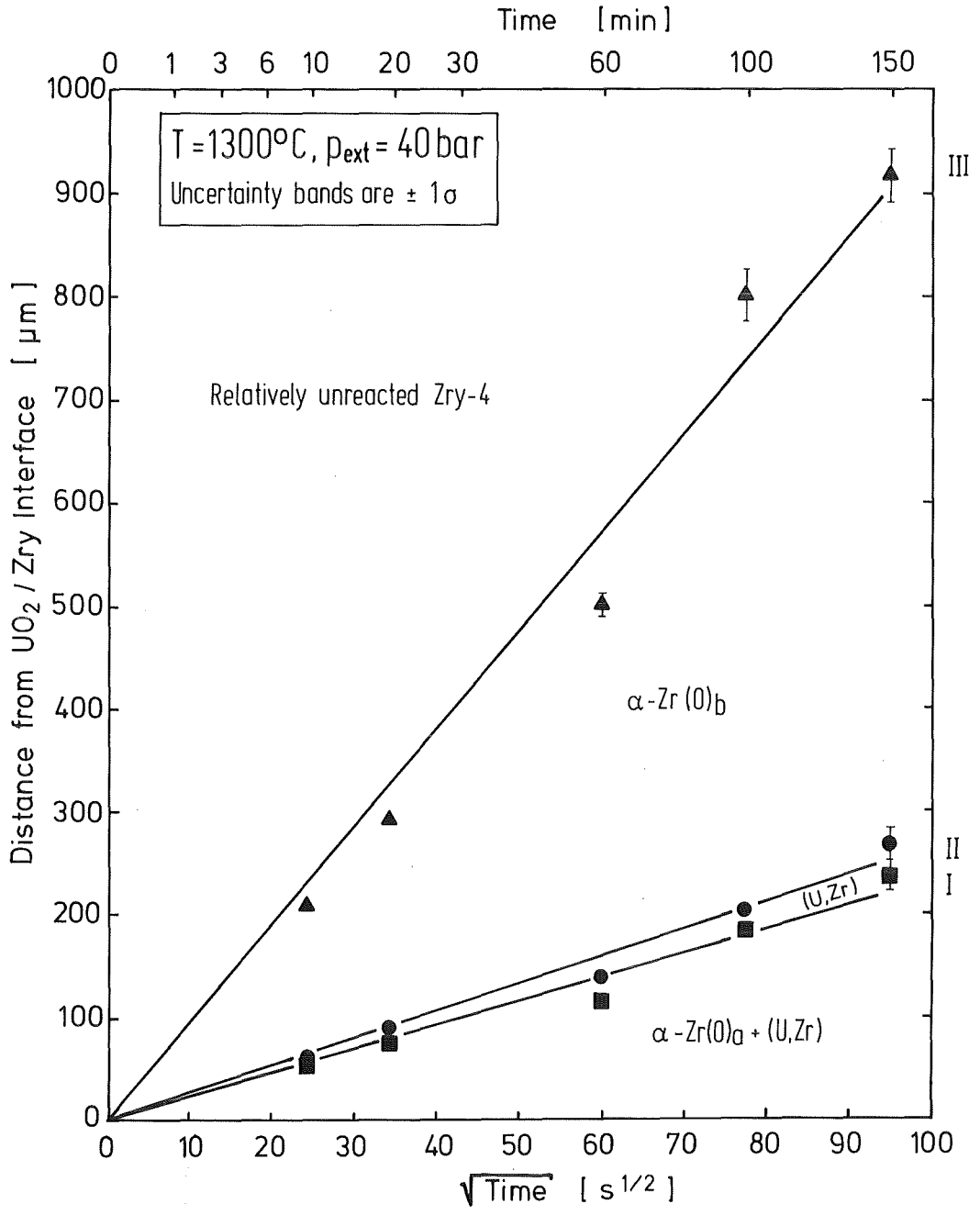

Figure 14: UO_2/Zry-4 reaction zone thickness versus $\sqrt{time}$ ($s^{1/2}$) at 1300°C

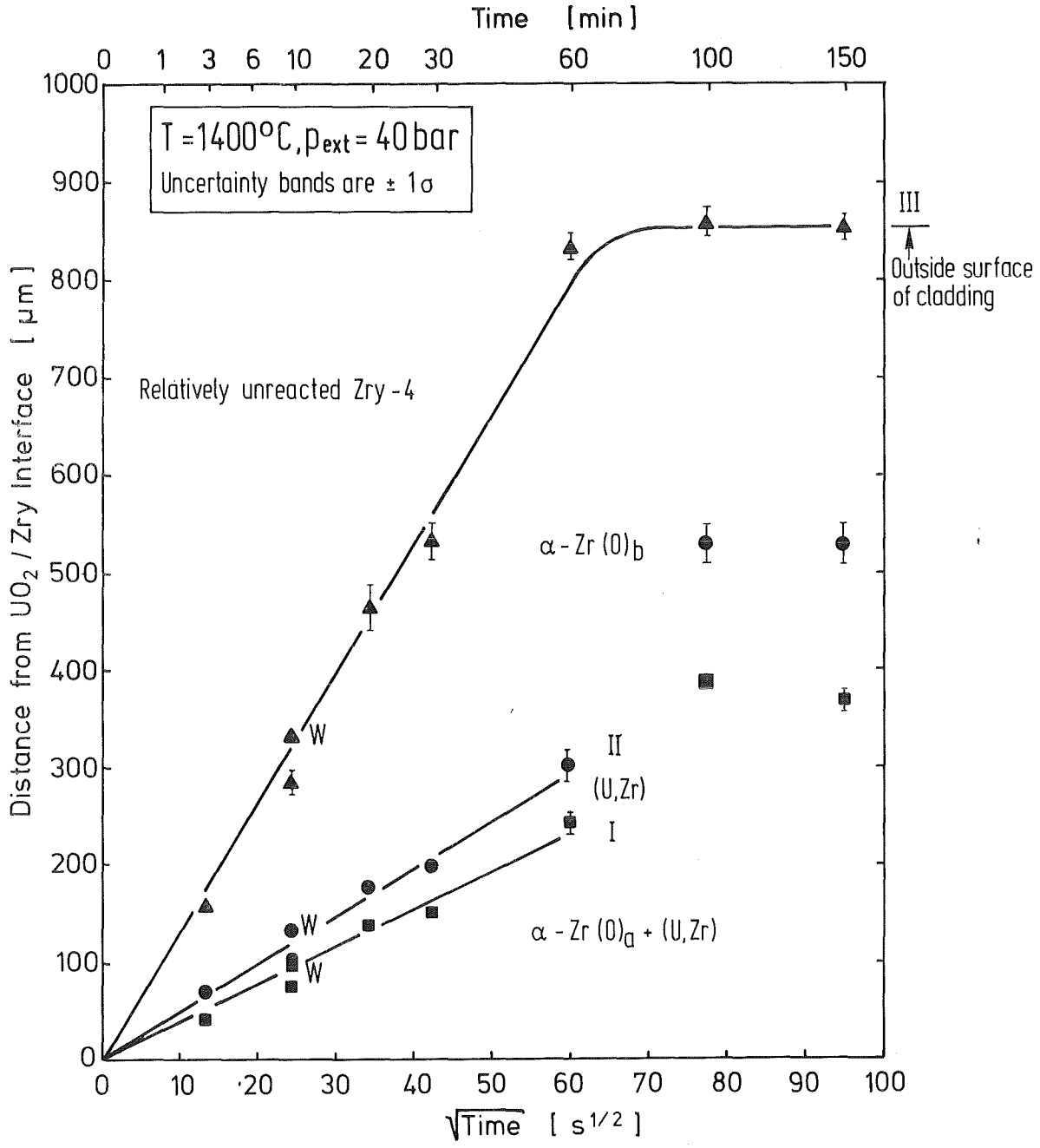

Figure 15: UO_2/Zry-4 reaction zone thickness versus $\sqrt{time}$ ($s^{1/2}$) at 1400°C

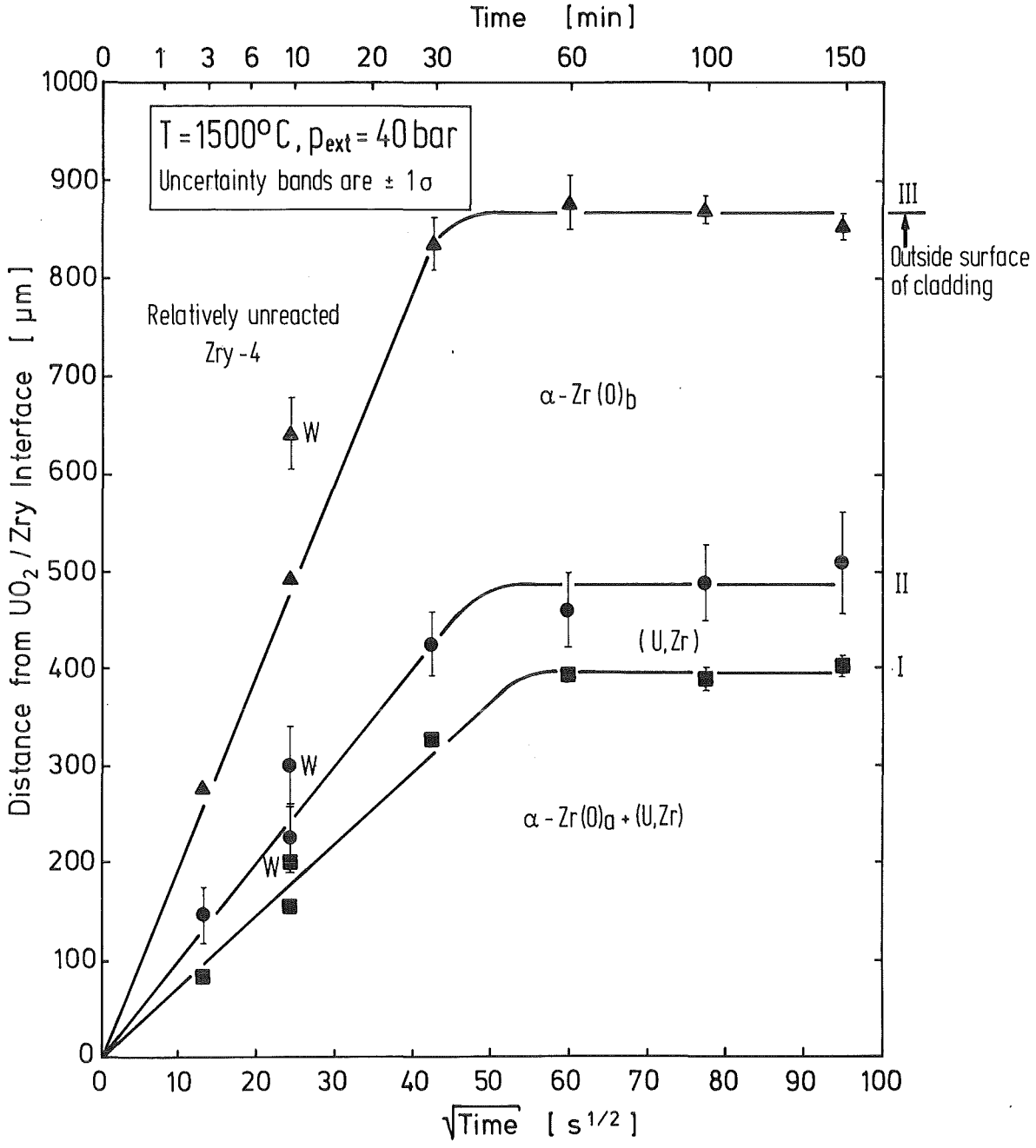

Figure 16: UO_2/Zry-4 reaction zone thickness versus $\sqrt{time}$ ($s^{1/2}$) at 1500°C

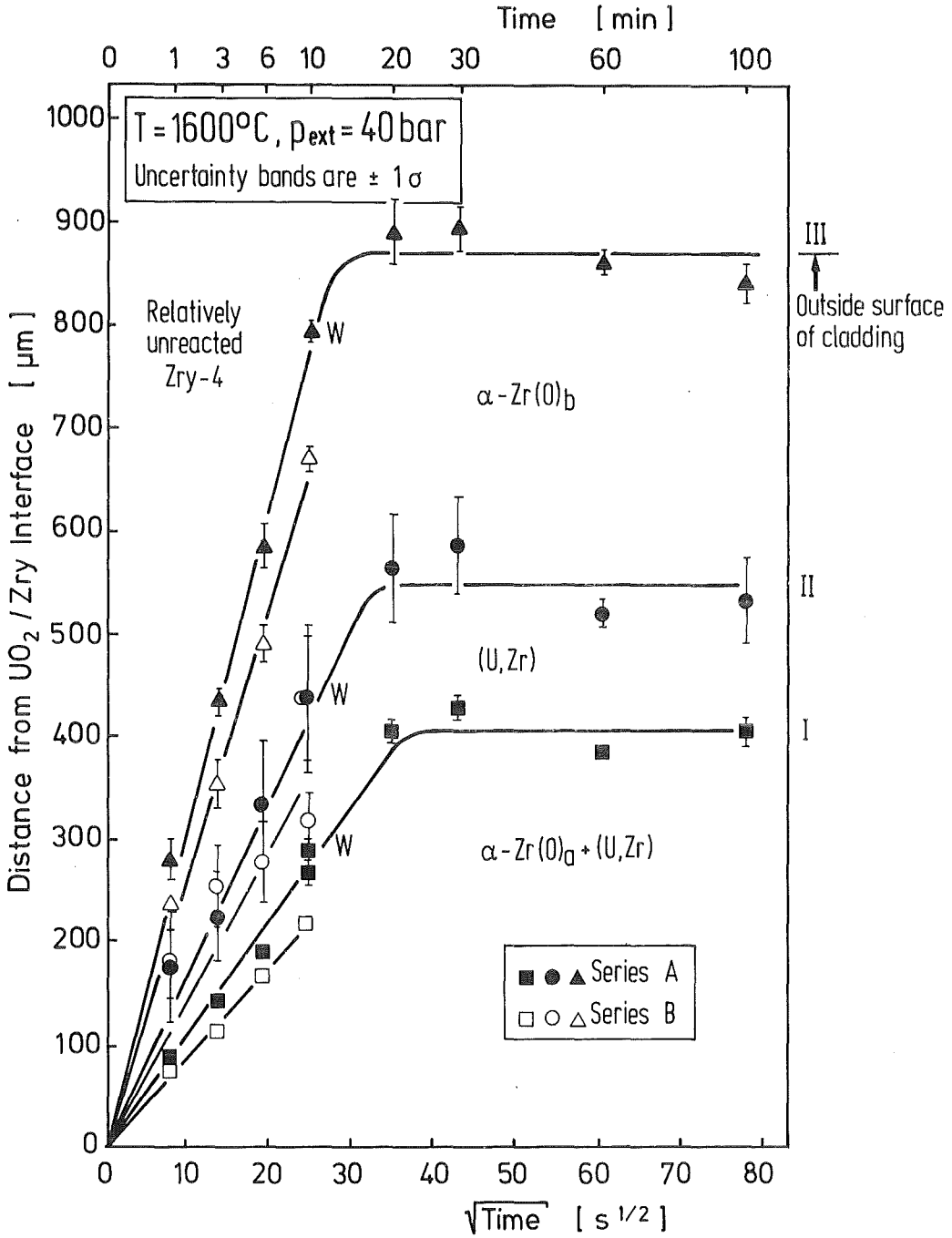

Figure 17: UO_2/Zry-4 reaction zone thickness versus $\sqrt{time}$ ($s^{1/2}$) at 1600°C

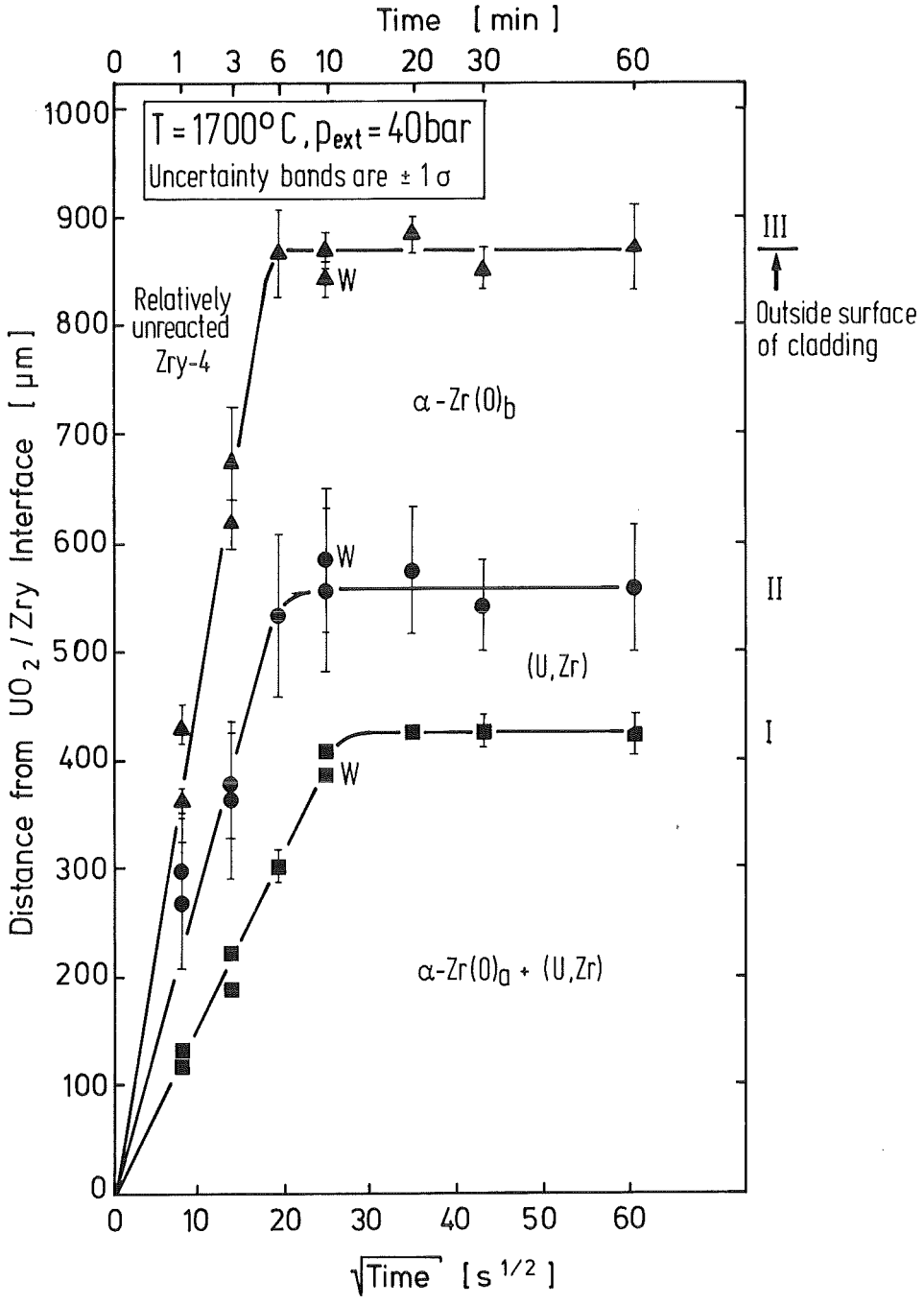

Figure 18: UO_2/Zry-4 reaction zone thickness versus $\sqrt{time}$ ($s^{1/2}$) at 1700°C

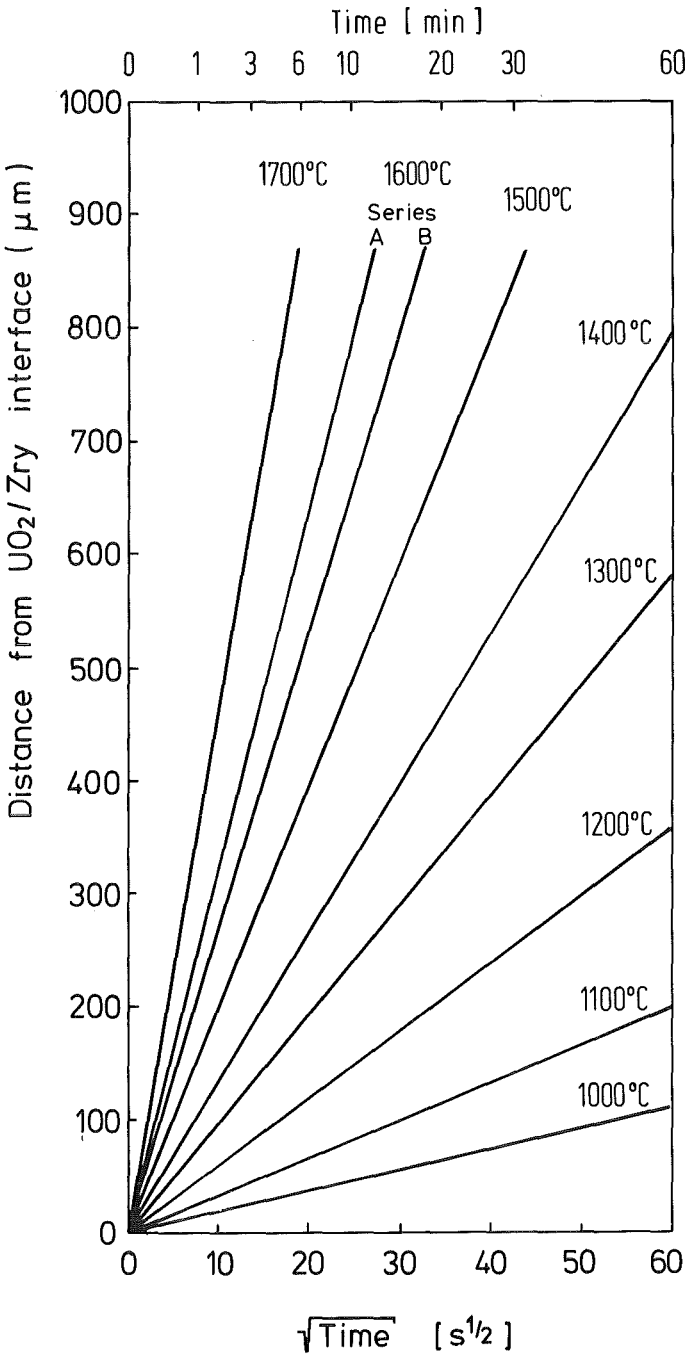

Figure 19: UO_2/Zry-4 total reaction zone thickness versus $\sqrt{time}$ ($s^{1/2}$) from 1000 to 1700°C

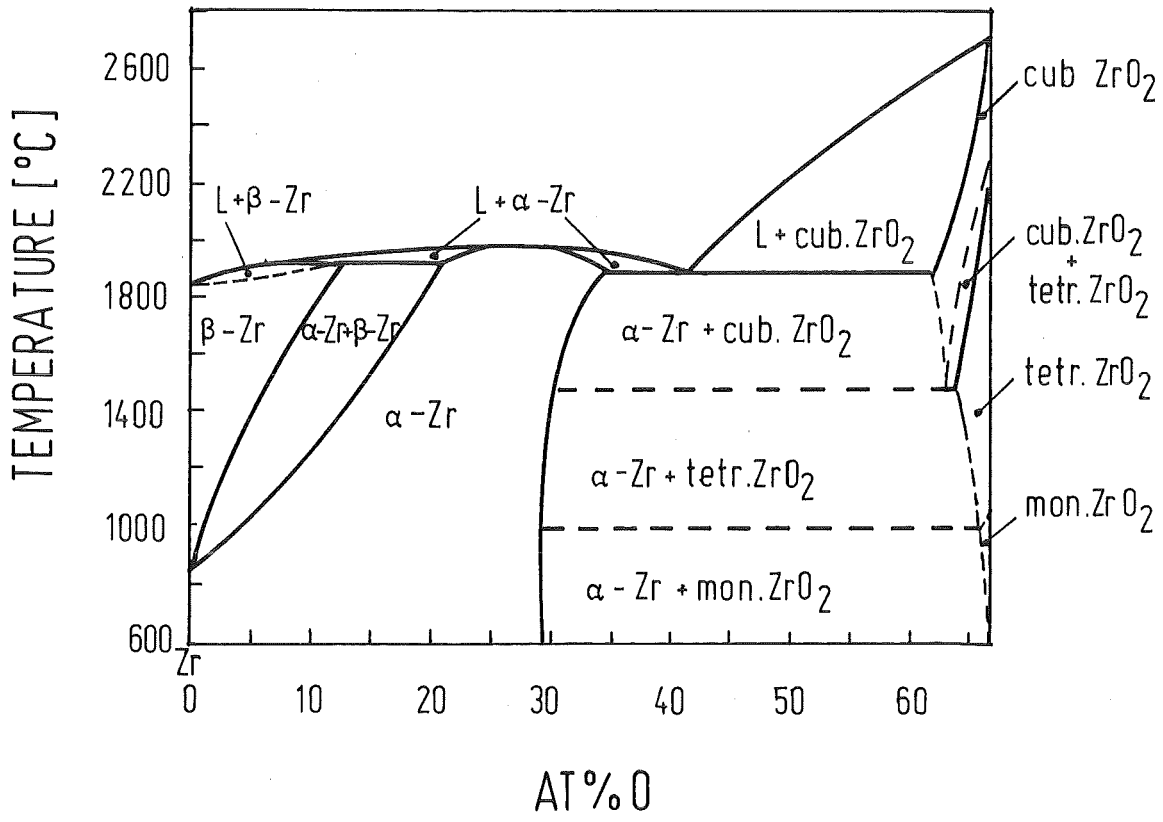

Figure 20: Zr-ZrO_2 phase diagram

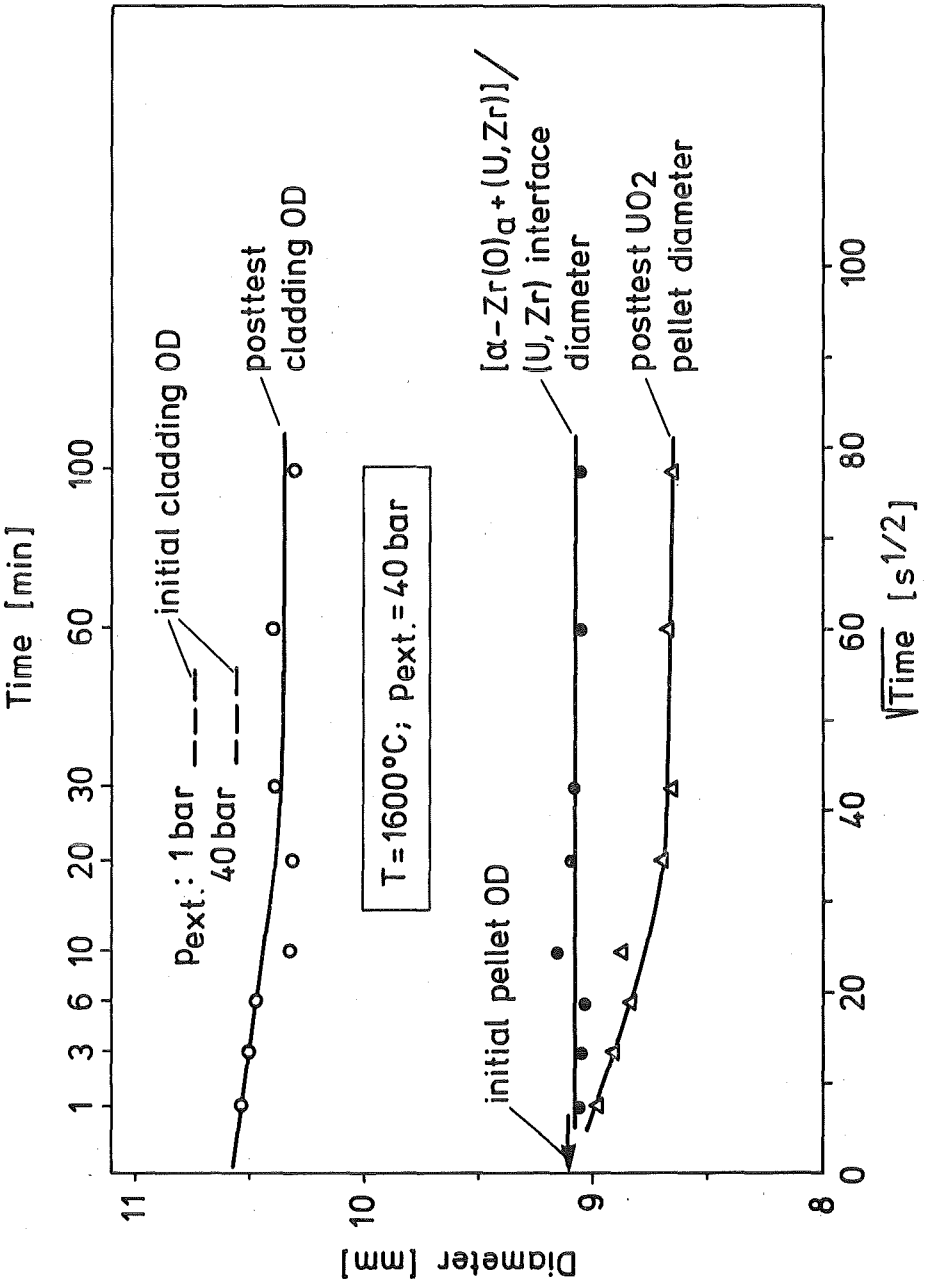

Figure 21: Cladding and reaction layer interface diameters versus time at 1600°C

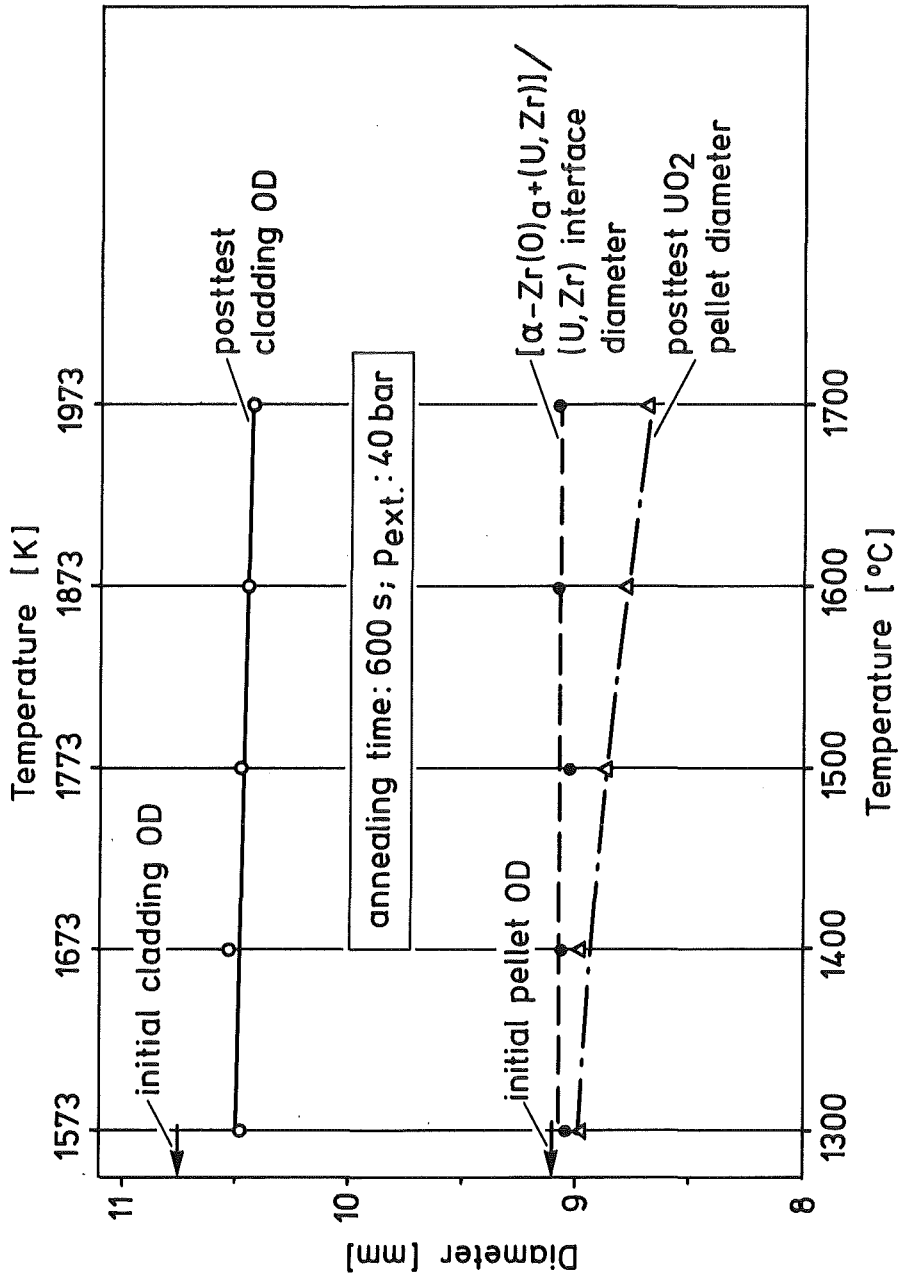

Figure 22: Cladding and reaction layer interface diameters versus temperature after 10 minutes

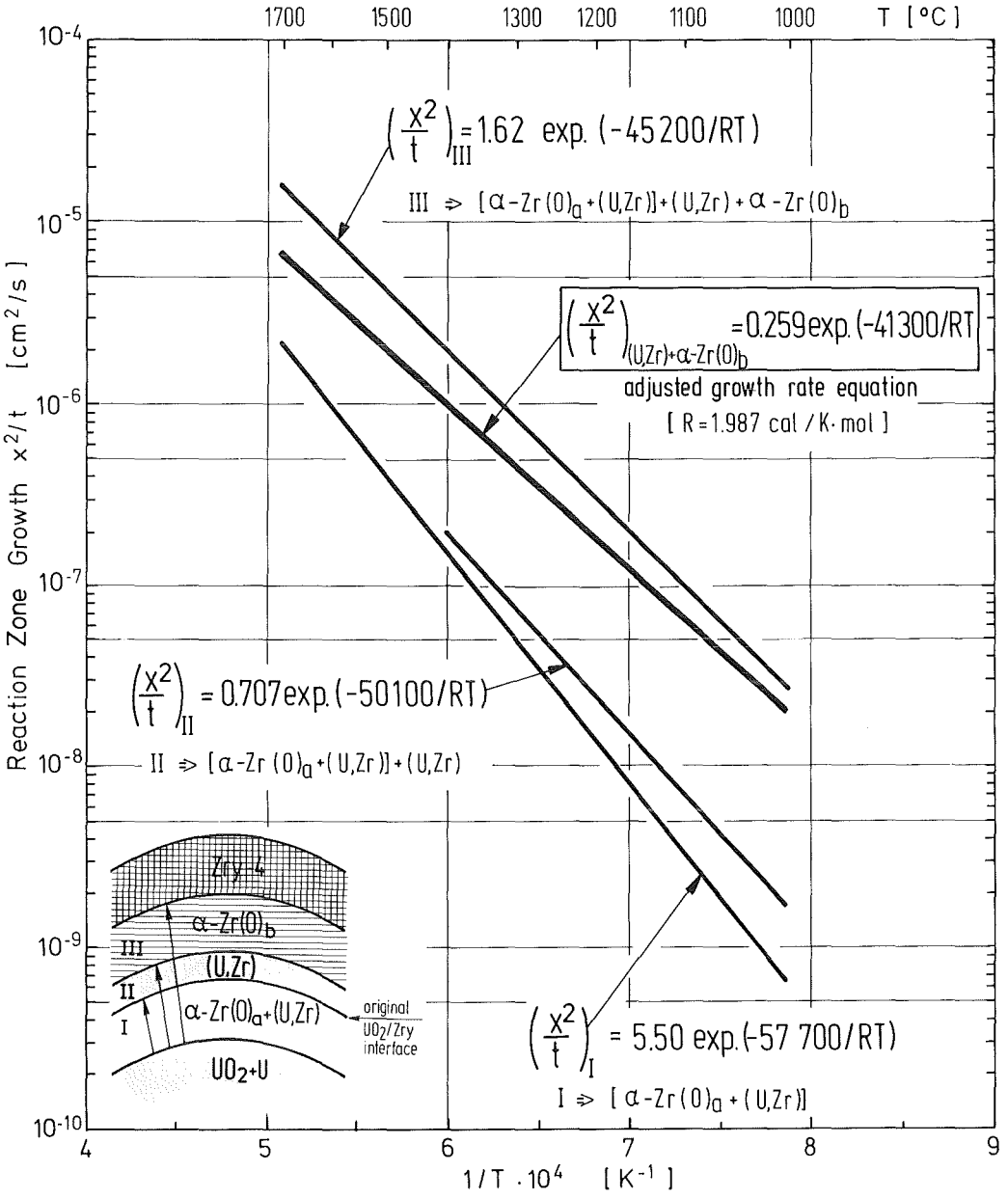

Figure 23: UO_2/Zry-4 reaction zone growth as a function of reciprocal temperature

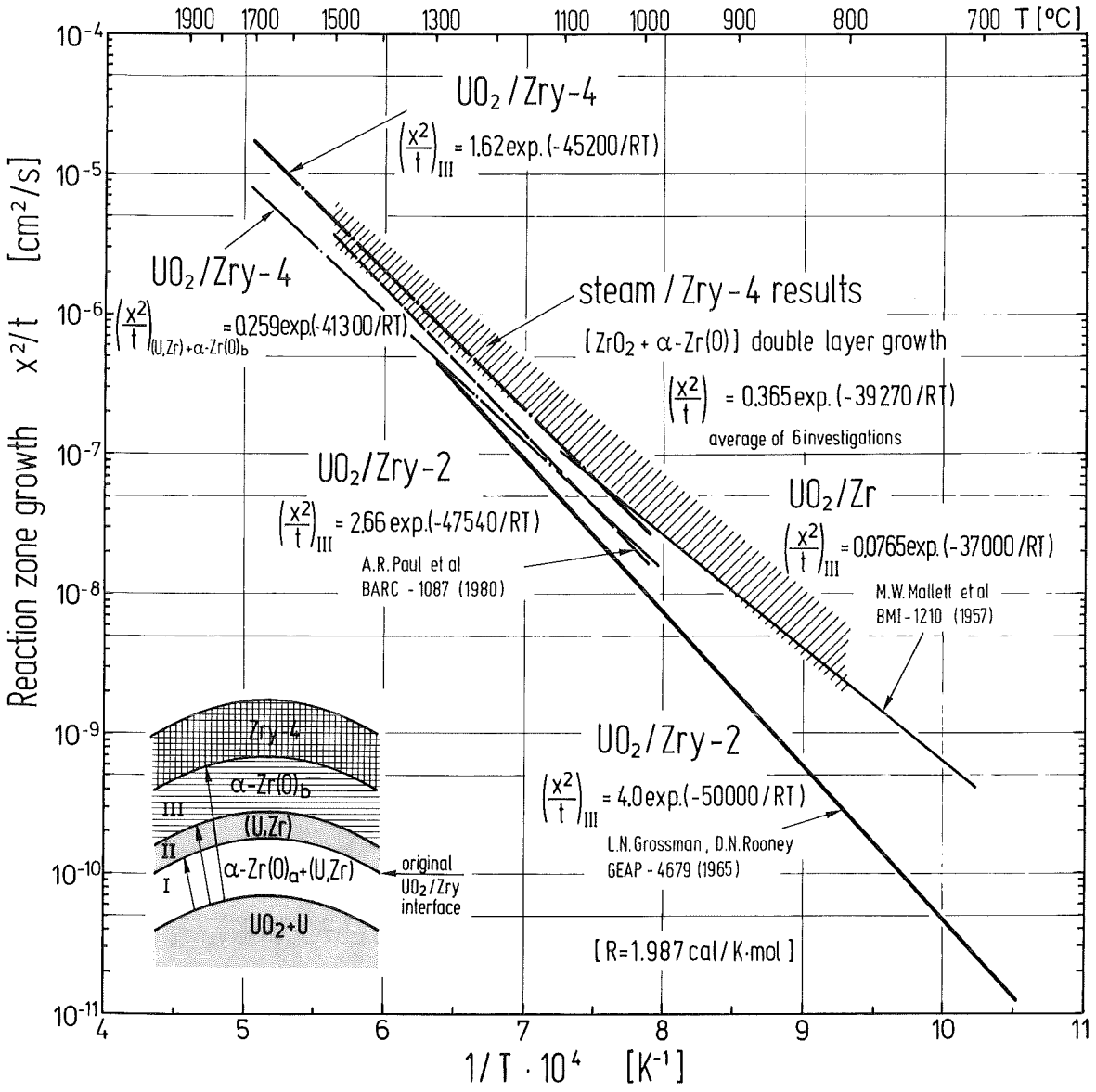

Figure 24: Comparison of the growth rate equations for the UO_2/Zry and steam/Zry reactions

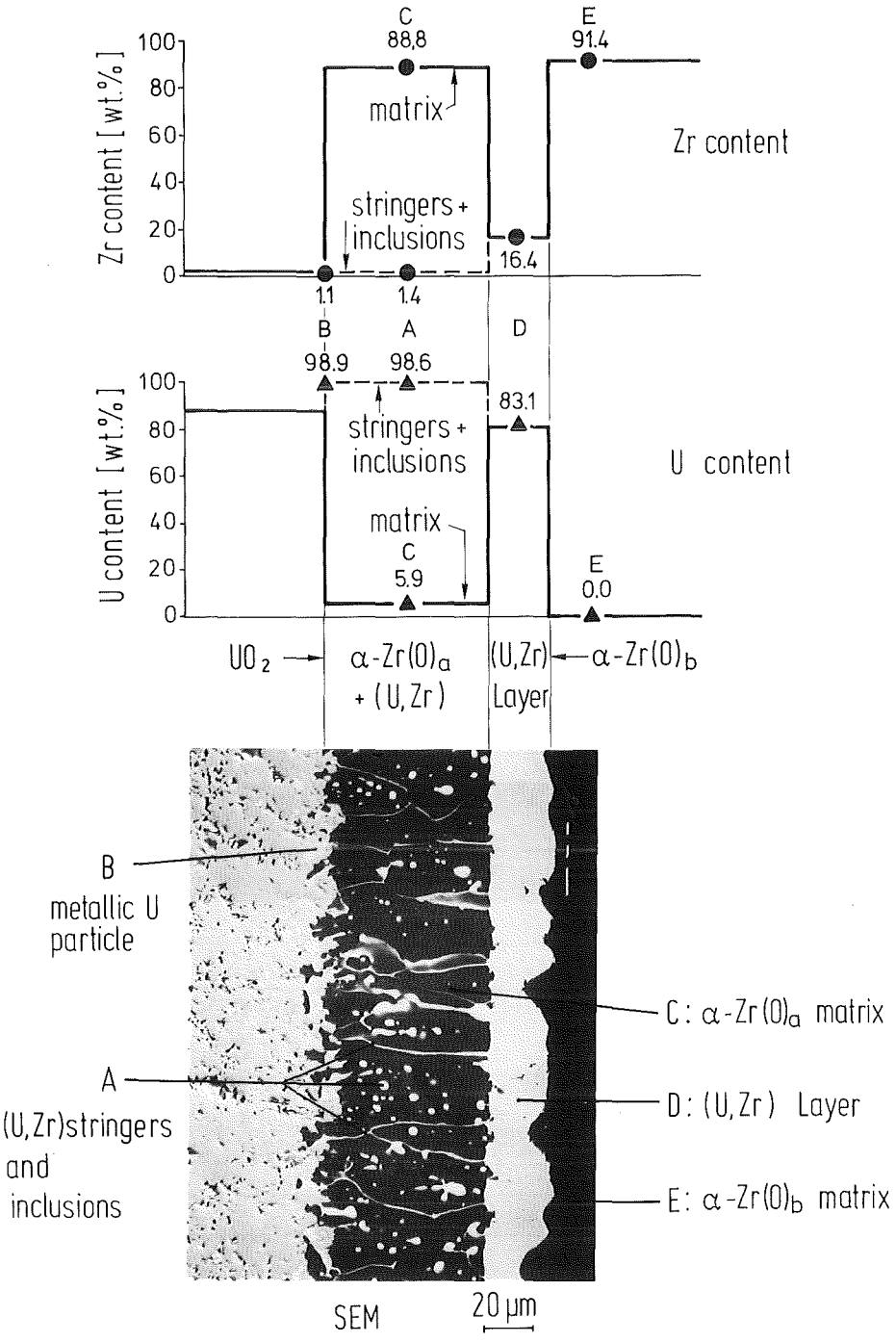

Figure 25: Zr and U contents of the UO_2/Zry-4 layers at 1500°C after 6 min (electron microprobe analysis)

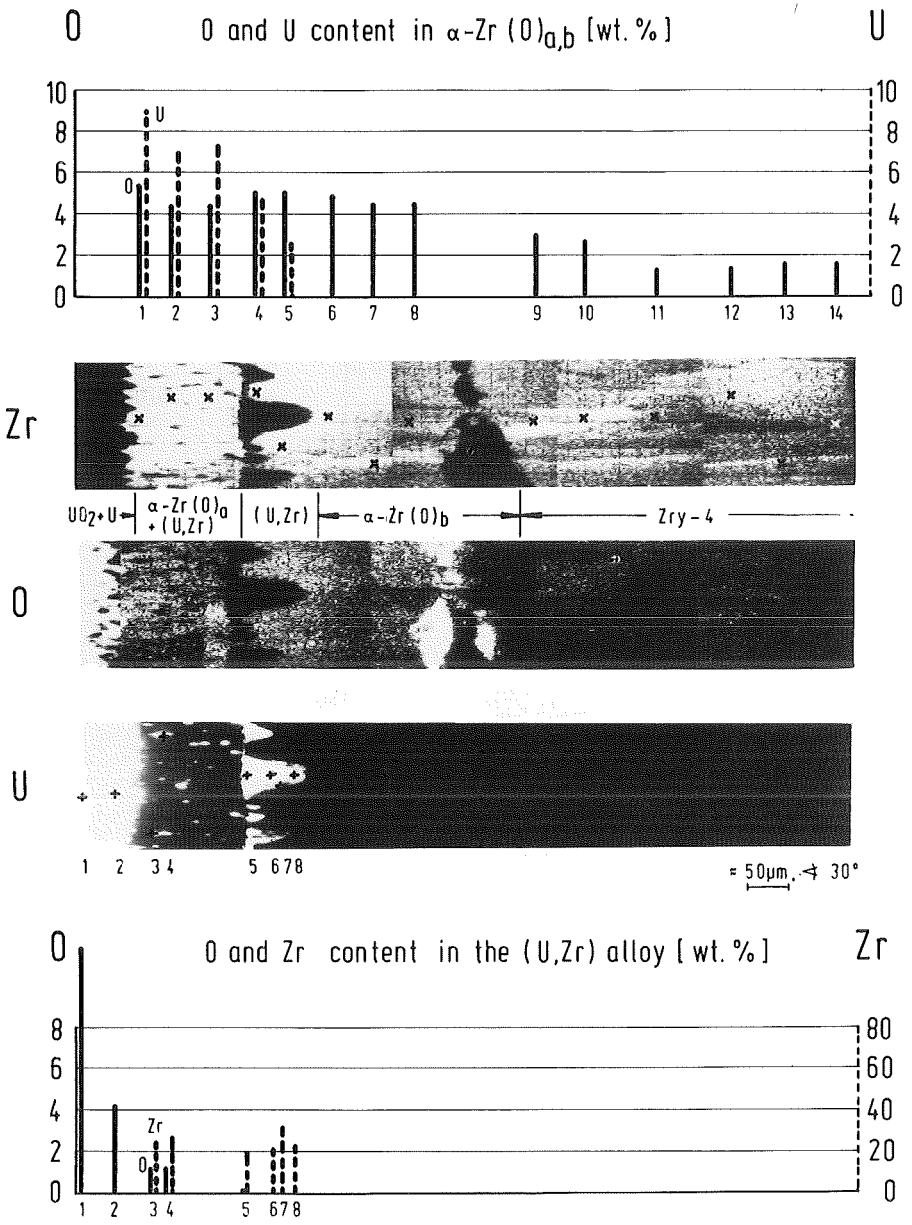

Figure 26a: U, Zr, and O contents of the UO_2/Zircaloy-4 reaction zones at 1500°C after 6 min

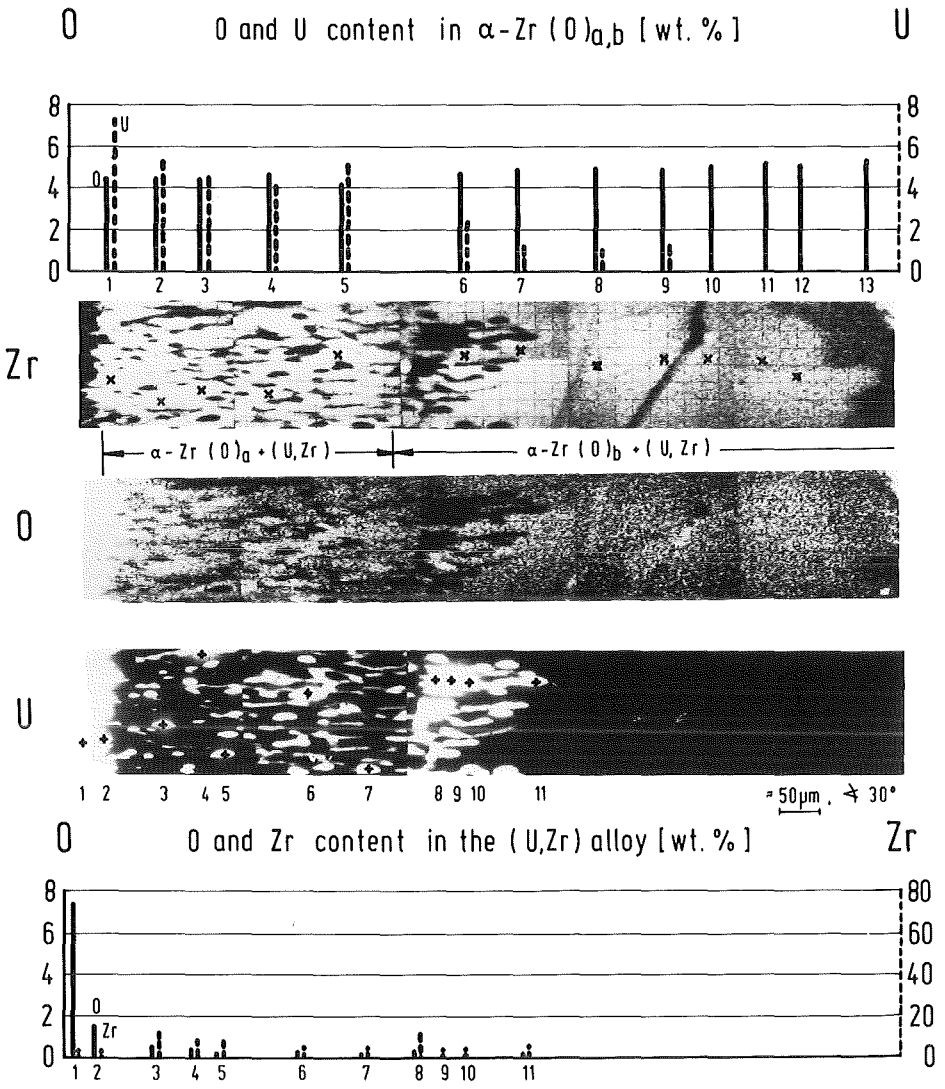

Figure 26b: U, Zr, and O contents of the UO_2/Zircaloy-4 reaction zones at 1500°C after 30 min

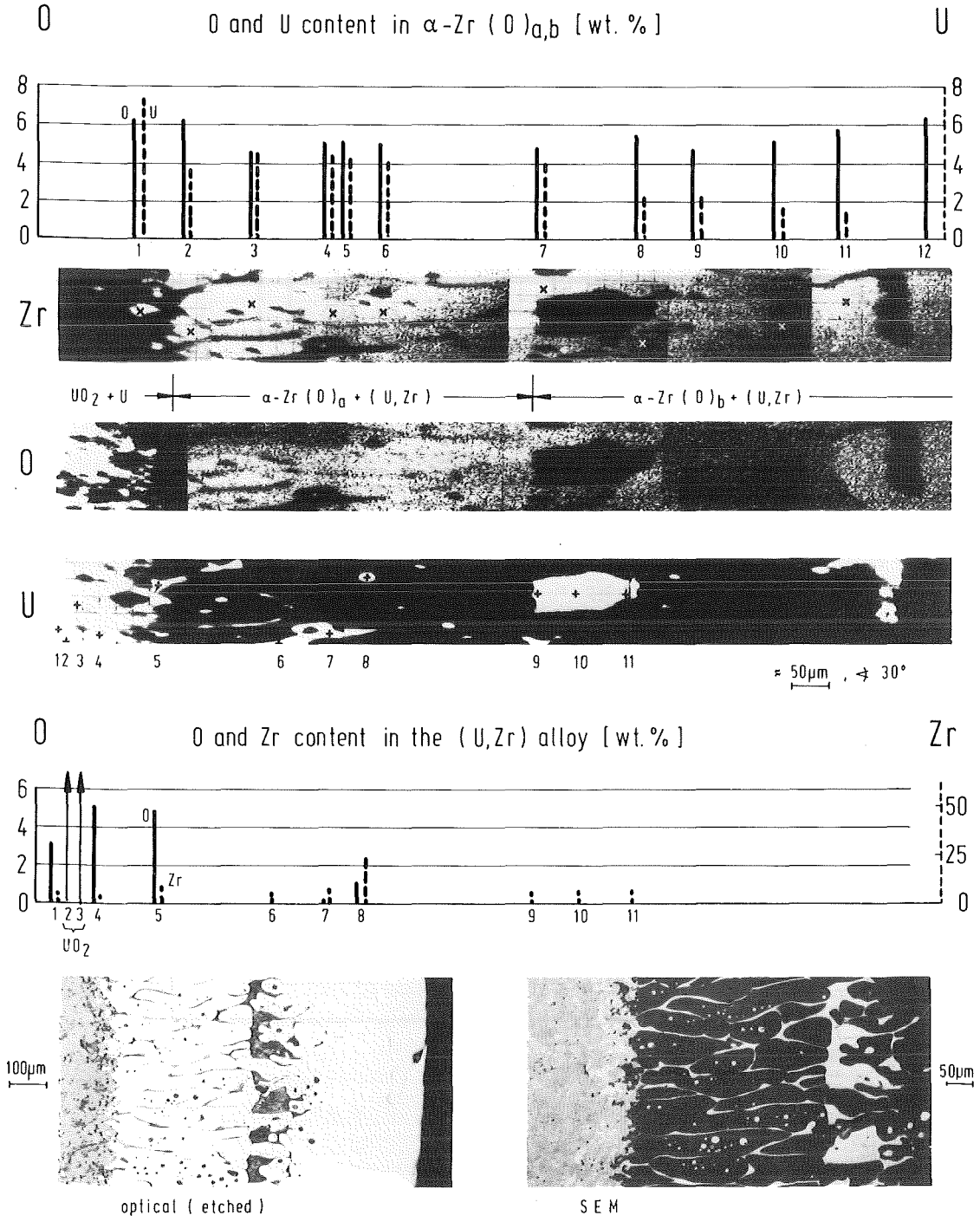

Figure 26c: U, Zr, and O contents of the UO_2/Zircaloy-4 reaction zones at 1500°C after 100 min

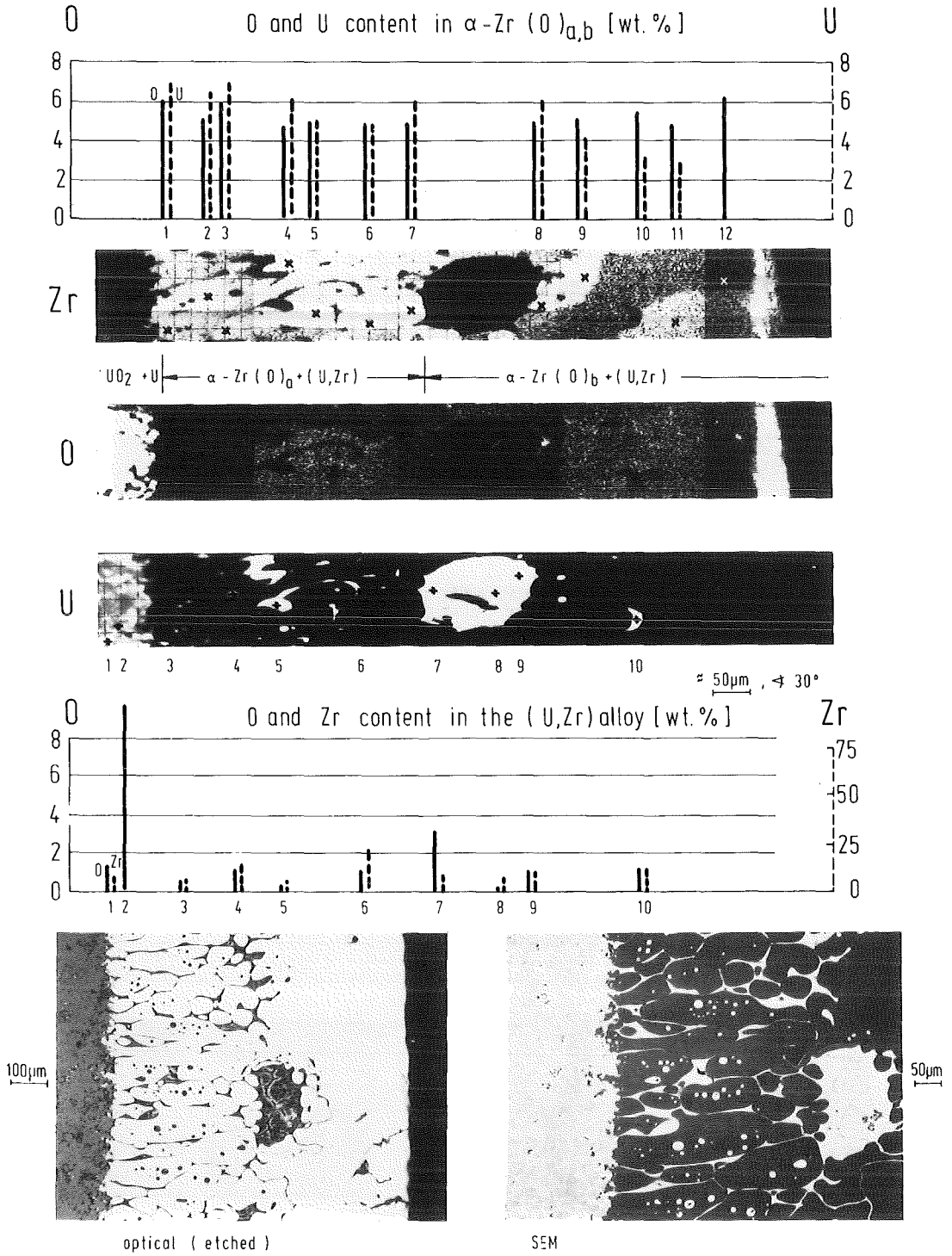

Figure 26d: U, Zr, and O contents of the UO_2/Zircaloy-4 reaction zones at 1500°C after 150 min

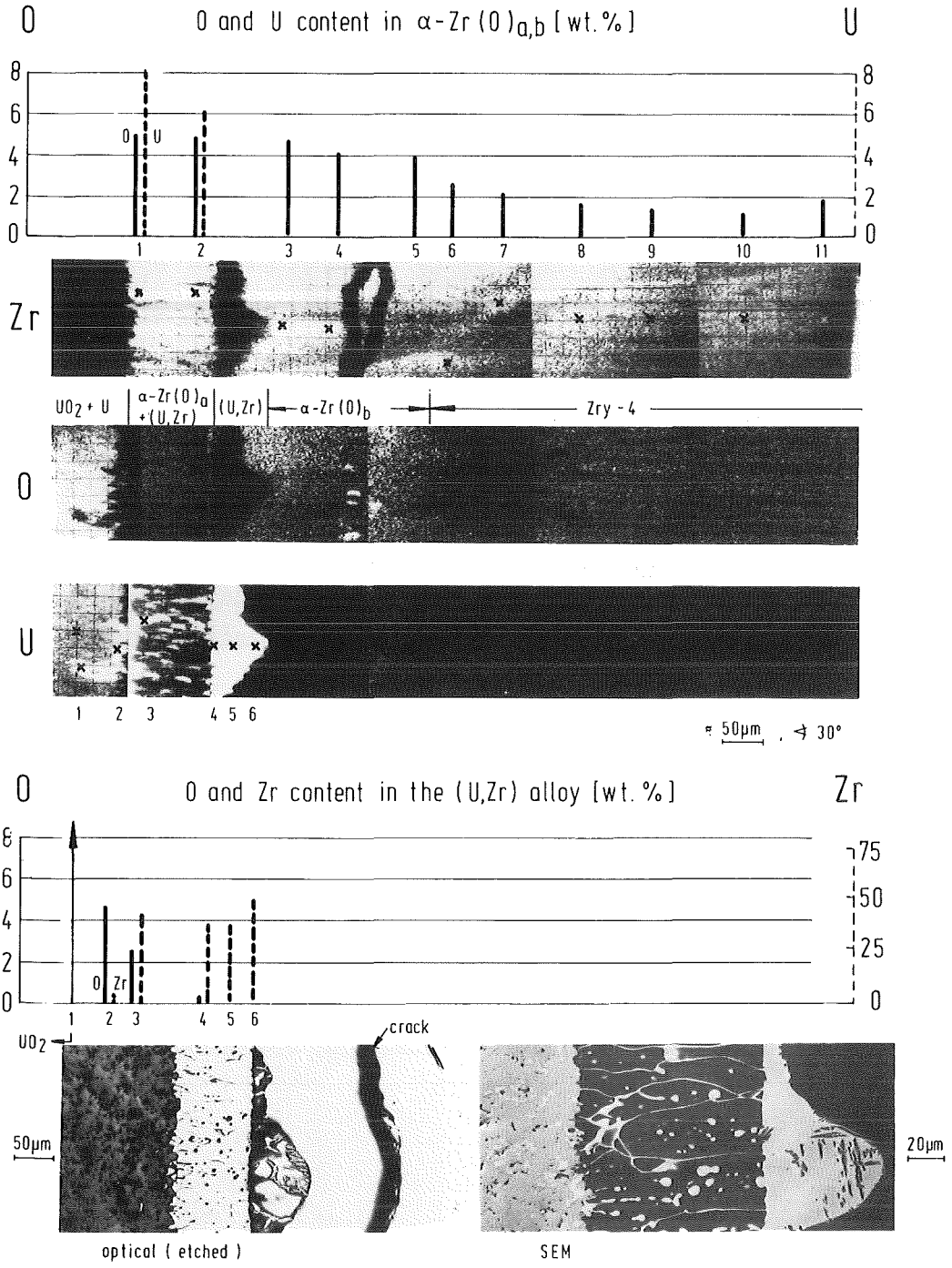

Figure 27a: U, Zr, and O contents of the UO_2/Zircaloy-4 reaction zones at 1600°C after 3 min

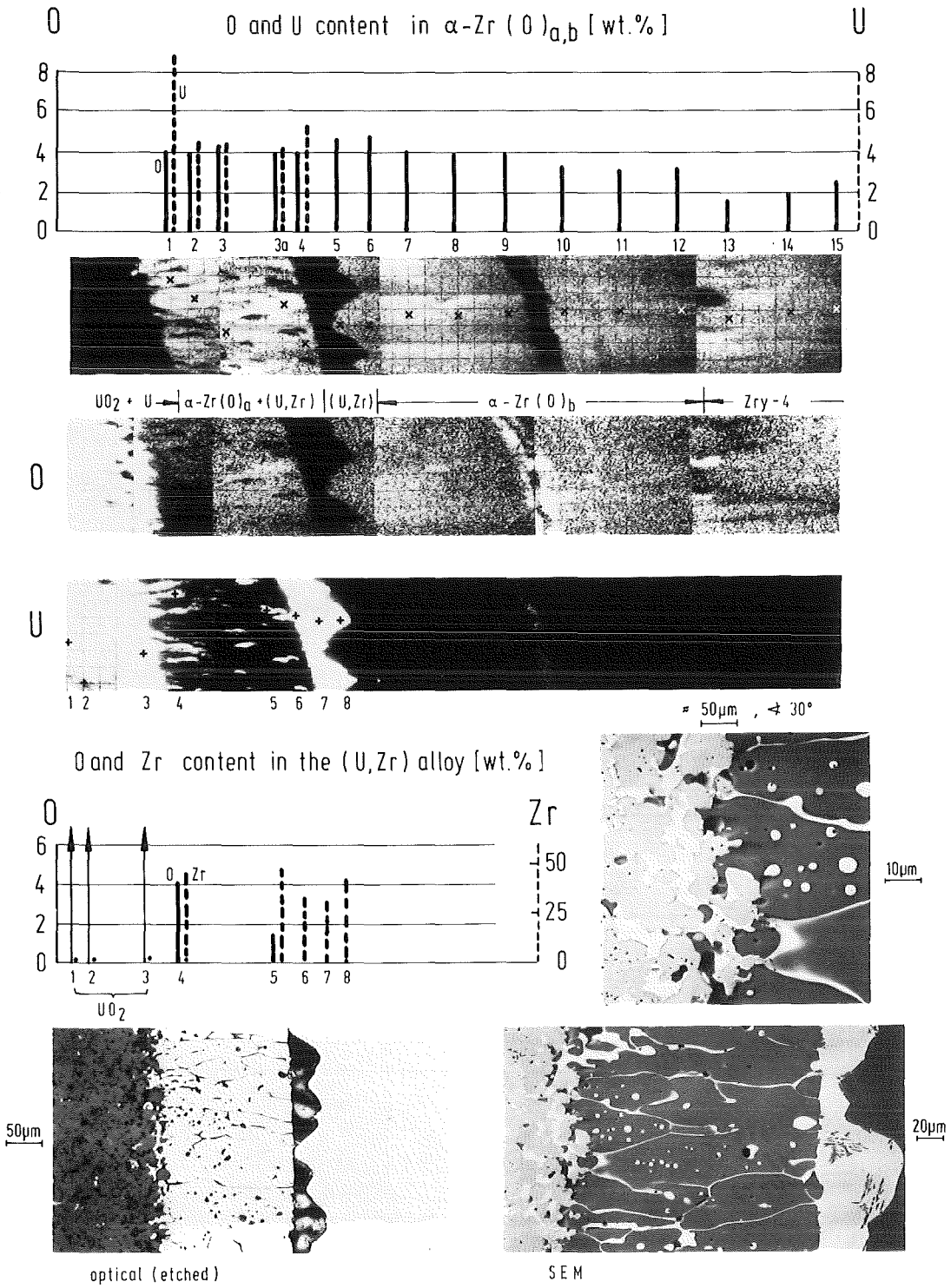

Figure 27b: U, Zr, and O contents of the UO_2/Zircaloy-4 reaction zones at 1600°C after 20 min

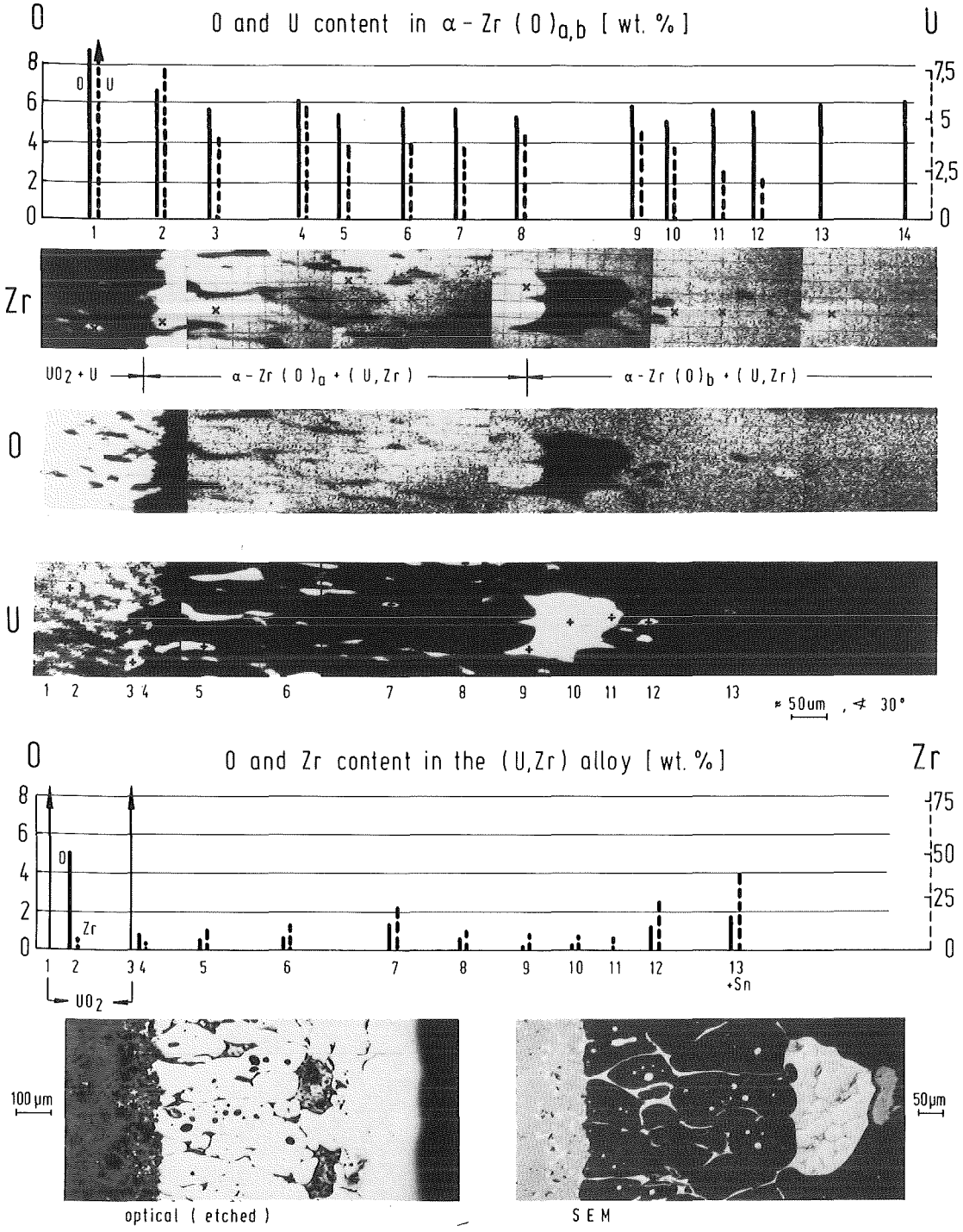

Figure 27c: U, Zr, and O contents of the UO_2/Zircaloy-4 reaction zones at 1600°C after 100 min

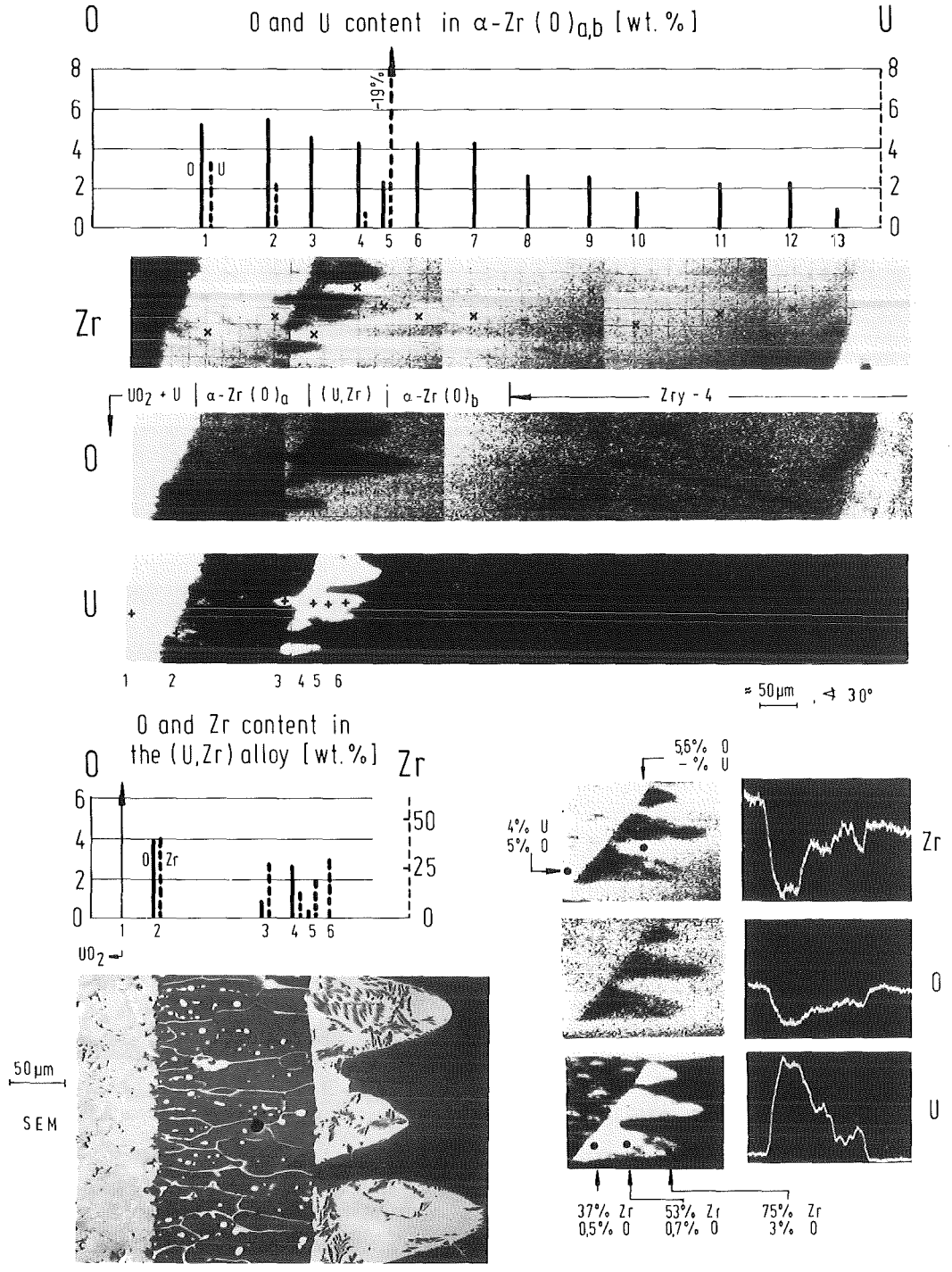

Figure 28a: U, Zr, and O contents of the UO_2/Zircaloy-4 reaction zones at 1700°C after 3 min

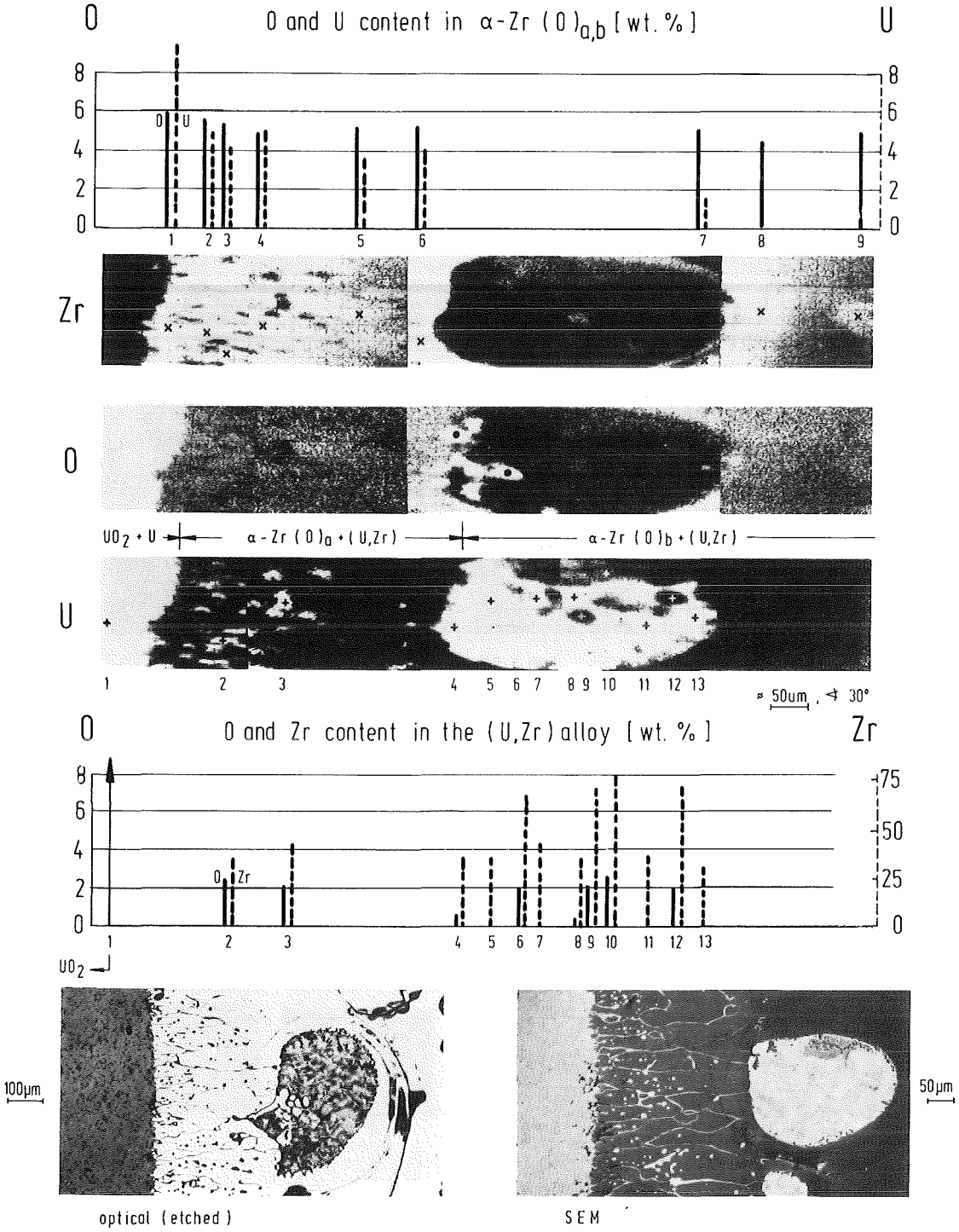

Figure 28b: U, Zr, and O contents of the UO_2/Zircaloy-4 reaction zones at 1700°C after 10 min

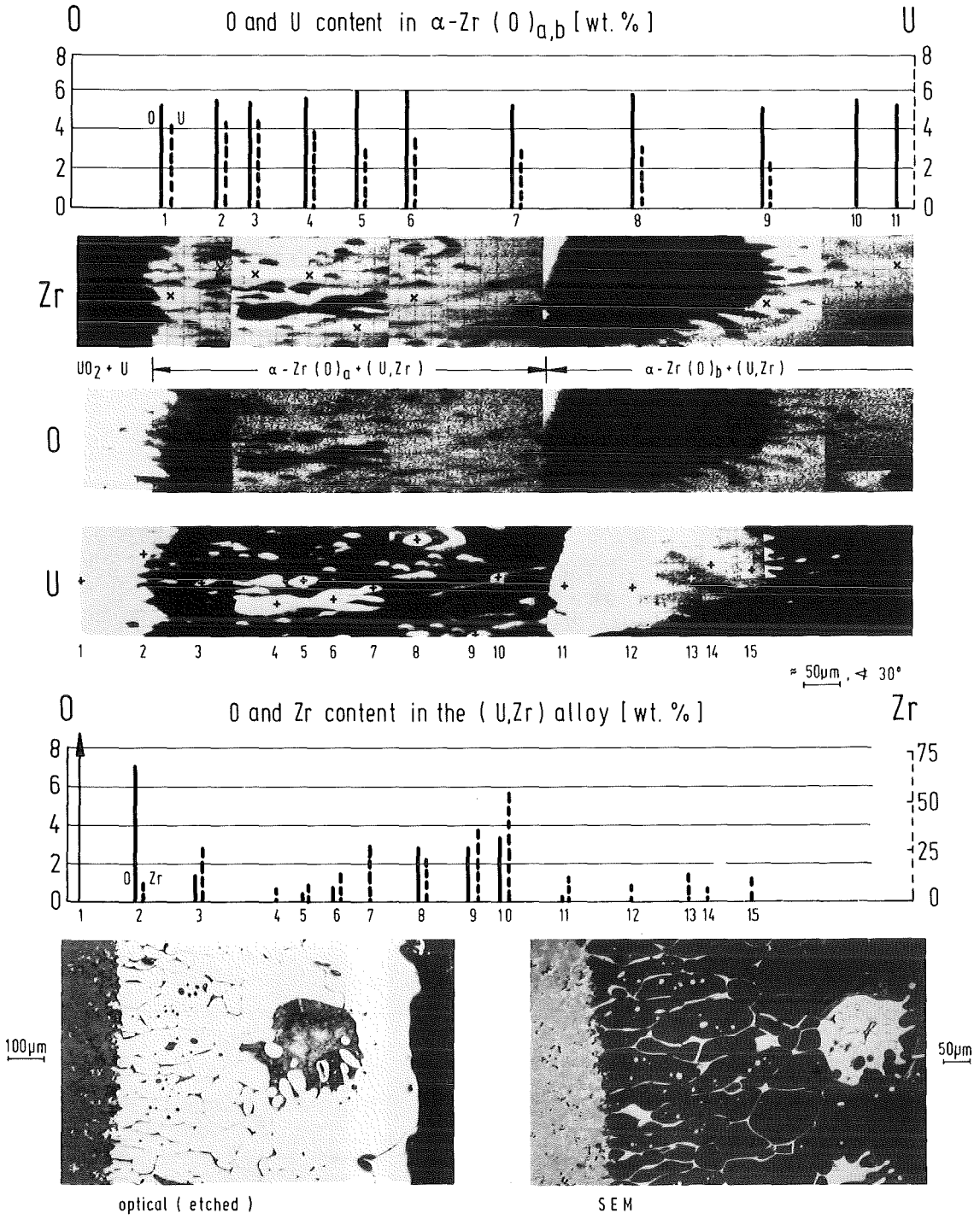

Figure 28c: U, Zr, and O contents of the UO_2/Zircaloy-4 reaction zones at 1700°C after 60 min

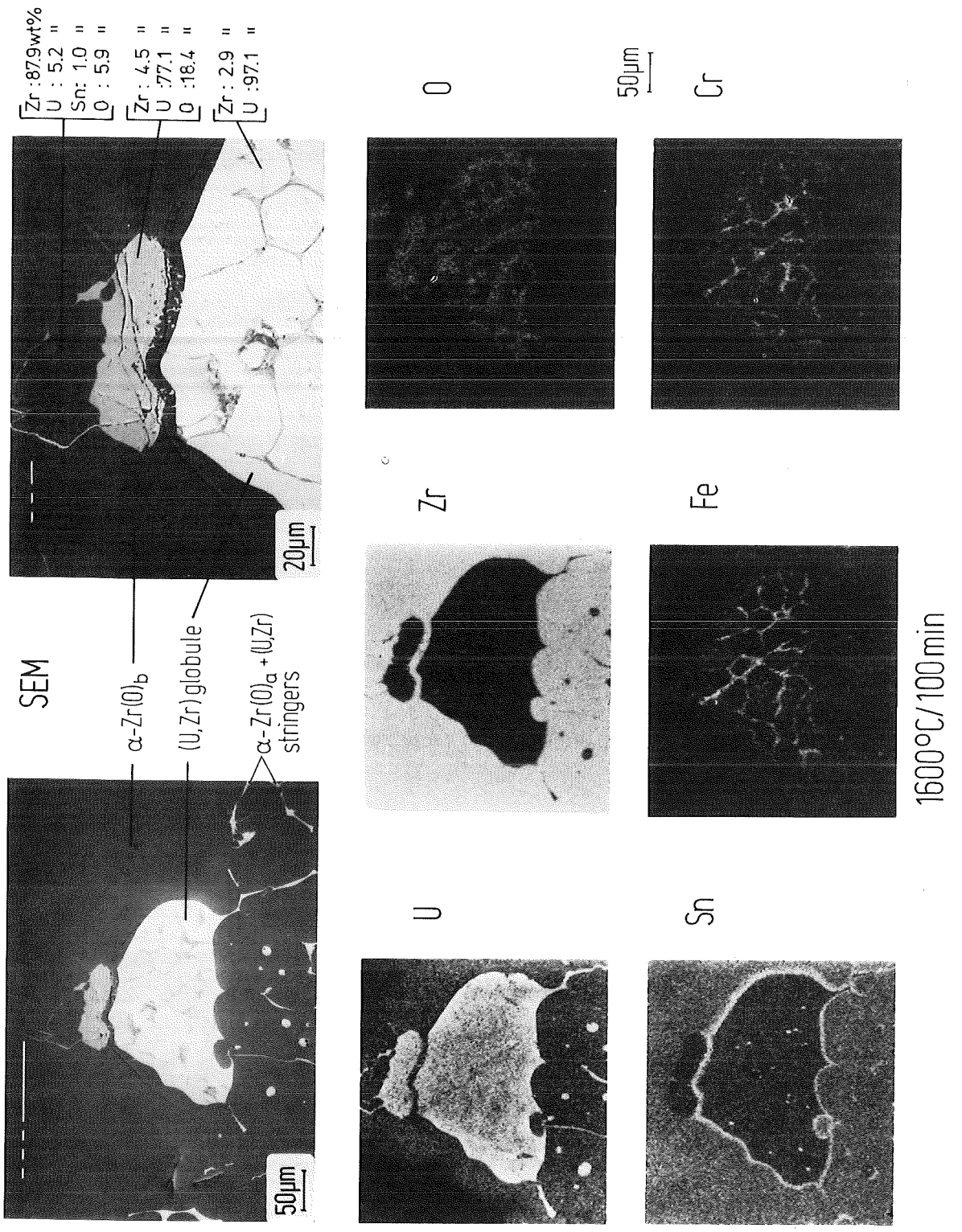

Figure 29: (U,Zr) reaction layer at 1600°C after 100 minutes (electron microprobe analyses)

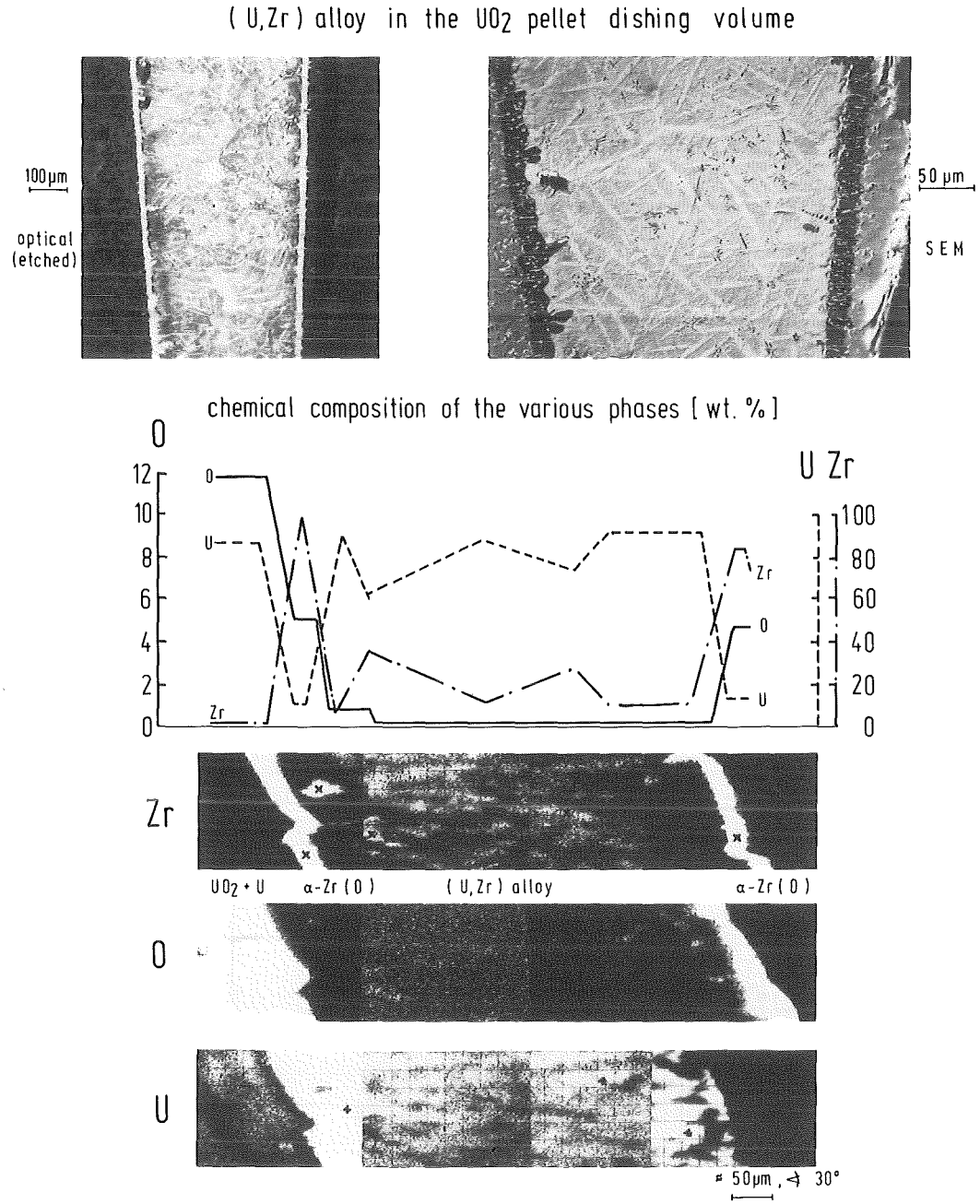

Figure 30: Chemical interaction between the liquid (U,Zr) alloy [which flows into the pellet dishing volumes due to the external overpressure] and UO_2 at 1700°C after 60 min

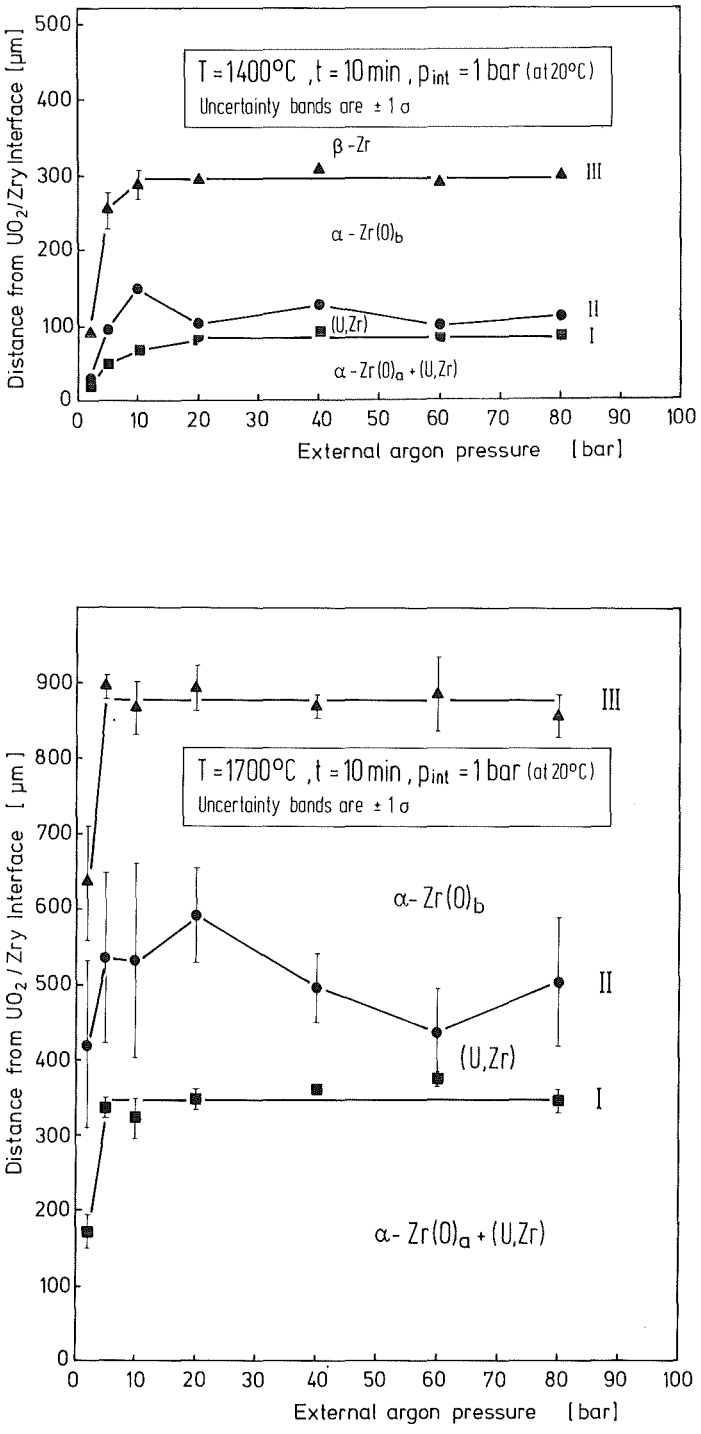

Figure 31: UO_2/Zry-4 reaction zone thickness versus external argon pressure at 1400 and 1700°C (annealing time 10 minutes)

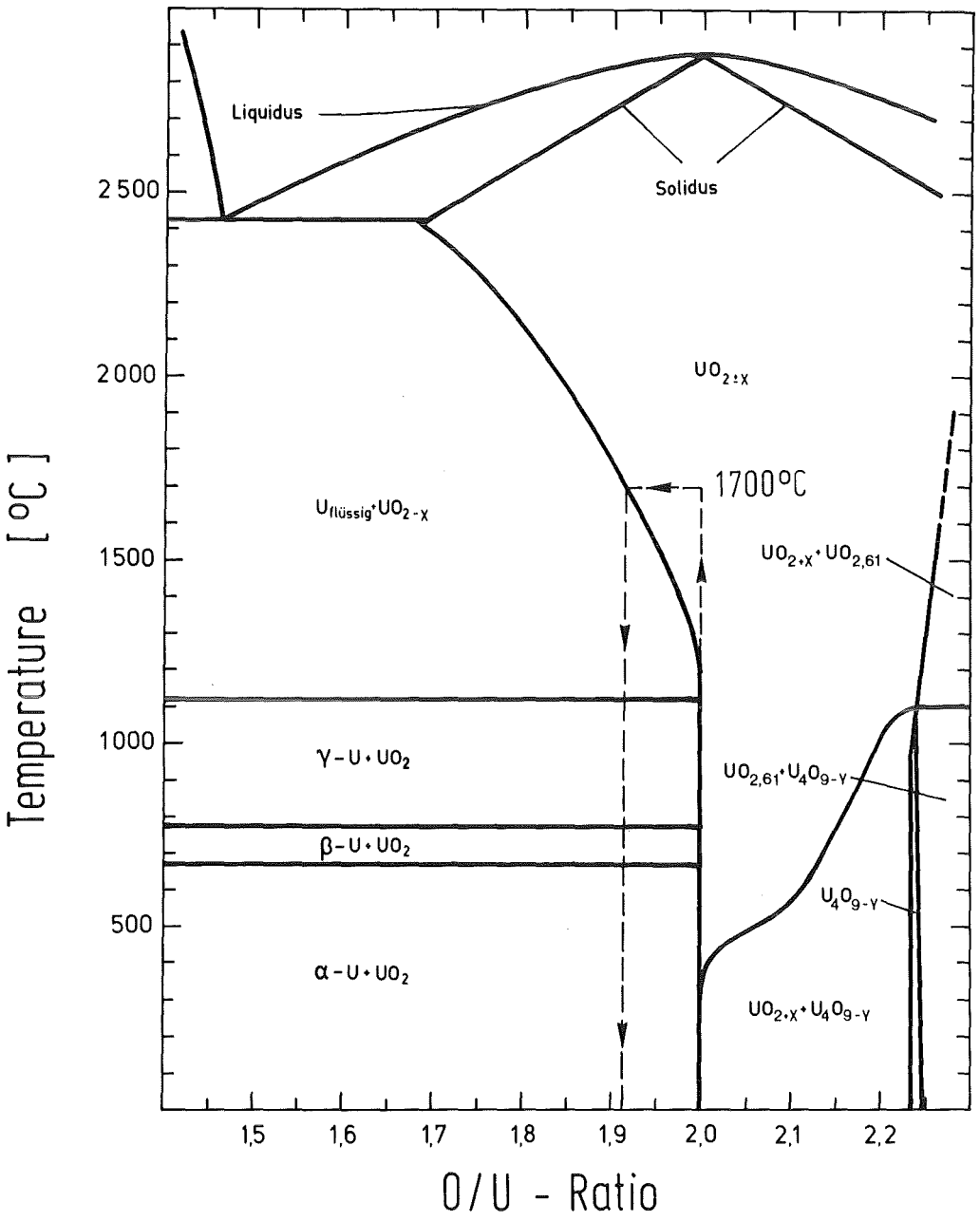

Figure 32: Detail of the U-O phase diagram

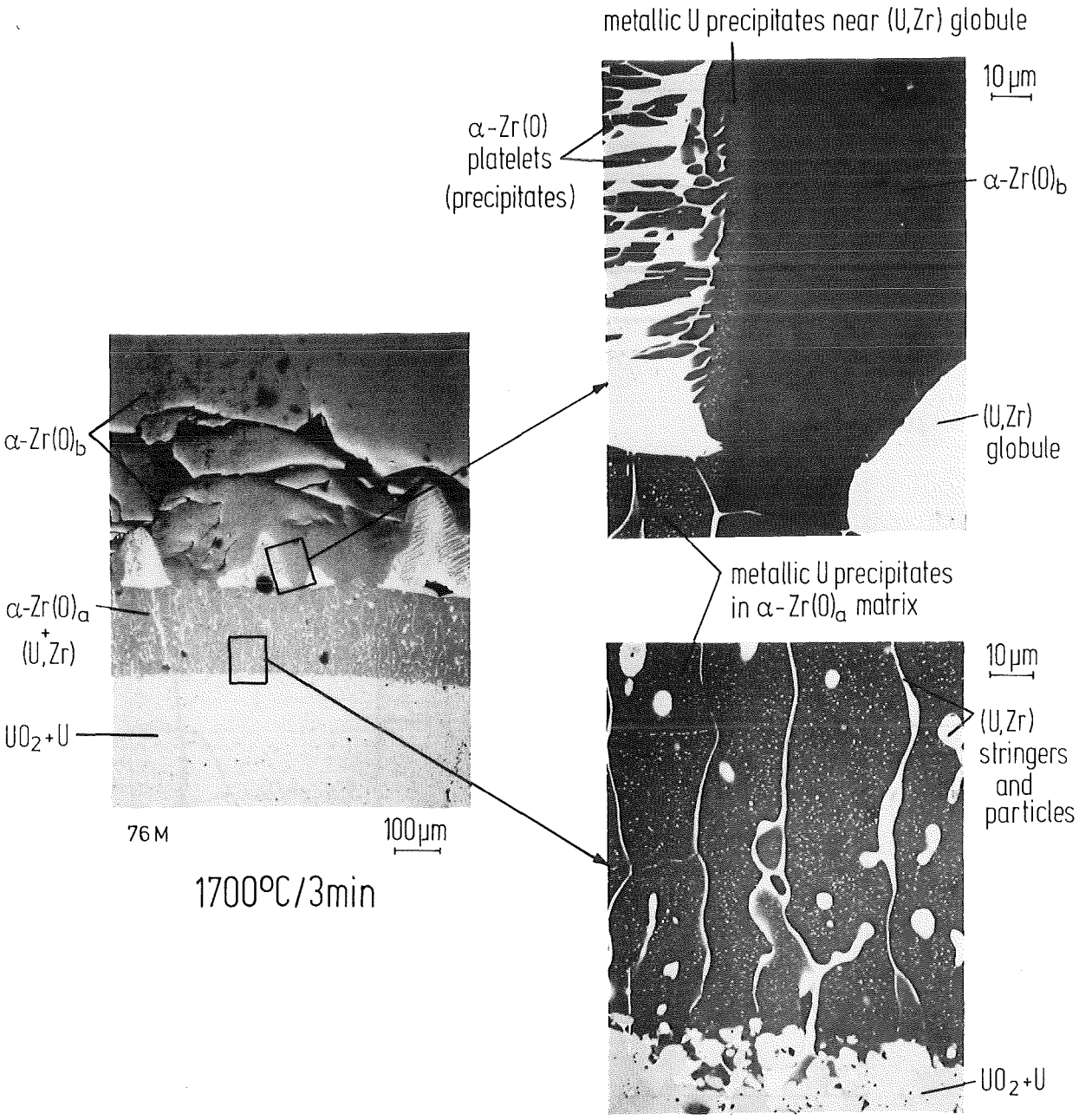

Figure 33: Metallic U precipitates in α-Zr(O)$_a$ matrix after 3 min at 1700°C (SEM photographs)

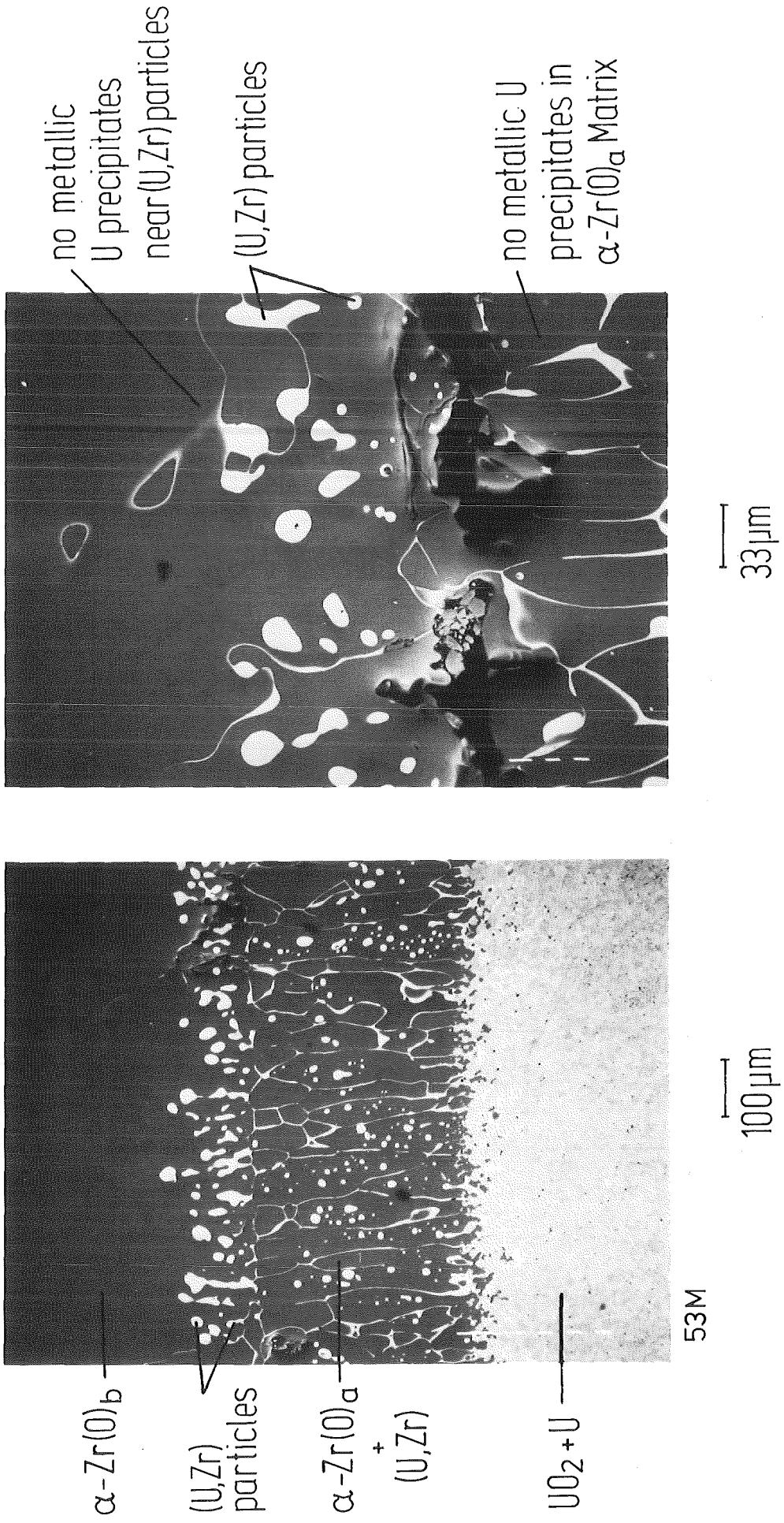

Figure 34: Appearance of (U,Zr) alloy layer after 100 minutes at 1400°C (SEM photographs)

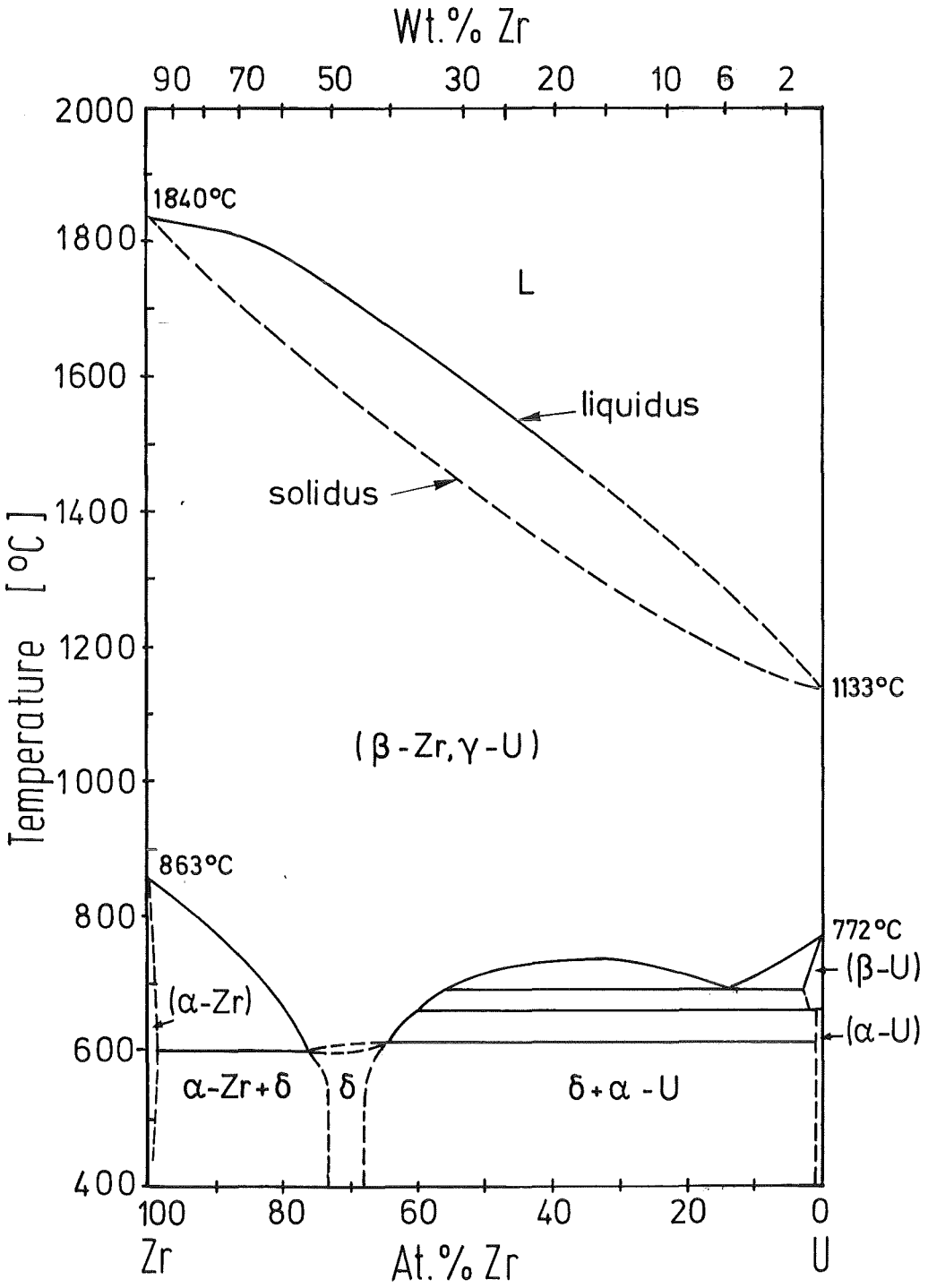

D. Summers - Smith (1954)
A.N. Holden, W.E. Seymour (1956)

Figure 35: U-Zr phase diagram

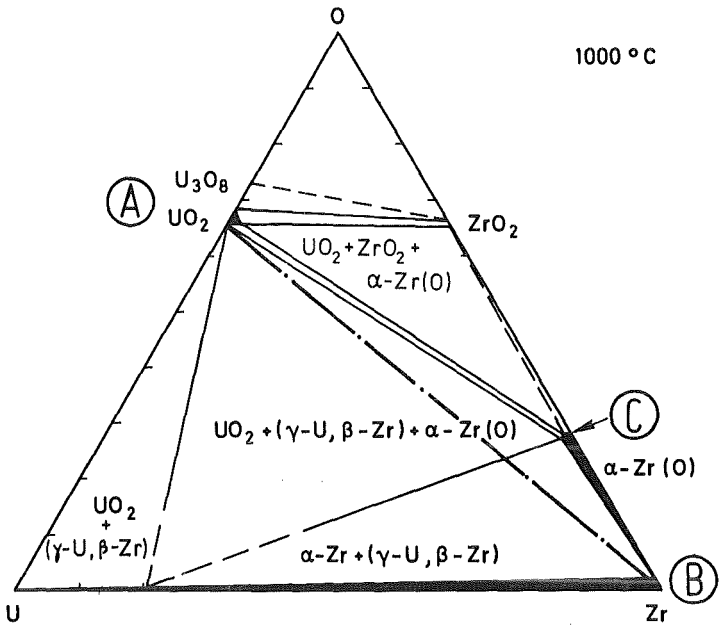

A→B represents the initial UO_2/Zr tie line

Figure 36: Equilibrium phase diagram of the (U-Zr-O) ternary system at 1000°C

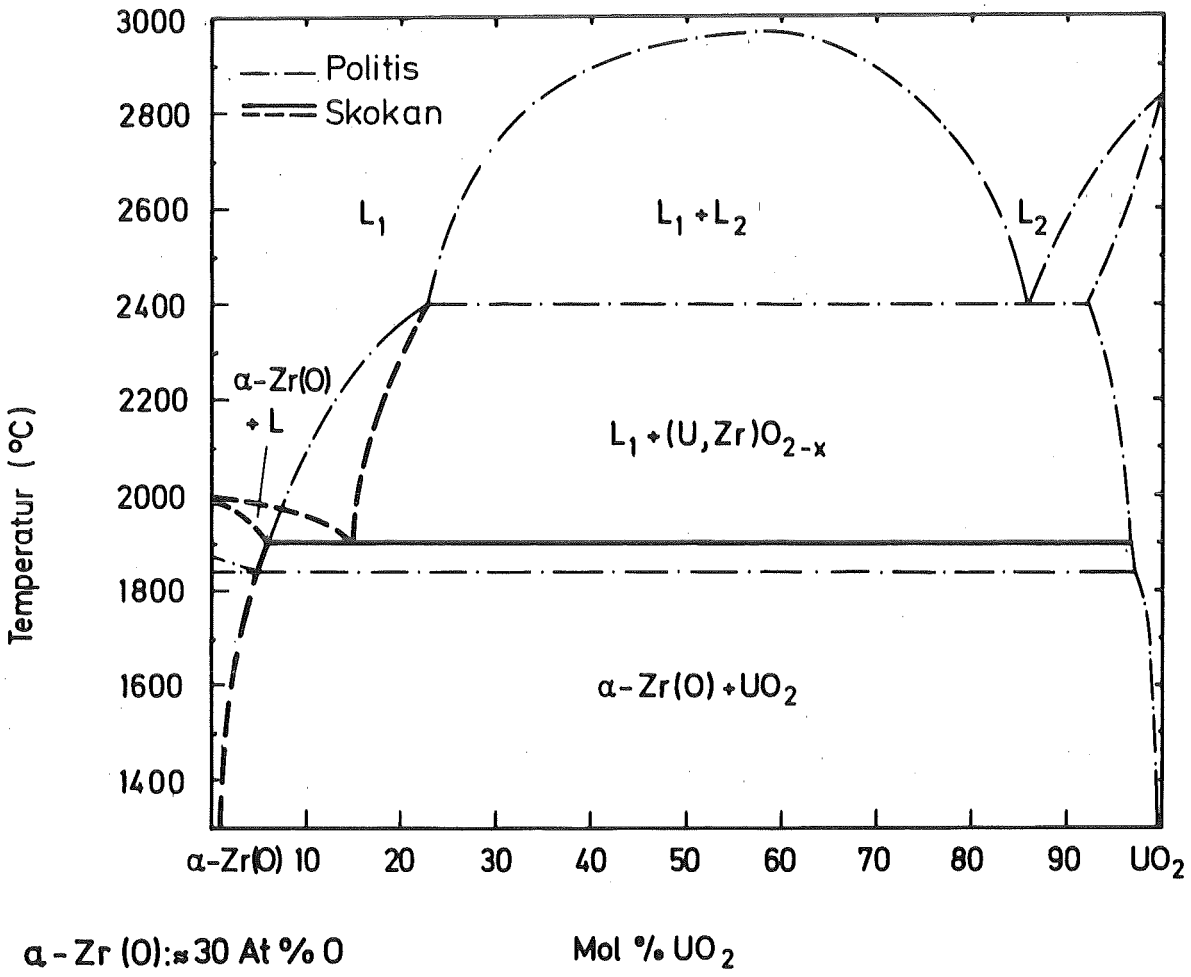

Figure 37: Quasi-binary α-Zr(O)/UO_2 phase diagram (oxygen-saturated α-Zr(O) with 30 at.% oxygen) /29,36/.

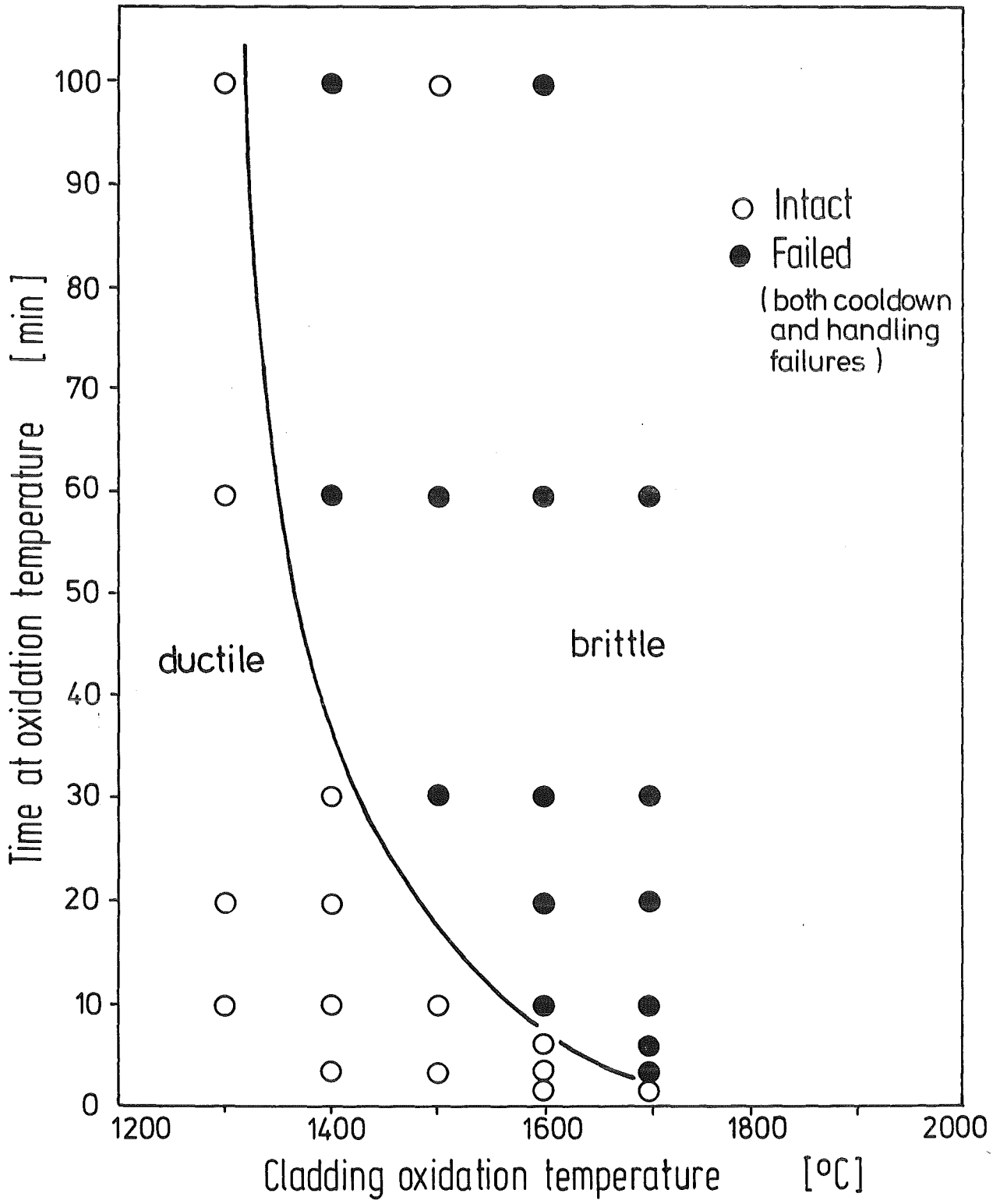

Figure 38: Failure map for the out-of-pile UO_2/Zry-4 specimens

APPENDIX

Statistical Treatment of the UO_2/Zry-4 Interaction Data

1. Parabolic Reaction Kinetics

The growth rate of the UO_2/Zry interaction layers is assumed to be controlled by the diffusion of oxygen from UO_2 to zircaloy within the cladding. The growth rate is proportional to the current oxide layer thickness and has been experimentally observed to be an Arrhenius function of temperature. Therefore, the growth rate can be expressed as:

$$\frac{dx}{dt} = A \frac{1}{x} \exp\left(\frac{-B}{RT}\right) \qquad (1)$$

where
- x = layer thickness (cm)
- t = time (s)
- R = 1.987 (cal/mole-K)
- T = temperature (K)
- A,B = constants to be determined.

Integrating equation (1) for zero layer thickness at zero time yields:

$$\frac{x^2}{t} = 2A \exp\left(\frac{-B}{RT}\right). \qquad (2)$$

Taking logarithms of equation (2) gives a linear equation:

$$\ln (x^2/t) = \ln (2A) - \frac{B}{RT} . \qquad (3)$$

Letting
- $y = \ln (x^2/t)$
- $a_o = \ln (2A)$
- $a_1 = -\frac{B}{R}$
- $z = \frac{1}{T}$,

then

$$y = a_o + a_1 z. \qquad (4)$$

The constants a_o and a_1 may be estimated by the method of least squares. The correct model is assumed to be:

$$y_i = \hat{y}_i + e_i \qquad (5)$$

where y_i = observed value
$\hat{y}_i$ = predicted value
e_i = random error.

The method estimates the constants by minimizing the sum over n data points of the squared errors with respect to each constant /1/:

$$\begin{aligned} S &= \sum_{i=1}^{n} e_i^2 \\ &= \sum_{i=1}^{n} (y_i - \hat{y}_1)^2 \\ &= \sum_{i=1}^{n} (y_i - a_o - a_1 z_i)^2 \qquad (6) \end{aligned}$$

$$\frac{\partial S}{\partial a_o} = \sum_{i=1}^{n} (-2)\,(y_i - a_o - a_1 z_i)$$

$$\frac{\partial S}{\partial a_1} = \sum_{i=1}^{n} (-2z_i)(y_i - a_o - a_1 z_i).$$

Setting the partial derivatives to zero leads to a set of so-called normal equations:

$$\sum_{i=1}^{n} y_i = n\,a_o + a_1 \sum_{i=1}^{n} z_i$$

$$\sum_{i=1}^{n} y_i z_i = a_o \sum_{i=1}^{n} z_i + a_1 \sum_{i=1}^{n} z_i^2 \qquad (7)$$

which may be solved for a_o and a_1 directly.

Normal equations for the nonlinear form of equation (1) could likewise have been formulated. However, they would have required an iterative solution scheme. If the assumption is now made that the errors on $\ln(x^2/t)$ are normally distributed, as is frequently justified, then the linearization process

can be shown to lead to estimates of a_o and a_1 which may be superior to estimates determined from the nonlinear form of the equation /2/.

The estimators of a_o and a_1 obtained from the data can be expressed as:

$$\hat{a}_1 = \frac{\sum_{i=1}^{n} (y_i - \bar{y})(z_i - \bar{z})}{\sum_{i=1}^{n} (z_i - \bar{z})^2}$$

$$\hat{a}_o = \bar{y} - \hat{a}_1 \bar{z} \qquad (8)$$

where $\bar{y} = \frac{1}{n} \sum_{i=1}^{n} y_i$

$\bar{z} = \frac{1}{n} \sum_{i=1}^{n} z_i$.

Using these estimators, equations were developed for each of the reaction zones and are given here in the form of equation (2) in cm^2/s:

$$\begin{aligned} x^2/t &= 5.50 \exp(-57{,}700/RT) \quad \text{Zone I} \\ x^2/t &= 0.707 \exp(-50{,}100/RT) \quad \text{Zone II} \\ x^2/t &= 1.62 \exp(-45{,}200/RT) \quad \text{Zone III} \\ x^2/t &= 0.259 \exp(-41{,}300/RT) \quad \text{Zone III-Zone I.} \end{aligned} \qquad (9)$$

For the reaction zone adjusted with respect to the position of the original UO_2/Zry-4 interface (Zone III - Zone I), the average thickness of Zone I for each specimen was subtracted from the Zone III data and the regression performed as usual. Since Zone I was very uniform, this introduced only a small error into the adjusted reaction zone equation. The standard error of estimate of y on z is defined as:

$$s_{y.z} = \left[\frac{1}{n-2} \sum_{i=1}^{n} (y_i - \hat{y}_i)^2\right]^{1/2} \qquad (10)$$

and determined for each equation as:

$$\begin{aligned} s_{y.z}\,(I) &= 0.243 \\ s_{y.z}\,(II) &= 0.213 \\ s_{y.z}\,(III) &= 0.257 \\ s_{y.z}\,(III\text{-}I) &= 0.299. \end{aligned} \qquad (11)$$

Note that the standard errors of estimate are given for ln (x^2/t).

Confidence intervals at a 95% confidence level for a_o and a_1 are given by:

$$a_o = \hat{a}_o \pm t_{(n-2,0.975)} \left[\frac{\sum_{i=1}^{n} z_i^2}{n \sum_{i=1}^{n} (z_i - \bar{z})^2} \right]^{1/2} s_{y.z}$$

$$a_1 = \hat{a}_1 \pm t_{(n-2,0.975)} \left[\frac{s_{y.z}}{\left[\sum_{i=1}^{n} (z_i - \bar{z})^2 \right]^{1/2}} \right] \qquad (12)$$

where t is the 0.975 percentile value of Student's t distribution with n-2 degrees of freedom. Confidence intervals for the constants given in equations (9) are then determined from.

$$\begin{aligned} 2A &= \exp(a_o) \\ &= \exp\left[\hat{a}_o \pm t_{(n-2,0.975)} s_{a_o}\right] \\ B &= -Ra_1 \\ &= -R\left[\hat{a}_1 \pm t_{(n-2,0.975)} s_{a_1}\right] \end{aligned} \qquad (13)$$

where s_{a_o} and s_{a_1} are the estimated standard deviations of a_o and a_1 as defined by (12). The upper and lower confidence limits were found to be:

$$\begin{aligned} 2A\ (I) &= (6.61 \ , \ 4.57) \\ 2A\ (II) &= (0.944 \ , \ 0.502) \\ 2A\ (III) &= (2.06 \ , \ 1.27) \\ 2A\ (III\text{-}I) &= (0.342 \ , \ 0.196) \\ B\ (I) &= (58{,}400 \ , \ 57{,}100) \\ B\ (II) &= (51{,}200 \ , \ 49{,}100) \\ B\ (III) &= (46{,}000 \ , \ 44{,}400) \\ B\ (III\text{-}I) &= (42{,}200 \ , \ 40{,}000) \end{aligned} \qquad (14)$$

Confidence limits for predicted values of $y = \ln(x^2/t)$ can be estimated at the 95% confidence level by:

$$y_p = y_o \pm t_{(n-2,0.975)} s_{y.z} \left[\frac{n+1 + (z_o - \bar{z})^2 / s_z^2}{n-2} \right]^{1/2} \qquad (15)$$

where y_p = predicted value of y corresponding to $z=z_o$ for the population

y_o = predicted value of y corresponding to $z=z_o$ from equation (9)

s_z^2 = sample variance of z.

These curves (from equation (15)) are shown in Figure 1 for each equation.

2. General Case

Equation (1) and the analysis following explicitly assumed that time and reaction layer thickness could be incorporated into a single dependent variable, i.e., that the reaction kinetics are exactly parabolic. To investigate the more general case where time is also an independent variable, the reaction rate can be assumed to be proportional to the inverse of the thickness raised to a power m which is determined from the data:

$$\frac{dx}{dt} = A \frac{1}{x^m} \exp\left(-\frac{B}{RT}\right). \tag{16}$$

Integrating:

$$\frac{1}{m+1} x^{m+1} = At \exp\left(-\frac{B}{RT}\right) \tag{17}$$

and taking logarithms gives:

$$\ln x = \left(\frac{1}{m+1}\right) \ln [A(m+1)] - \left(\frac{1}{m+1}\right) \frac{B}{RT} + \left(\frac{1}{m+1}\right) \ln t. \tag{18}$$

Letting

$$\begin{aligned} y &= \ln x \\ a_o &= \left(\frac{1}{m+1}\right) \ln [A(m+1)] \\ a_1 &= -\left(\frac{1}{m+1}\right) \frac{B}{R} \\ a_2 &= \frac{1}{m+1} \end{aligned} \tag{19}$$

$$z_1 = \frac{1}{T} \qquad (19)$$

$$z_2 = \ln t,$$

then $$y = a_o + a_1 z_1 + a_2 z_2.$$

The normal equations are derived as before, and the resulting equations of the form:

$$\frac{x^{m+1}}{t} = (m+1)\,(A)\,\exp\left(\frac{-B}{RT}\right)$$

are:

$$\frac{x^{1.96}}{t} = (1.96)(2.75)\,\exp\,(-57{,}100/RT) \quad \text{Zone I}$$

$$\frac{x^{2.04}}{t} = (2.04)(0.391)\,\exp\,(-51{,}100/RT) \quad \text{Zone II} \qquad (20)$$

$$\frac{x^{2.10}}{t} = (2.10)(0.808)\,\exp\,(-46{,}400/RT) \quad \text{Zone III}$$

$$\frac{x^{2.14}}{t} = (2.14)(0.114)\,\exp\,(-42{,}800/RT) \quad \text{Zone III-Zone I}$$

with standard errors of estimates:

$$s_{y.z_1z_2}\,(I) = 0.121$$

$$s_{y.z_1z_2}\,(II) = 0.106 \qquad (21)$$

$$s_{y.z_1z_2}\,(III) = 0.126$$

$$s_{y.z_1z_2}\,(III\text{-}I) = 0.145.$$

Note that the standard errors of estimate are given for ln x.

Confidence internals for the regression coefficients a_o, a_1, and a_2 and for the predicted values y_p can be determined as before, but with more complexity /3/. In particular, the constants A,B, and m are all functions of a_o, a_1, and a_2.

3. References

3.1 M.R. Spiegel, Statistics, Schaum's Outline Series, McGraw-Hill, 1972.

3.2 P.G. Hoel, Introduction to Mathematical Statistics, John Wiley and Sons, Inc., 1971.

3.3 D.F. Morrison, Multivariate Statistical Methods, McGraw-Hill, 1978.

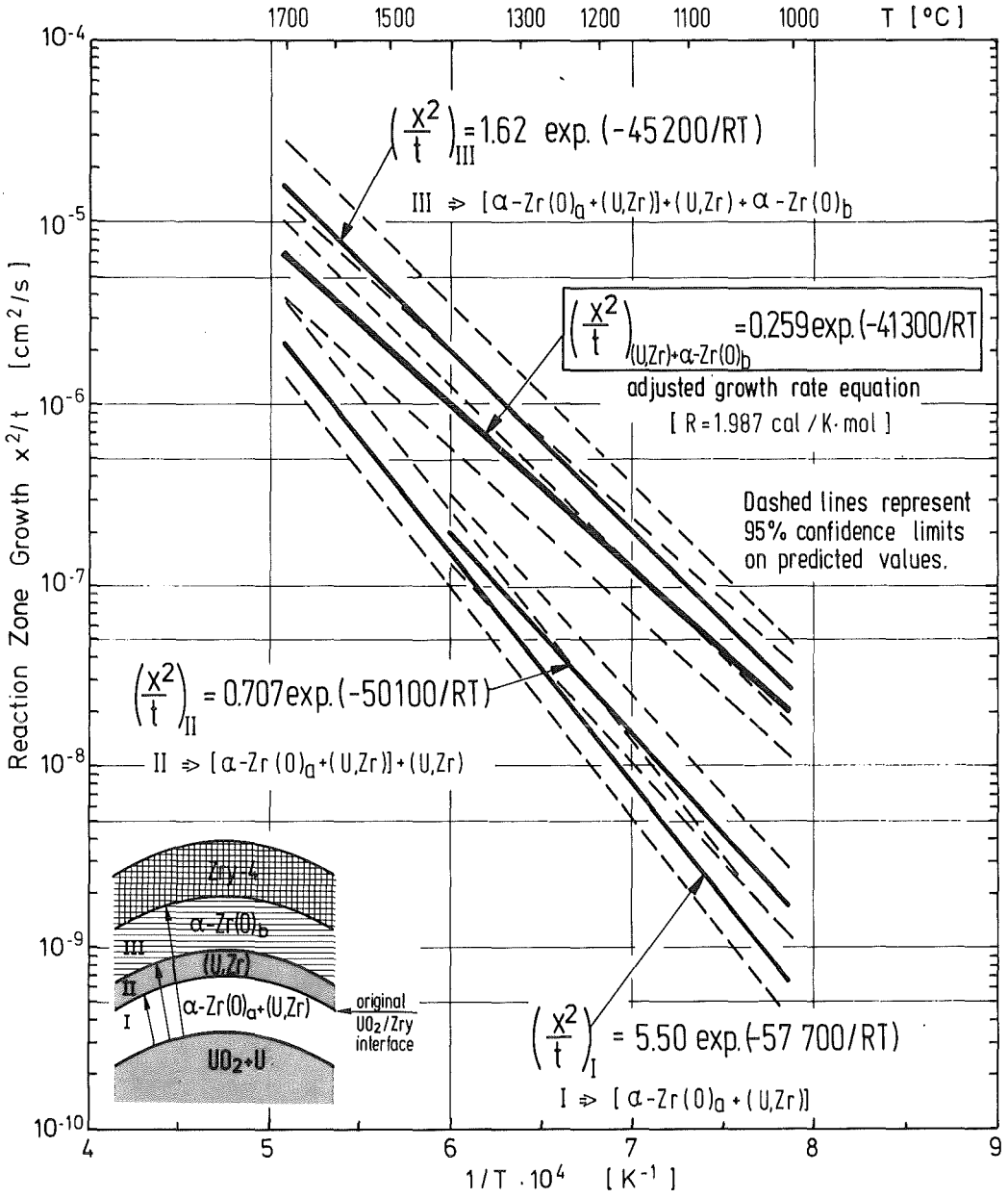

Figure 1 : UO_2/Zry-4 reaction zone growth as a function of reciprocal temperature